

PROTEOME ANALYSIS OF HYDROGEN PRODUCTION MECHANISM OF
RHODOBACTER CAPSULATUS GROWN ON DIFFERENT GROWTH
CONDITIONS

A THESIS SUBMITTED TO
THE GRADUATE SCHOOL OF NATURAL AND APPLIED SCIENCE
OF
MIDDLE EAST TECHNICAL UNIVERSITY

BY

BEGÜM PEKSEL

IN PARTIAL FULFILLMENT OF THE REQUIREMENTS
FOR
THE DEGREE OF MASTER OF SCIENCE
IN
BIOTECHNOLOGY

FEBRUARY 2012

Approval of the thesis:

**PROTEOME ANALYSIS OF HYDROGEN PRODUCTION MECHANISM OF
RHODOBACTER CAPSULATUS GROWN ON DIFFERENT GROWTH
CONDITIONS**

submitted by **BEGÜM PEKSEL** in partial fulfillment of the requirements for the degree of **Master of Science in Biotechnology Department, Middle East Technical University** by,

Prof. Dr. Canan Özgen _____
Dean, Graduate School of **Natural and Applied Sciences**

Prof. Dr. Nesrin Hasırcı _____
Head of Department, **Biotechnology**

Prof. Dr. Meral Yücel _____
Supervisor, **Biology Department., METU**

Dr. Yavuz Öztürk _____
Co-supervisor, **Marmara Research Center, TÜBİTAK**

Examining Committee Members:

Prof. Dr. Hüseyin Avni Öktem _____
Biology Dept., METU

Prof. Dr. Meral Yücel _____
Biology Dept., METU

Assist. Prof. Dr. Çağdaş Son _____
Biology Dept., METU

Dr. Ebru Özgür _____
METU-MEMS

Dr. Yavuz Öztürk _____
Marmara Research Center, TÜBİTAK

Date: 10.02.2012

I hereby declare that all information in this document has been obtained and presented in accordance with academic rules and ethical conduct. I also declare that, as required by these rules and conduct, I have fully cited and referenced all material and results that are not original to this work.

Name, Last name : Begüm PEKSEL

Signature :

ABSTRACT

PROTEOME ANALYSIS OF HYDROGEN PRODUCTION MECHANISM OF RHODOBACTER CAPSULATUS GROWN ON DIFFERENT GROWTH CONDITIONS

Peksel, Begüm

M.Sc., Department of Biotechnology

Supervisor : Prof. Dr. Meral Yücel

Co-Supervisor : Dr. Yavuz Öztürk

February 2012, 120 pages

Rhodobacter capsulatus is a versatile organism capable of growing on different growth conditions including photofermentation in the presence of carbon source, aerobic respiration, anaerobic respiration in the presence of an external electron acceptor such as DMSO. The photofermentative growth of *R.capsulatus* results in hydrogen production which stands out as an environmentally harmless method to produce hydrogen and accepted as one of the most promising process. Due to the serious problems such as as global climate change and environmental pollution caused by the fossil fuels, there is an increasing requirement for a clean and sustainable energy source. Furthermore, the ability of *R.capsulatus* to fix nitrogen, to use solar energy makes it a model to study various aspects of its metabolism. Thus the goal of this study is to increase the potential in biohydrogen production with the photofermentative bacteria and to investigate the proteins playing roles in different growth modes of the bacteria.

In the present study, protein profiles of *Rhodobacter capsulatus* grown on respiratory, anaerobic respiratory and photofermentative growth modes were obtained. LC-MS/MS system is used to analyze the proteome as a high throughput technique. Physiological analysis such as HPLC for the analysis of the carbon source consumption, GC and analysis of pigments were carried out to state the environmental conditions. As a result, total of 460 proteins were identified with 17 proteins being unique to particular growth condition. Ratios of the proteins in different growth conditions were compared and important proteins were highlighted.

Keywords: *Rhodobacter capsulatus*, PNS bacteria, biohydrogen production, LC-MS/MS, proteomics, photofermentation, aerobic respiration of *R.capsulatus*, anaerobic respiration of *R.capsulatus*, DMSO

ÖZ

FARKLI KOŞULLARDA BÜYÜTÜLEN RHODOBACTER CAPSULATUS BAKTERİSİNİN HİDROJEN ÜRETİM MEKANİZMASININ PROTEOMİKS YÖNTEMİ İLE ANALİZİ

Peksel, Begüm

Yüksel Lisans, Biyoteknoloji Bölümü

Tez Yöneticisi : Prof. Dr. Meral Yücel

Ortak Tez Yöneticisi: Dr. Yavuz Öztürk

Şubat 2012, 120 sayfa

Rhodobacter capsulatus, karbon kaynağı varlığında fotofermentasyon, aerobik solunum, DMSO gibi harici electron akseptörü varlığında anaerobik solunum yapabilen, çok yönlü büyüeyebilen bir organizmadır. *Rhodobacter capsulatus*'un fotofermentasyon ile büyümesi hidrojen üretimi ile sonuçlanır ki bu çevreye zarar vermeyen bir hidrojen üretme metodudur ve gelecek vaadeden bir yöntem olarak göze çarpmaktadır. Fosil yakıtların sebep olduğu küresel iklim değişikliği ve çevre kirliliği gibi ciddi problemlerden dolayı, temiz ve sürdürülebilir bir enerji kaynağına ihtiyaç duyulmaktadır. Ayrıca *Rhodobacter capsulatus* azotu bağlaması ve solar enerjiyi kullanabilmesi gibi özellikleri dolayısıyla birçok metabolik olay için model bir organizmadır. Bu sebeplerden dolayı, bu çalışma fotofermentatif bakteri kullanarak biyohidrojen üretimini arttırmak ve farklı büyüme koşullarında büyüeyen bakterilerde önemli rolleri olan proteinleri incelemek amaçlanmaktadır.

Bu alıřmada, *Rhodobacter capsulatus* bakterisinin solunum, anaerobik solunum ve fotofermentatif byme kořullarındaki protein profilleri elde edilmiřtir. Yksek verimlilięe sahip LC-MS/MS sistemi proteomu incelemek iin kullanılmıřtır. Karbon kaynaęının tketimini analiz etmek iin HPLC, GC analizi ve pigment analizi gibi fizyolojik analizler bakterinin iinde bulunduęu evresel kořulları belirlemek iin uygulanmıřtır. Sonu olarak, 17 tanesi belirli bir kořula zg olmak zere 460 tane protein tanımlanmıřtır. Farklı kořullardaki proteinlerin oranları karřılařtırılmıř ve nemli proteinler vurgulanmıřtır.

Anahtar Kelimeler: *Rhodobacter capsulatus*, PNS bakterisi, biyohidrojen retimi, LC-MS/MS, proteomiks, fotofermentasyon, *R.capsulatus* aerobic solunum, *R.capsulatus* anaerobik solunum, DMSO

To my family,

ACKNOWLEDGEMENTS

First of all, I would like to express my sincere gratitude to my supervisor Prof. Dr. Meral Yücel for her invaluable guidance, advice, support and for the opportunities that made me involved in very innovative, informative scientific environments and gave me chance to work with great scientists. Also I would like to thank to my co-supervisor Dr. Yavuz Öztürk for his contribution to this study through his advices, recommendations and for his support during my visit in Marmara Research Center.

I would also like to thank Prof. İnci Erođlu and Prof. Ufuk Gündüz for their guidance and support.

I am very grateful for Dr. Ebru Özgür for considerable contribution to my study through her advices, it was precious to have discussions with her.

I would like to thank the examining committee members, Prof. Dr. Hüseyin Avni Öktem and Assist. Prof. Dr. Çağdaş Son for evaluating my thesis.

It is a pleasure to thank my labmates Dominic Deo Androga, Nilüfer Afşar, Pelin Sevinç, Endam Özkan, Muazzez Gürkan Dođan, Efe Boran, Emrah Sađır, Görkem Baysal and Gülşah Pekgöz for their friendship, assistance and contributions. It was great to share the same bench, to spend time with you in and out of the lab.

I would like to express my gratitude to Dr. A. Tarık Baykal for his guidance during protein isolation, LC-MS/MS experiments and data analysis. I would also like to thank Emel Akgün, Melis Savaşan Söğüt and Ebru Çayır for their help and friendship during my visit in TÜBİTAK- Marmara Research Center.

I would like to thank Tufan Öz, Dr.Cengiz Balođlu and Dr.Remziye Yılmaz for their advices and help throughout my study. I also acknowledge Gülten Orakçı for her help and guidance with the HPLC and GC analyses.

I owe sincere thanks to Dr. Ferhan Ayaydın not only for the microscopy part of this study, but also for his invaluable guidance and contribution to my scientific notion. I've learned so much from him throughout the "International Training Course-Biological Research Center, Szeged, HUNGARY" that I really enjoyed being part of.

Besides the scientific part, it is indispensable to thank my friends Nilay Grgener and Gzde Kumař for their very precious friendship and encouragement. I am grateful for your contributions to my life, personality and the time we share.

At last but not least, I am indebted to my family Sabahattin Saim Peksel, Hlya Peksel, Melike Peksel and Orkun Peksel not only for being there supporting me no matter what, but also letting me be who I am since the day I was born. There is no proper way to express my gratitude to you, but I would like to say that I am so happy to be a part of our family.

This research was supported by METU with DAP project (BAP No: BAP-07.02.2011-003), LTP Project (BAP No: BAP 07.02.2011.101), TBTAK 1001 Project 108T455 and the EU 6th Framework Integrated Project 019825 (HYVOLUTION).

TABLE OF CONTENTS

ABSTRACT	iv
ÖZ.....	vi
ACKNOWLEDGEMENTS.....	ix
TABLE OF CONTENTS.....	xi
LIST OF TABLES.....	xv
LIST OF FIGURES	xvi
LIST OF SYMBOLS AND ABBREVIATIONS	xix
CHAPTERS.....	1
1. INTRODUCTION	1
1.1 Hydrogen as the Future Energy Carrier.....	1
1.2 Hydrogen Production.....	2
1.3 Biohydrogen Production.....	6
1.3.1 Biophotolysis of water.....	6
1.3.2 Dark Fermentation.....	8
1.3.3 Photofermentation.....	9
1.3.4 Hybrid Systems.....	10
1.3.5 Microbial Electrolysis Cells.....	11
1.4 Purple Non-Sulfur Bacteria.....	12
1.5 Physiology, Metabolism and Global responses of PNS bacteria.....	14
1.5.1 Carbon Assimilation metabolism in PNS bacteria.....	15
1.5.2 Hydrogen Production Metabolism in PNS bacteria.....	17
1.5.3 Tetrapyrrole Metabolism of PNS Bacteria, Pigments and Photosynthesis ..	19
1.6 Proteomics	23

1.6.1	LC-MS/MS	25
1.7	Proteomics studies of PNS bacteria	26
1.8	Aim of this study.....	27
2.	MATERIALS AND METHODS.....	28
2.1	The Microorganism.....	28
2.2	Culture media.....	28
2.2.1	Growth medium	28
2.2.2	Hydrogen producing medium	28
2.2.3	Solid medium.....	29
2.2.4	Stock medium	29
2.3	Experimental set-up	29
2.3.1	Pre-cultivation of the bacteria.....	29
2.3.2	Experimental conditions	30
2.3.3	Sampling procedures.....	31
2.4	Analysis	33
2.4.1	Cell density measurement.....	33
2.4.2	Gas composition analysis.....	33
2.4.3	Organic Acid analysis.....	33
2.4.4	Photosynthetic pigment analysis.....	34
2.4.5	Microscopy analysis	34
2.4.6	Sodium dodecyl sulfate Polyacrylamide Gel Electrophoresis (SDS-PAGE).....	35
2.5	Proteome analysis	35
2.5.1	Protein isolation	35
2.5.2	Sample Preparation for LC-MS/MS	36
2.5.3	LC-MS/MS method	36
2.5.4	LC-MS/MS Data Analysis.....	38
3.	RESULTS AND DISCUSSIONS.....	40
3.1	Physiological Analysis of <i>R.capsulatus</i> under different growth conditions	40
3.1.1	Growth of <i>R.capsulatus</i> under different conditions	40
3.1.2	Optimization of DMSO concentration for the anaerobic respiratory growth condition	42
3.1.3	Analysis of Pigmentation in <i>Rhodobacter capsulatus</i> grown under different conditions.....	44

3.1.4	Analysis of top gas of <i>Rhodobacter capsulatus</i> grown under different conditions.....	47
3.1.5	Physiological Analysis of the samples used for LC-MS/MS experiments ..	50
3.1.6	Visualization of <i>Rhodobacter capsulatus</i> using fluorescence microscope ..	51
3.2	LC-MS/MS Analysis	53
3.2.1	Optimization of Protein isolation and Protein quantification	53
3.2.2	Quality assessment of the LC-MS/MS data.....	56
3.2.3	Identification of Proteins of <i>Rhodobacter capsulatus</i> by LC-MS/MS.....	58
3.3	Protein Profiles of <i>Rhodobacter capsulatus</i> Grown on Different Growth Conditions.....	61
3.3.1	Comparison of the protein levels in anaerobic respiratory growth in the presence of DMSO vs aerobic respiratory growth	64
3.3.2	Comparison of the protein levels in anaerobic photofermentative growth in the presence of illumination vs aerobic respiratory growth	67
3.3.3	Comparison of the protein levels in anaerobic photofermentative growth in the presence of illumination vs anaerobic respiratory growth in the presence of DMSO	69
4.	CONCLUSIONS	73
	REFERENCES	75
	APPENDICES	84
A.	COMPOSITION OF THE GROWTH AND EXPERIMENTAL MEDIA.....	84
B.	SAMPLE HPLC CHROMATOGRAM AND CALIBRATION CURVES.....	87
C.	COMPONENTS OF THE SOLUTIONS USED IN SDS POLYACRYLAMIDE GEL ELECTROPHORESIS.....	90
D.	CELL COUNT EXPERIMENTS AND MICROSCOPY IMAGES	92
E.	BACTERIA DRY CELL WEIGHT CURVES	93
F.	SAMPLE NANO-DROP SPECTRUM FOR ISOLATED PROTEINS.....	94
G.	PRINCIPLE COMPONENT ANALYSIS.....	95

H. PROTEIN DETERMINATION AND QUANTIFICATION BY PROGENESIS SOFTWARE.....	97
I. LIST OF IDENTIFIED PROTEINS BY LC-MS/MS METHOD.....	100

LIST OF TABLES

TABLES

Table 1.1 Hydrogen production summary table	4
Table 1.2 Different growth modes of PNS bacteria.....	14
Table 3.1 Concentration of UPX extracted proteins and peptides after trypsinization followed by lyophilization	55
Table 3.2 Unique peptides identified in a particular growth mode.....	64
Table 3.3 Changes in the protein levels in anaerobic respiratory growth in the presence of DMSO vs aerobic respiratory growth	65
Table 3.4 Changes in the protein levels in anaerobic photofermentative growth in the presence of illumination vs aerobic respiratory growth	67
Table 3.5 Changes in the protein levels in anaerobic respiratory growth in the presence of DMSO vs anaerobic photofermentative growth in the presence of illumination.....	70
Table A.1 The composition of MPYE medium for 1 L.....	84
Table A.2 The components of the growth and experimental media	85
Table A.3 The composition of the 10X vitamin solution	86
Table A.4 The composition of 10X trace element solution	86
Table B.1 HPLC analysis of LC-MS/MS samples	89
Table C.1 The composition of 10X SDS Running Buffer	90
Table C.2 The composition of 6X Loading Buffer.....	90
Table C.3 The composition of the SDS Polyacrylamide gel	91
Table C.4 The composition of Coomassie Gel stain and destaining solution.....	91
Table I.4 The list of identified proteins by LC-MS/MS and PLGS software	100

LIST OF FIGURES

FIGURES

Figure 1.1 Alternative methods for Hydrogen Production	2
Figure 1.3 Photofermentative pathways of PNS bacteria	9
Figure 1.4 Schematic illustration of microbial electrolysis cell	11
Figure 1.5 The microscopic images of <i>Rhodobacter capsulatus</i> grown in darkness and photosynthetic conditions emphasizing intercytoplasmic membranes	13
Figure 1.6 Different electron transfer pathways	16
Figure 1.7 Reactions of central carbon metabolism in purple nonsulfur bacteria	17
Figure 1.8 The general view of H ₂ related pathways in PNS bacteria	18
Figure 1.9 Overview of the tetrapyrrole biosynthetic pathway with the major intermediates and products	20
Figure 1.9 The schematic illustration of the major components involved in the photosynthetic reactions	22
Figure 1.10 Atomic force microscopy image of a photosynthetic membrane	23
Figure 1. 11 Strategies for MS-based proteomic analysis	25
Figure 2.1 Illustration of streak plate technique	30
Figure 2.2 Illustration of Argon Flush	31
Figure 2.4 Picture of the Waters Synapt HDMS.....	37
Figure 2.5 Schematic illustration of the LC-MS/MS system.....	38
Figure 3.2 Acetate consumption graph of <i>R.capsulatus</i> for different growth conditions	42
Figure 3.3 The growth profile of <i>Rhodobacter capsulatus</i> for different DMSO concentrations (0mM, 30mM, 40mM and 50mM)	43
Figure 3.4 Acetate consumption graph of <i>Rhodobacter capsulatus</i> for different DMSO concentrations (0mM, 30mM, 40mM and 50mM)	44

Figure 3.5 Absorption spectra of intact cells of <i>Rhodobacter capsulatus</i> grown on different growth conditions.....	45
Figure 3.6 Absorption spectra of acetone/methanol extracted <i>Rhodobacter capsulatus</i> cells grown on different growth conditions	46
Figure 3.7 Absorption spectra of <i>Rhodopseudomonas acidophila</i>	47
Figure 3.8 Gas chromatogram for different growth conditions	49
Figure 3.9 Bacteriochlorophyll concentration graph for different growth conditions .	51
Figure 3.10 Fluorescence microscopy images of <i>Rhodobacter capsulatus</i>	52
Figure 3.11 SDS-PAGE gel (12%) picture of proteins extracted with different extraction buffers stained with Coomassie	54
Figure 3.12 SDS-PAGE gel (12%) image of UPX extracted samples stained with Coomassie.....	56
Figure 3.14 Principle Component analysis of identified peptides in all growth conditions.....	58
Figure 3.15 Plot of charge/mass ratio versus retention time of analyzed peptides by LC-MS/MS	59
Figure 3.16 The pie-chart representation of gene ontology according to biological processes	60
Figure 3.17 The pie-chart representation of gene ontology according to molecular function	61
Figure 3.19 Schematic representation of unique spectra, peptides and proteins identified for different growth conditions.....	63
Figure B.1 Sample HPLC chromatogram for Aerobic respiratory growth condition..	87
Figure B.2 Sample HPLC chromatogram for Anaerobic photofermentative growth condition	88
Figure B.3 Sample HPLC chromatogram for Anaerobic respiratory growth condition in the presence of DMSO.....	88
Figure B.4 Calibration Curve for Acetic Acid.....	89
Figure D.1 Phase-contrast image of <i>R.capsulatus</i> used in cell counting experiments.	92
Figure E.1 Dry cell weight calibrataion curve of <i>Rhodobacter capsulatus</i>	93

Figure F.1 A representative Nano-Drop spectrum for Protein readings at 280nm	94
Figure G-1 Geometrical steps for finding components of principal component analysis	96
Figure H-1 Representation of protein identification by Progenesis software	97
Figure H-2 Representation of peptide quantification by the feature on mass/charge ratio vs retention time graph	98
Figure H-3 Box plot representation of Light harvesting protein B 870 alpha subunit of <i>Rhodobacter capsulatus</i>	99

LIST OF SYMBOLS AND ABBREVIATIONS

ATP	Adenosine triphosphate
Bchl	Bacteriochlorophyll
BP Medium	Bieble Pfening Medium
CBB pathway	Calvin-Benson-Bassham pathway
DMS	Dimethylsulfide
DMSO	Dimethyl sulfoxide
EMRT	Exact mass retention time
ESI	Electrospray ionization
FASP	Filter Aided Sample Preparation
GGPP	Geranylgeranyl pyrophosphate
GO	Gene ontology
IEA	Internatiol energy agency –in the text given
LB	Lysogeny Broth
LC-MS	Liquid chromatography- Mass spectrometry
LC-MS/MS	Liquid chromatography tandem mass spectrometry
MALDI	Matrix assisted Laser desorption/ionization
MEC	Microbial electrolysis cell
NAO	Nonyl acridine orange
OD	Optical density
PCA	Principle Components Analysis

PI	Propidium iodide
PLGS	ProteinLynx Global Server
PNS	Purple non-sulfur
RC	Reaction Center
<i>R.capsulatus</i>	<i>Rhodobacter capsulatus</i>
RUBISCO	Ribulose biphosphate carboxylase/oxygenase
SDS	Sodium dodecylsulfate
TMAO	Trimethylamine N oxide
UPLC	Ultra performance liquid chromatography
UPX	Universal Sample Extraction Buffer

CHAPTER 1

INTRODUCTION

1.1 Hydrogen as the Future Energy Carrier

Undoubtedly, energy demand of the world is increasing along with the CO₂ emissions and depletion of the fossil fuels. The industrialized world's economy is highly dependent on the availability of fossil fuels. The growing economy with urbanization and industrialization will result in depletion of the world's reservoirs, increased pollution and oil price concurred with an economic crisis. According to International Energy Agency (IEA) global energy related emissions of CO₂ will increase 20% and reach 36.4 gigatonnes in 2035 with a reflection of long-term global temperature increase of more than 3.4°C, however encouragement of renewable energy deployment may reduce emissions by 3.4 gigatonnes (World Energy Outlook 2011 Factsheet). The results of CO₂ increase and in turn temperature raise may be listed as the increase in the frequency and intensity of extreme weather events such as floods, droughts and hurricanes which causes changes in agricultural yields, biological extinctions and glacial retreat (Züttel *et al*, 2010). Furthermore the 32.8% of energy is supplied by oil with the highest crude oil production in Middle East region and 61.7% oil is consumed in transportation sector together with 5.5% of natural gas and 0.4% of coal in 2009 (International Energy Agency). The situation addresses the substantial and undeniable demand for a new environmentally friendly energy source and energy carrier that can be used in transportation.

Hydrogen produces only water when reacted with oxygen in an internal combustion engine or a fuel cell and that makes it a clean non-polluting fuel. Hydrogen has 34 kcal/g heat of combustion which is 3 times of petroleum (10.3-8.4 kcal/g) and 4 times of coal (7.8 kcal/g) (Jain, 2009). 1 kg of hydrogen contains the same energy of 2.1 kg natural gas and 2.8kg gasoline (US Department of Energy, Hydrogen Analysis Research Center). It has the highest energy to mass ratio. Hydrogen production is location independent, thus it doesn't require

long distance transport which consumes energy itself and may provide energy where electricity is not available such as remote areas. These properties make hydrogen not only a renewable energy source, but also a good energy carrier. However it is important to note that for hydrogen to be an environmentally friendly fuel, it should be produced from solar light or a renewable source such as wind power, hydropower or biomass.

Although hydrogen is being attractive for its energy carrying properties, it is important to highlight its use in the industry for the hydrogenation of many products such as heavy oils, foods and reduction of nitrate, perchlorate and other oxidized water pollutants. For these purposes the yearly H_2 demand is approximately 10^8 m^3 (at 1 atm) in the United States (Lee, 2010).

1.2 Hydrogen Production

Hydrogen can be generated by various processes. Primary energy source and production technologies are important to classify hydrogen production methods. Fig. 1.1 states the alternative methods from energy sources and production technologies.

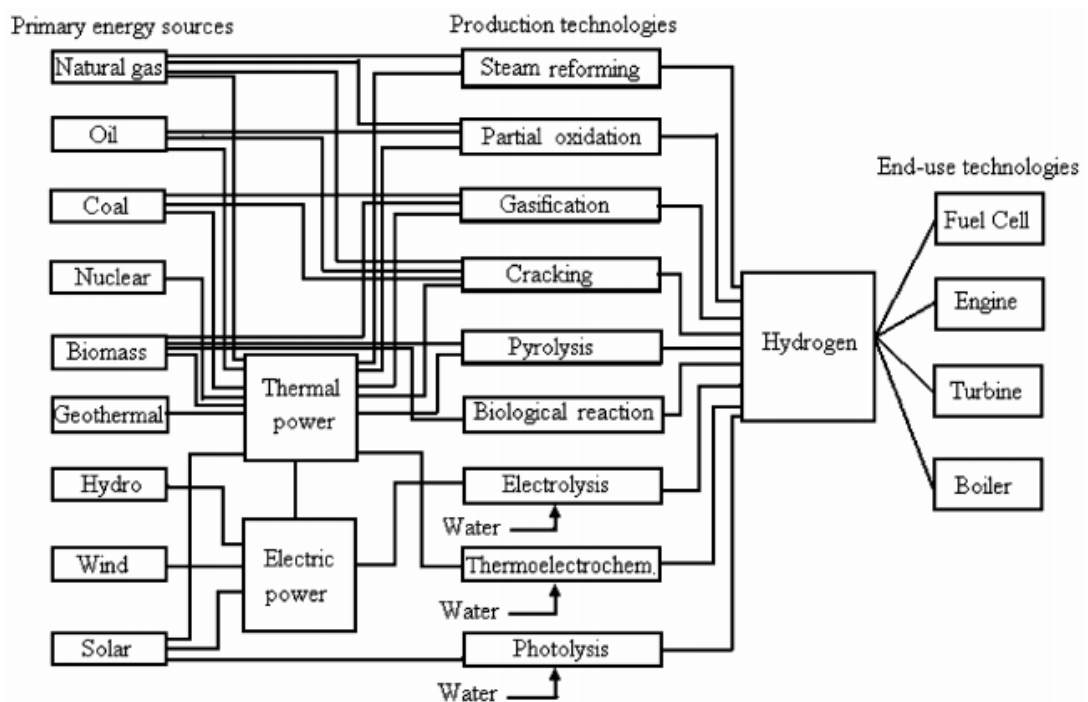


Figure 1.1 Alternative methods for Hydrogen Production (Balat *et al*, 2008)

Hydrogen can be produced using fossil fuels as a source with the methods as follows:

- Steam reforming of natural gas or thermal power obtained from coal, oil etc. is the least expensive method and used to produce hydrogen with the maximum conversion (Kothari *et al*, 2008). Briefly, it is an endothermic catalytic process and requires hydrocarbons to be processed. A very important disadvantage of the method is the large quantities of CO₂ emission and removal of tar is necessary (Levin *et al*, 2010).
- Partial oxidation is the second widely used method of hydrogen production. It is an endothermic process as steam reforming. All kinds of fuels can be used. However it emits CO together with CO₂. Also H₂/CO ratio is low (Holladay *et al.*, 2009).
- Gasification resembles partial oxidation and based on partial oxidation of materials such as coal and biomass. Thus this is a non-biological method to produce hydrogen from biomass. Highly efficient H₂ production may be obtained with this method (Ishida *et al*, 2006). However there is a significant amount of tar that must be separated as well as gasses like CO, CO₂, CH₄ that can be formed during the process. Solar gasification on the other hand has good hydrogen yields, but requires effective collector plates (Das *et al*, 2008).
- Thermal cracking process involves the utilization of oxygen and steam in proper extents with natural gas. Heat is required to run the process, but still in the case of methane the efficiency is comparable to partial oxidation and steam reforming (Bicakova *et al.*, 2010).
- Pyrolysis is another method which produces hydrogen from biomass with a mixture of gasses such as CH₄, CO₂, CO, N₂. This method offers reduced emissions, however fouling by the carbon formed is the main challenge (Holladay *et al.*, 2009).
- Electrolysis process requires water and in the simplest form it uses electricity to split water molecule into hydrogen and oxygen.

- Photolysis process in which solar energy is used to produce hydrogen, however the efficiency is low (Bicakova *et al.*, 2010)
- Thermochemical methods imply for the decomposition of water into its molecules with the use of chemical reactions to initiate the process (Bicakova *et al.*, 2010)
- Biological Production requires the participation of a microorganism and explained in detail in the following sections.

Among the listed processes hydrogen is virtually produced using natural gas (40%), heavy oils (30%), coal (18%) together with electrolysis (4%) and biomass (1%) (Das *et al.*, 2008). The industrial way of producing hydrogen takes place with the consumption of fossil fuels except the applications consuming electricity produced from hydro or wind power (Kothari *et al.*, 2008). Thus these processes cannot be considered as environmentally friendly. On the contrary, biological way of hydrogen production, which will be addressed in depth in the following part, is not only environmentally friendly but also makes the recycling of wastes possible as they are used as biomass. The efficiencies of these processes are summarized in Table 1.1.

Table 1.1 Hydrogen production summary table (adapted from Levin *et al.*, 2010)

Process	Feedstocks	Conversion efficiencies	Co-products	References
Steam reforming	Methane, glycerol, alcohols, polyols, sugars, organic acids	70–85% ^d	CO, CO ₂ , C ₁₀ –C ₂₂ carbon chains	McHugh, 2005; Muradov, 2008
Aqueous reforming	Glycerol, alcohols, polyols, sugars, organic acids	35–100% ^d	CO, CO ₂ , alkanes, alcohols, polyols, organic acids	Milliken, 2008; Reichman, 2007; Wen, 2008

Table 1.1 Continued

Electrolysis	H ₂ O + electricity	50–60% ^c	Nil	Sorensen, 2005
Partial oxidation	Hydrocarbons ^a	60–75% ^d	N/A	McHugh, 2005
Biomass gasification	Biomass ^b	35–50% ^d	CO, CO ₂ , CH ₄	Guoxin, 2009
BioH₂: photolysis	H ₂ O + sunlight	0.5% ^f	Nil	Turner, 2008
BioH₂: photo-fermentation	Organic acids + sunlight	0.1% ^g	CO ₂	Turner, 2008
BioH₂: dark fermentation	Biomass ^c	60–80% ^h	CO ₂	Turner, 2008; Levin, 2004
<p>BioH₂ : Biohydrogen production</p> <p>Nil: only H₂ is produced.</p> <p>N/A: data not available.</p> <p>a Glycerol, alcohols, polyols, sugars, organic acids.</p> <p>b Lignocellulosic biomass.</p> <p>c Lignocellulosic biomass and/or lignocellulose hydrolysis products (five and/or six carbon sugars).</p> <p>d Thermal efficiency: based on higher heating values.</p> <p>e Lower heating value of hydrogen produced divided by the electrical energy used to generate the hydrogen. Does not include purification.</p> <p>f Solar conversion to hydrogen via water splitting using light energy. Does not include purification.</p> <p>g Solar conversion to hydrogen by catabolism of organic acids using light energy. Does not include purification.</p> <p>h Maximum theoretical yield of 4 moles H₂ per mole glucose catabolized.</p>				

1.3 Biohydrogen Production

Biological hydrogen production process includes use of inexhaustible resources such as sunlight and electrons from H₂O or organic acids and requires a biological system such as a microbial organism or enzymes (Das *et al*, 2008). Another advantage of the system is the use of biomass which may be obtained from food or industrial wastes, thus hydrogen production will also play role in recycling (Lee *et al*, 2010).

The process operates at ambient temperature and atmospheric pressure due to the essentiality of the biological systems. The drawbacks of the biological systems making them yet to be commercially unavailable are the stability and efficiency (Kothari *et al*, 2008).

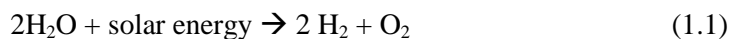
Biohydrogen production processes can be classified as follows:

- Biophotolysis of water (direct or indirect biophotolysis)
- Dark fermentation
- Photofermentation
- Hybrid systems
- Microbial Electrolysis cells (Lee *et al*, 2010; Das *et al*,2008)

1.3.1 Biophotolysis of water

Photosynthetic hydrogen production is the biological process that generates hydrogen from water using sunlight. There are two types of biophotolysis: direct biophotolysis and indirect biophotolysis.

In direct biophotolysis, solar energy is captured by the photosynthetic apparatus and the energy is used to convert water into stored chemical energy by the following general reaction:



Photosystem I and II are both responsible for this process. The energy captured by photosystem II (PSII) is used to split water to evolve oxygen. Photosystem I (PSI) can either uses this energy to reduce CO₂ or forms H₂ in the prescence of hydrogenase (Das *et al*, 2008). As shown in the scheme (Fig. 1.2) solar energy is absorbed by the reaction centers (RC) of PSII and PSI. Then the electrons travel through pheophytins (Pheo) to redox

intermediates (RI) or to ferredoxins (Fd) which transfers electrons to hydrogenases (H) to from hydrogen.

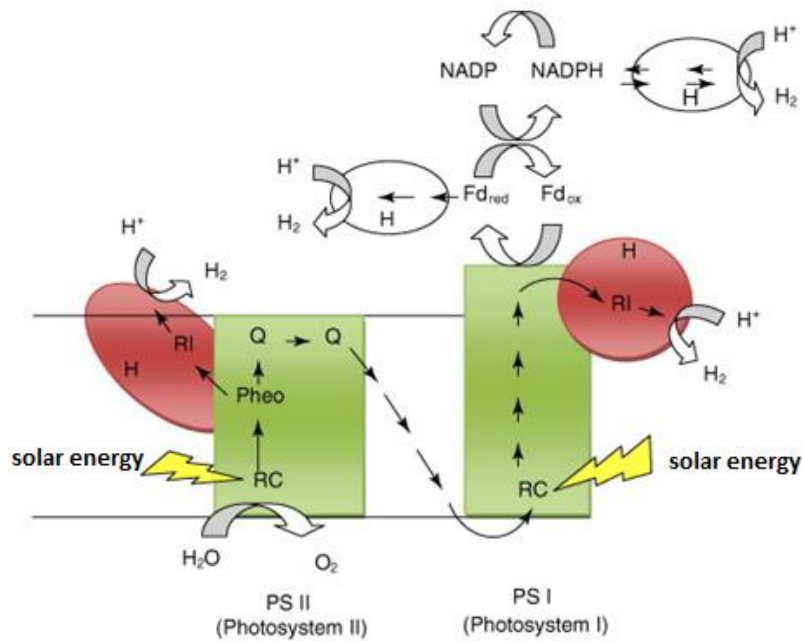
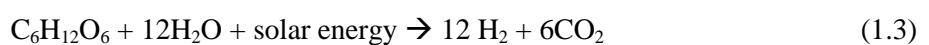
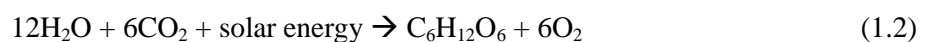


Figure 1.2 Direct Biophotolysis (Lee *et al*, 2010)

Green Algae have the capability of performing direct biophotolysis, but the system requires saturated light intensities. O₂ produced by the process however has inhibitory effect on hydrogenases in even very low concentrations. Sparging inert gas to the system to sustain the partial pressure of O₂ low, use of O₂ absorbers or making hydrogenase more O₂ tolerant are some resolutions, however still the system is not efficient to overcome the weighty cost (Hallenback *et al*, 2002).

Indirect biophotolysis is carried out by cyanobacteria which are a very diverse group of prokaryotic photosynthetic organisms, known as blue-green algae, thus they have pigments such as chlorophyll α , caretenoids etc. Indirect biophotolysis reaction involves two steps:



The system involves several enzymes including;

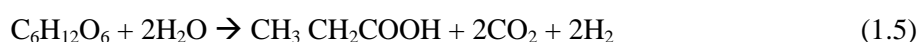
- nitrogenases which are involved in nitrogen reduction and produces hydrogen as a by-product
- uptake hydrogenases which are involved in reoxidation of H₂ to produce H₂O to assure the redox balance
- bidirectional hydrogenases which catalyze both synthesis and oxidation of H₂ (Levin *et al*, 2004)

During indirect biophotolysis, CO₂ fixation followed by O₂ generation and nitrogen fixation followed by H₂ production occurs separately, thus inhibition of hydrogenases by O₂ is prevented. However, the process still has low photochemical efficiencies due to low light conversion efficiencies and cost (Das *et al*, 2008).

1.3.2 Dark Fermentation

Dark fermentation is an anaerobic process and involves the oxidation of carbon rich substrates. Starch based materials, lignocellulosic materials are some substrates to be used, however various waste waters such as molasses, starch hydrolysate, glycerol waste etc. are more attractive to be processed in dark fermentation due to cost and waste recycling purposes (Hallenbeck *et al*, 2002; Chong *et al*, 2009). Fermentation reactions can be operated at mesophilic (25–40°C), thermophilic (40–65°C), extreme thermophilic (65–80°C), or hyperthermophilic (>80°C) temperatures.

The bacteria needs to dispose the electrons formed during oxidation of the substrates. Under aerobic conditions, O₂ serves as the final electron acceptor and keeps the redox balance. On the other hand, under anaerobic conditions, carbon sources are oxidized to short-chain organic acids such as acetic acid, butyric acid etc. and protons act as the electron acceptors and reduced to molecular H₂ (Das *et al*, 2008). The equations for glucose as substrate, acetic acid and butyric acid as the products are given in the following:



The organic acids produced in the fermentation process cause an increase in acidity and in turn H_2 production is inhibited, thus pH is needed to be maintained in the range of 5-6. Moreover the partial pressure of hydrogen in the liquid phase affects the production because of its effect on hydrogenase (Chong *et al*, 2009).

Dark fermentation offers high H_2 production rates, nevertheless yields are low due partial composition of the substrates. Combining this process with a microbial system that produces H_2 from the products of the dark fermentation is a promising solution while also serious environmental pollution will be eliminated (Lee *et al*, 2010).

1.3.3 Photofermentation

Photofermentation is carried by purple non-sulfur (PNS) bacteria via assimilation of organic acids such as acetic acid, lactic acid etc. and mainly by the activity of nitrogenase system under photoheterotrophic conditions (under light and in the absence of oxygen) (Das *et al*, 2008). The equation of photofermentation reaction for acetic acid is as follows:

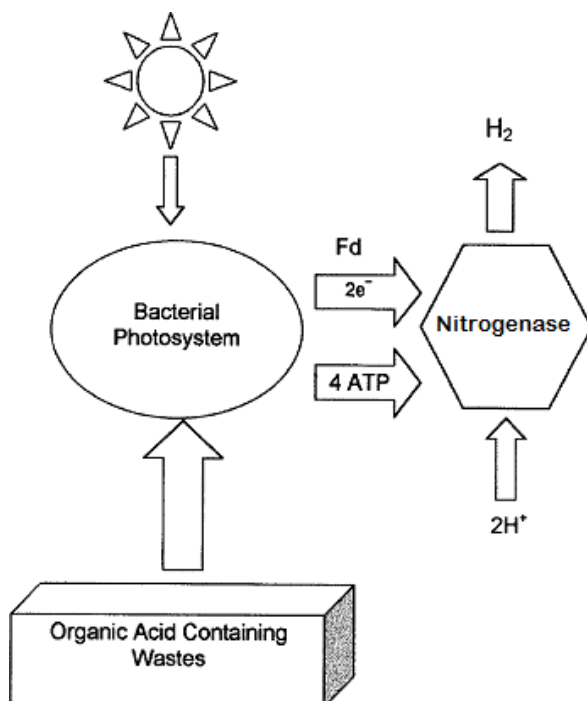
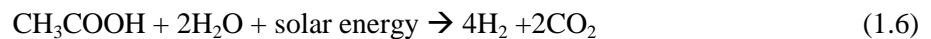


Figure 1.3 Photofermentative pathways of PNS bacteria (Hallenbeck *et al*, 2002)

As shown in Fig. 1.3, light energy absorbed by PS is used to produce H₂ by nitrogenase enzyme. The absence of PSII in this system eliminates the O₂ related drawbacks. However presence of uptake hydrogenase causes reduced efficiencies due to its H₂ consumption activity. Genetically modified strains that lack uptake hydrogenase are produced and have higher hydrogen production efficiencies (Öztürk *et al.*, 2006; Kars *et al.*, 2009). Another bottleneck of the system is low light conversion efficiencies. The reactor design to increase the surface area or light diffusing capability, using co-cultures with different light utilization characteristics are some solutions that can be used to increase the efficiency (Das *et al.*, 2008).

1.3.4 Hybrid Systems

Hybrid systems aim to compensate the drawbacks of individual hydrogen production processes. In dark fermentation alone, hydrogen yields are low due to incomplete digestion of carbon rich substrates. Dark fermentation and photofermentation coupled systems hence intends the complete digestion of the feedstock. In such an integrated system, carbon rich sources are digested to short-chain organic acids during first dark fermentation step. Then the organic acids are further utilized in the second photofermentation step. Hydrogen production occurs in both processes and the carbon source is totally reduced to CO₂. Thus this system has increased yields compared to both processes alone (Eroglu *et al.*, 2011). Dark fermentation and photofermentation processes can be operated in sequential or in combined forms in which the processes are consecutive or simultaneous, respectively. In a recent review by Argun *et al.*, sequential fermentors are introduced to have higher yields and productivities (2011).

Another hybrid system proposed by Melis *et al.*, targets the low light conversion efficiency of photofermentation with the use of green algae (2006). Normally green algae photosynthesize and produce O₂ which in turn inhibits the nitrogenase system and hydrogen production. However as an advantage, green algae have the ability to utilize visible spectrum of light in the range of 400-700nm. Compared to near infrared spectrum in 700-950 nm range which is absorbed by PNS bacteria, 400-700nm range has more than two times the energy content of photosynthetically active radiation (Melis *et al.*, 2006). The system proposed, controls the photosynthesis/respiration rate of the green algae by sulfur deficiency, thus co-culture of green algae and PNS bacteria becomes possible resulting in better utilization of solar energy in a wider wavelength range and higher efficiencies.

1.3.5 Microbial Electrolysis Cells

This emerging technology combines the bacterial metabolism with electrochemistry. Microorganisms present in the anode oxidize an organic compound i.e. acetate, ethanol, butyrate and transfer released electrons to anode with the conductive solid. With this connection electrons reach to the cathode, where they react with H_2O to produce hydrogen. The scheme of a microbial electrolysis cell (MEC) is given in Fig. 1.4. A power supply is connected to boost the electrons to cathode, because the produced electrons have lower redox potential to reduce H_2O to H_2 (Geelhoed *et al*, 2010). The major advantage of the system is high H_2 yields and can be combined to fermentation processes. Nevertheless the system still requires an external supply, the voltage must be balanced in order to direct electrons and high-efficiency materials are needed for membranes and electrodes (Lee *et al*, 2010)

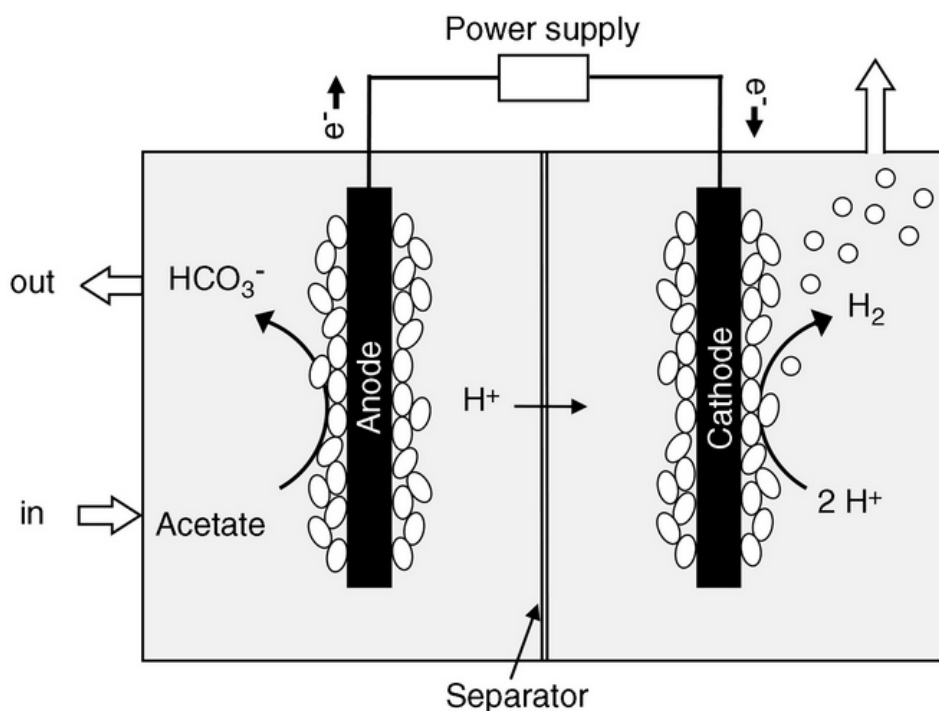


Figure 1.4 Schematic illustration of microbial electrolysis cell (Geelhoed *et al*, 2010)

1.4 Purple Non-Sulfur Bacteria

Purple non-sulfur bacteria (PNS) belong to a large group of bacteria called α -Proteobacteria. The members are versatile and able to grow well in phototrophic, respiratory or fermentative condition. For example *Rhodobacter capsulatus* can grow under light with either CO₂ or organic carbon, under dark by respiration either in aerobic conditions or anaerobic conditions with the presence of an electron acceptor, by fermentation or by chemolithotrophy (Madigan *et al*, 2009).

PNS bacteria have photosynthetic pigments giving various colors from olive-green, peach brown, brown, brown-red, red or pink to themselves. According to the species or the conditions the pigment content of the cells differs and give characteristic absorption spectra (Imhoff, 2006).

Most of the PNS bacteria are isolated from fresh waters, however they also occur in marine, hypersaline environments, soil and sewages (Imhoff, 2006).

Rhodobacter capsulatus which is used as a model organism to study various aspects of metabolism owing to its metabolic versatility is a member of PNS bacteria (Onder *et al*, 2010). It has been a favourite research tool in photosynthesis, energetics and nitrogen fixation together with molecular genetics' techniques. By Strnad *et al* genome sequence of *R. capsulatus* was published leading to initiate efforts for transcriptomic and proteomic studies (2010). First efforts to define complete proteome of this species were done by Onder *et al* under defined growth conditions and led to better understanding of the global distributions of the proteins and showed the importance of the identification of hypothetical proteins annotated in the genome (2008).

The full lineage of this rod-shaped (Fig. 1.5) gram-negative bacteria is in bacteria superkingdom, proteobacteria phylum, alphaproteobacteria class, Rhodobacterales order, Rhodobacteraceae family and Rhodobacter genus.

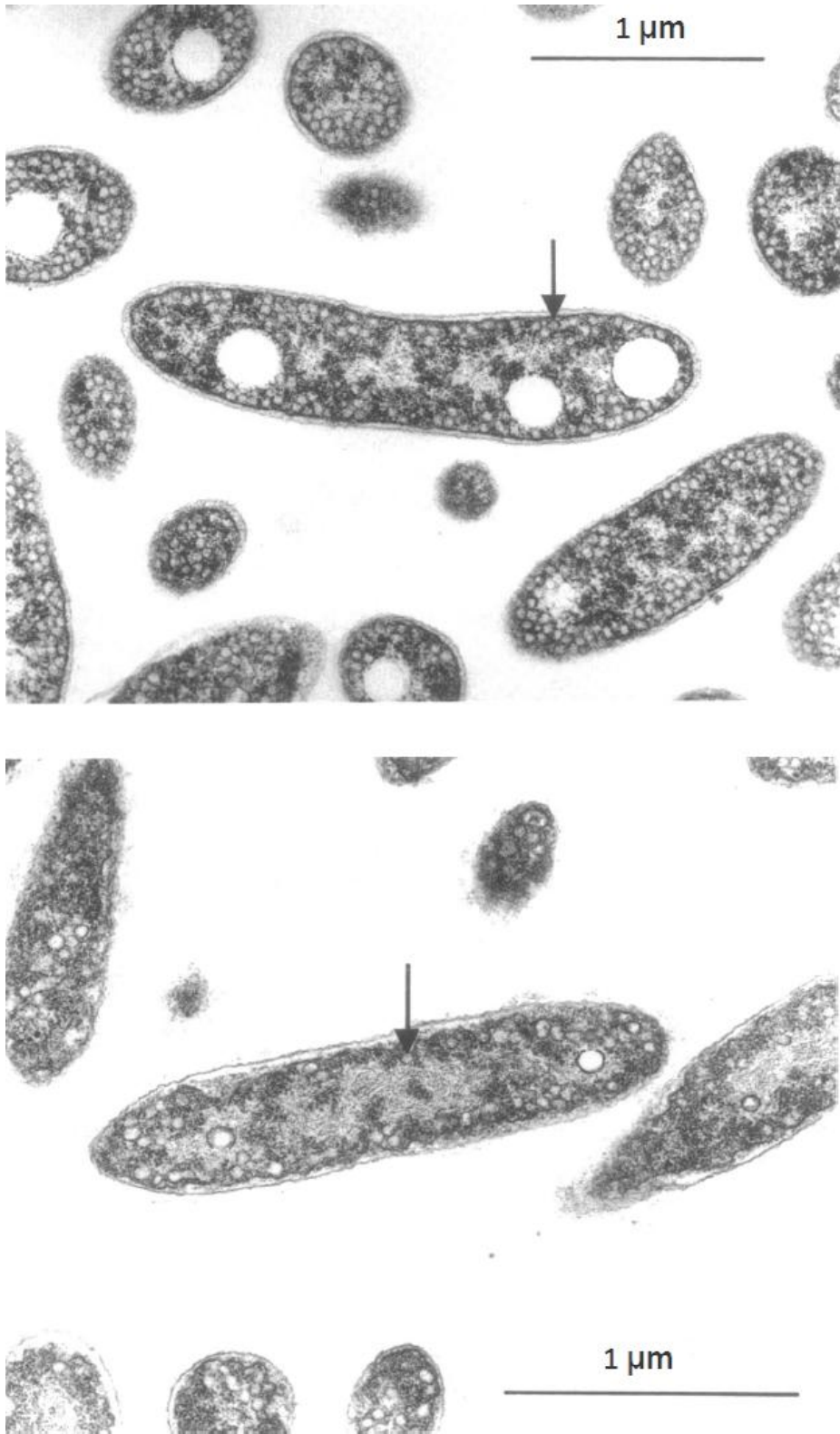


Figure 1.5 The microscopic images of *Rhodospirillum rubrum* grown in darkness and photosynthetic conditions emphasizing intercytoplasmic membranes (adapted from Madigan *et al*, 1979)

1.5 Physiology, Metabolism and Global responses of PNS bacteria

As emphasized previously, this remarkable versatile organism is able to survive in different conditions because the metabolism and physiology of PNS bacteria changes as it adapts to environmental conditions. These conditions and mode of growth was shown in table 1.2 to introduce the aspects of the metabolism.

Table 1.2 Different growth modes of PNS bacteria (compiled from Koku et al, 2002 and Kars et al, 2010)

Mode of Growth	Carbon source	Energy source	
Photoheterotrophy	Organic carbon	Light	CBB pathway functions for redox homeostasis in the cell using CO ₂ as the electron acceptor. Hydrogen is produced under nitrogen limiting conditions.
Photoautotrophy	Inorganic carbon (CO ₂)	Light	In the prescence of illumination and CO ₂ CBB pathway functions for CO ₂ fixation. Rubisco enzyme is required in high amounts.
Aerobic respiration	Organic carbon	Organic carbon	In the prescence of oxygen. Better growth is observed compared to anaerobic respiration and fermentation.

Table 1.2 Continued

Anaerobic respiration	Organic carbon	Organic carbon	Under anaerobic conditions in the presence of an alternative electron acceptor such as DMSO or TMAO better growth is observed compared to fermentation
Fermentation	Organic carbon	Organic carbon	Under anaerobic dark conditions with no alternative electron acceptor. Poor growth

1.5.1 Carbon Assimilation metabolism in PNS bacteria

The ability of surviving in different conditions (aerobic, anaerobic, under light or dark etc.) and utilizing different substrates together with the advantage of easy genetic manipulation make PNS bacteria an interesting model to study carbon metabolism. Thus, aerobic and anaerobic electron transport chains of PNS bacteria which are diversely organized with the adaptive regulatory mechanisms have been studied with great interest (Zannoni, 2004).

Adenosine triphosphate (ATP) the energy carrier can be synthesized by fermentation, aerobic or anaerobic respiration and photosynthesis. The proton motive force which is the inducer of ATP synthesis is created by the electron transfer chains. The chains are formed by the transmembrane complexes connected by lipid and water soluble electron carriers. Therefore lipid soluble electron carriers are called quinones and water soluble electron carriers are called cytochromes (Junge and Jackson, 1982). The interactions and the organization of these chains enable bacteria to accommodate different conditions. The details of the electron transfer pathways in which the membranous (in black) and periplasmic (in red) components are shown distinctively in Fig. 1.6.

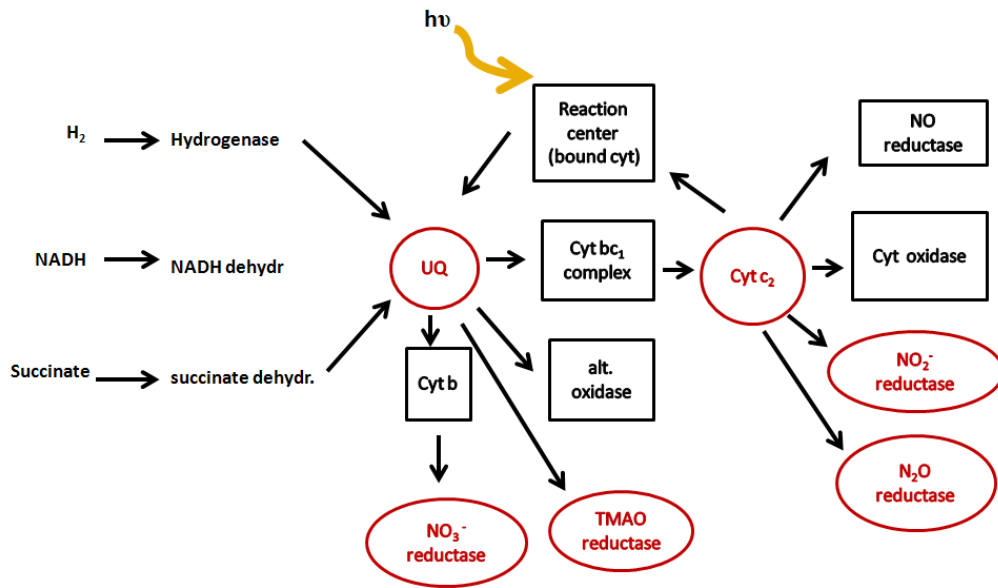


Figure 1.6 Different electron transfer pathways (adapted from Verméglio *et al*, 2004)

The respiratory chain, photosynthetic apparatus and terminal reductase of dimethyl sulfoxide (DMSO) and trimethylamine N-oxide (TMAO) which may serve as final electron acceptor during anaerobic respiration are expressed constitutively (Verméglio *et al*, 2004). However the ratio of this energy chains are regulated by light, oxygen concentrations and the presence of electron acceptors like nitrate. Under high light illumination and anaerobic conditions photosynthetic chain will be highly expressed inhibiting respiration, denitrification and reduction of DMSO either totally or partially with a very slow rate. However even the low oxygen availability in the environment will cause partial repression of the photosynthetic reactions. Under dark and anaerobic conditions bacteria use the available electron acceptor with the highest redox potential such as DMSO. Absence of illumination coupled with high oxygen presence will cause total repression of the photosynthetic reaction centers and antenna complexes (Sabaty *et al*, 1993). The reactions of the central carbon metabolism of PNS bacteria are shown in Fig. 1.7.

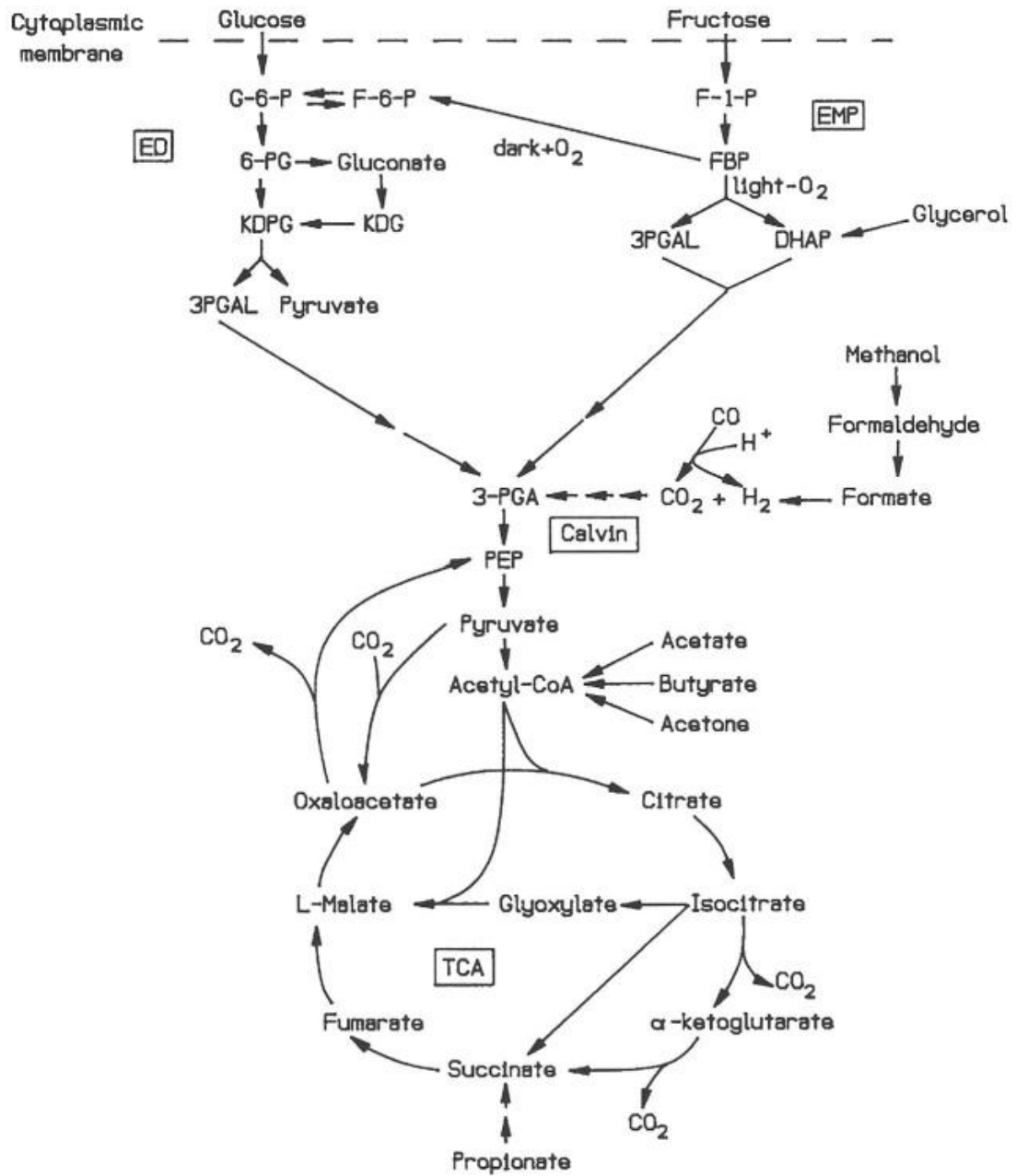


Figure 1.7 Reactions of central carbon metabolism in purple nonsulfur bacteria (Tabiata, 2004)

1.5.2 Hydrogen Production Metabolism in PNS bacteria

Hydrogen production occurs in the photoheterotrophic growth mode in the presence of an anaerobic atmosphere, illumination and organic acids. However, to direct the metabolism of

the bacteria towards hydrogen production nitrogen limitation is obligatory. Nitrogenase and hydrogenase enzymes build the basis of hydrogen production mechanism. In Fig. 1.8 schematic representation of H₂ related pathways is shown.

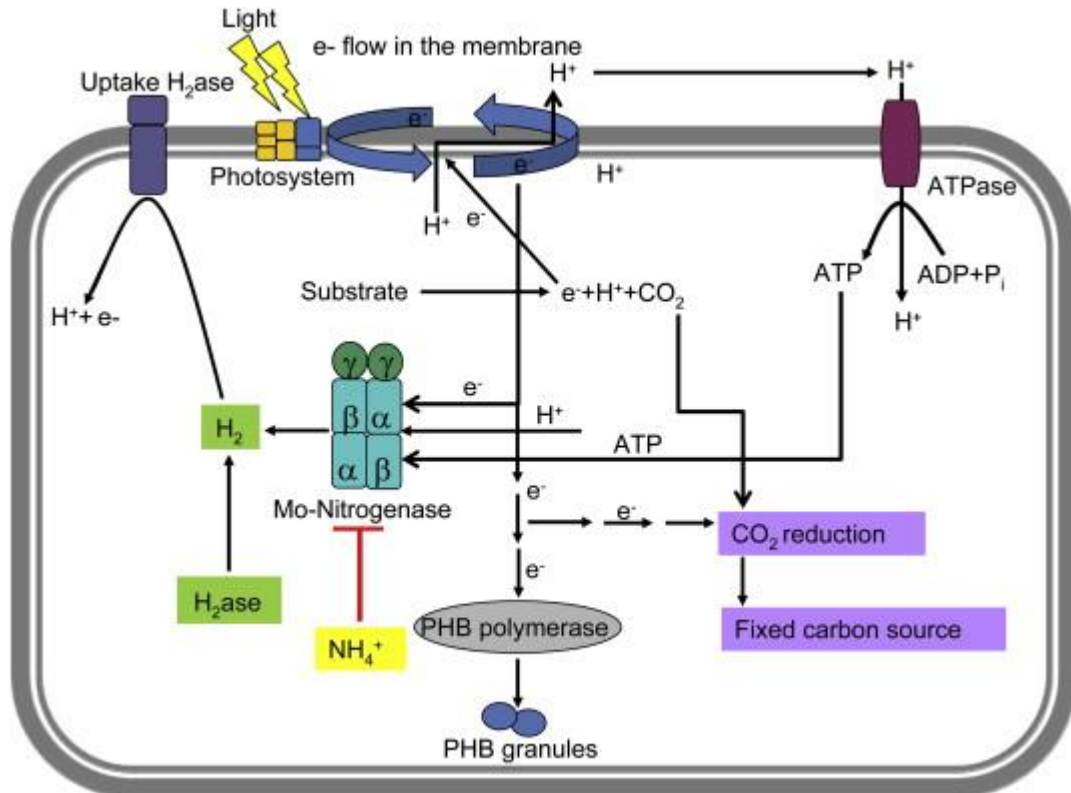
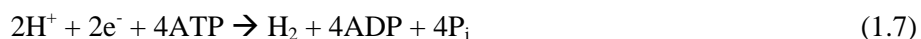


Figure 1.8 The general view of H₂ related pathways in PNS bacteria (Kars *et al*,2010)

During photofermentation, electron flow in the membrane obtained by the utilization of substrates and the solar energy creates the proton motive force for ATP production. Nitrogenase enzyme consumes ATPs to reduce protons to molecular hydrogen while reducing molecular nitrogen to ammonium (Kars *et al*, 2010). Nitrogenase is a highly conserved enzyme which catalyzes the reduction of molecular nitrogen (N₂) to NH₃, thus enables bacteria to use atmospheric nitrogen. As long as ammonium is present, the nitrogenase enzyme and nitrogen fixation is inhibited, because nitrogen fixation requires high energy (>16 ATP/1 N₂ molecule). Nitrogenase contains a unique iron-molybdenum cofactor (FeMo-co) which is the site for reduction. There are also nitrogenase enzymes alternative to Molybdenum-dependent nitrogenase (Mo-nitrogenase) such as vanadium dependent hydrogenase (V-nitrogenase) and iron-only nitrogenase (Fe-nitrogenase).

However Mo-nitrogenase has higher specific activity than V-nitrogenase and Fe-nitrogenase making it the preferred enzyme. It is important to note that since molybdenum is essential for the synthesis of the Mo-nitrogenase enzyme, bacteria has ABC-type high affinity molybdate uptake transporters (ModABC) to provide molybdenum even at low concentrations (Masepohl and Hallenbeck, 2010). Nitrogenase catalyzes the following reaction in the absence of molecular nitrogen and produces hydrogen:



Hydrogenases are the other diverse group of enzymes found in photosynthetic bacteria. The reaction they catalyze is as follows:



Likewise nitrogenases, they are classified according to the metal contents as Fe-hydrogenase, FeFe-hydrogenase and NiFe-hydrogenase. However they're also classified according to their preferences on hydrogen production or consumption as uptake-hydrogenase, bidirectional-hydrogenase and H₂ evolving hydrogenase (Kars *et al*, 2010; Schwarz *et al*, 2010). As a matter of fact, these enzymes regulate the H₂ turnover in the cell, thus balance the redox status and energy generation.

1.5.3 Tetrapyrrole Metabolism of PNS Bacteria, Pigments and Photosynthesis

Tetrapyrroles are the metal containing molecules that are the important due to their vital functions in both anabolic and catabolic metabolisms. The versatility of *Rhodobacter capsulatus*' metabolism depends on the use of tetrapyrroles to transfer electrons, to harvest light energy and to carry oxygen wouldn't be an overstatement (Zappa *et al*, 2010, Zeistra-Ryall, 2008)

There are two main species of tetrapyrrole in *Rhodobacter capsulatus* heme and bacterichlorophyll (Bchl). Cobalamins (vitamin B₁₂) are also synthesized in the tetrapyrrole biosynthetic pathway and used as cofactor for the enzymes. Glycine and succinyl-CoA is used to form δ-aminolevulinic acid which is the main precursor of this highly complex biosynthetic pathway (Zappa *et al*, 2010) In Fig. 1.9, the main steps and end-products of tetrapyrrole biosynthetic pathway are shown.

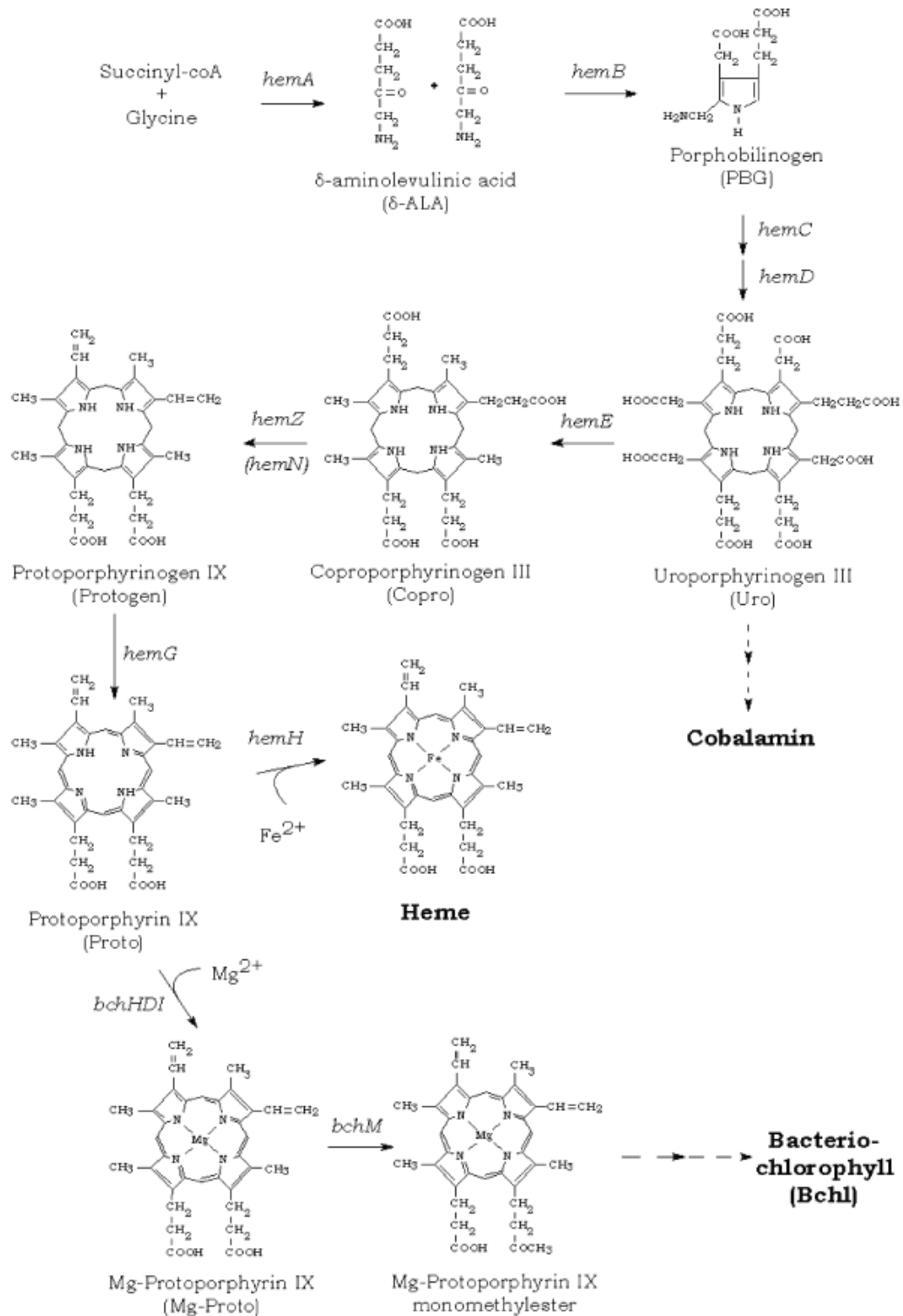


Figure 1.9 Overview of the tetrapyrrole biosynthetic pathway with the major intermediates and products (Smart *et al.*, 2004)

The biosynthesis of heme and Bchl are tightly controlled in the cell by the redox state and oxygen availability. Heme is needed for both respiration and photosynthesis whereas Bchl is involved only in photosynthesis. Many genes involved in Bchl and heme synthesis found in large operons and scattered over the genome having quite complex regulatory system interfering with the synthesis in many steps with various regulatory elements (Zeistra-Ryall, 2008). The main players of this regulatory network are as follows:

- **Reg A- Reg B** system which is the global regulator of *Rhodobacter capsulatus* has a direct affect on the tetrapyrrole synthesis. It is involved in positive transcriptional activation of the large *bchEJG* operon, which encodes various enzymes in Bchl synthesis, under anaerobic conditions (Willett *et al*, 2007).
- **CrtJ** is a redox responding transcription factor and aerobic repressor. It represses the synthesis of heme, Bchl and carotenoid synthesis genes under aerobic conditions (Elsen *et al*, 1998). Also apoproteins of the light harvesting and ubiquinol oxidase complexes are aerobically repressed with this regulator (Smart *et al*, 2004).
- **FnrL** is the redox regulator of the cell thus either represses or activates the genes involved in heme synthesis, however it has moderate effect (Smart *et al*, 2004).
- **AerR** is another aerobic repressor co-transcribed with CtrJ. It represses the genes involved in Bchl, apoprotein synthesis of light harvesting complex and ubiquinol oxidase complex (Smart *et al*, 2004).

Carotenoids on the other hand are isoprenoid pigments and have linear system of conjugated double bonds synthesized from its precursor geranylgeranyl pyrophosphate (GGPP). With this structure the chromophore can absorb light and dissipate the energy as heat. Carotenoids can thus harvest energy and play role in transferring this energy to chlorophylls. They also act as photoprotective pigments due to their ability to quench chlorophylls and singlet oxygen. Along with the diverse structure of carotenoids, they govern roles in membranes affecting the structure and fluidity or interactions with other proteins (Maresca *et al*, 2008).

Light harvesting (LH), antenna complexes and reaction centers are the membrane integrated protein-pigment machineries of the photosynthetic reactions. The integral membrane proteins of these machineries are bounded to bacteriochlorophyll a which absorbs light in the far-red region of the spectrum and carotenoids which absorb light in the green spectrum. There are two light harvesting complexes namely LH1 and LH2 having different light absorbing spectrums due to their structural differences (Law *et al*, 2004).

In the cells, the amount of LH2 is controlled by light intensity and oxygen partial pressure. Under low light intensities photosynthetic complexes are expressed in higher amounts, however in the semi-aerobic conditions, photosynthetic complexes are repressed by light (Gregor *et al*, 1999). On the other hand, LH1 is synthesized in fixed stoichiometric amounts with the reaction centers (RC) (Verméglio and Joliot, 1999). In the following figure (Fig. 1.9) the schematic organization of a photosynthetic membrane is shown.

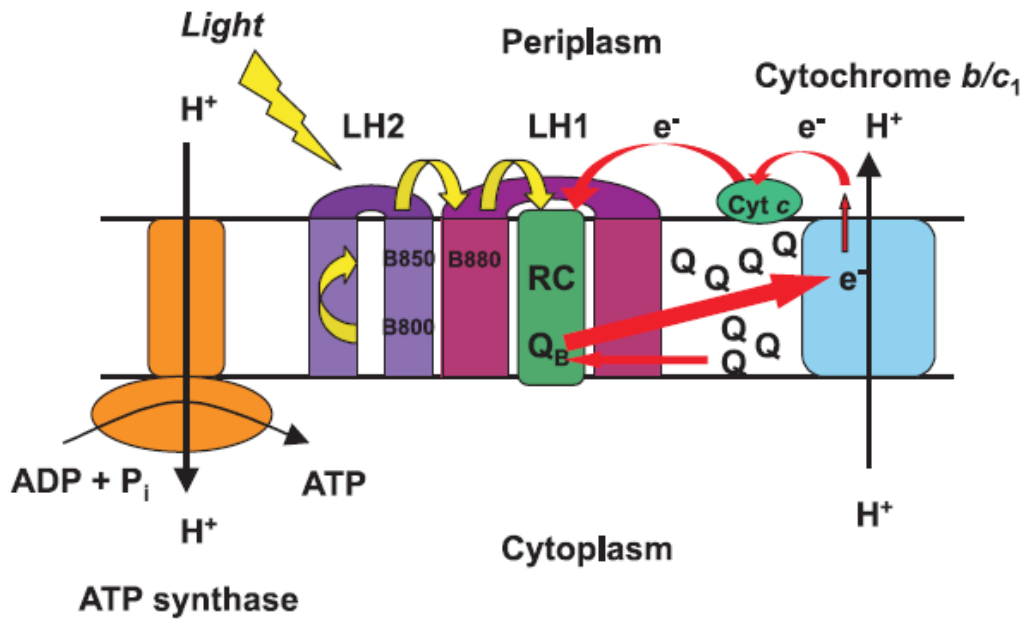


Figure 1.9 Schematic illustration of the major components involved in the photosynthetic reactions (Law *et al*, 2004)

As seen from the figure, LH is responsible for absorbing light, then energy is transferred to the RC which transfers the excitation energy to transmembrane redox difference. ATP-synthase synthesizes ATP and the cytochrome complex transfer electrons (Verméglio and Joliot, 1999). The components of the system are functionally linked and the organization of the proteins in the membrane determines the efficiency which is up to 95%. Furthermore the ecological habitat and the growth conditions play an important role in the organization (Scheuring *et al*, 2009). In Fig. 1.10 atomic force microscopy image of a photosynthetic membrane is shown, the rather smaller circles represent LH2 and the larger circular structures are the reaction centers.

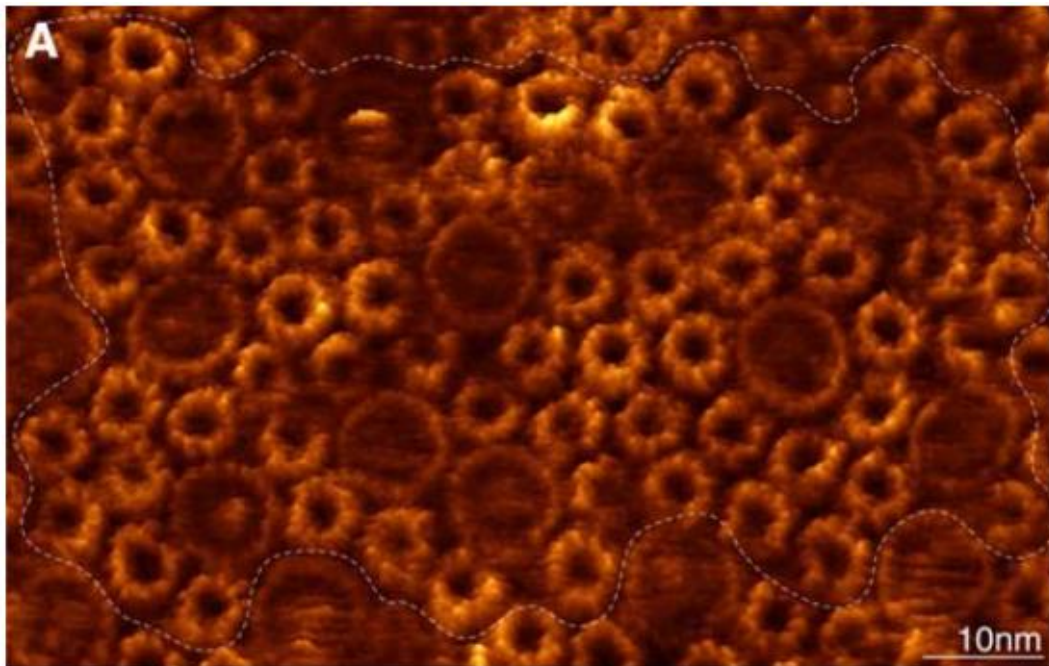


Figure 1.10 Atomic force microscopy image of a photosynthetic membrane (Scheuring *et al*, 2009)

1.6 Proteomics

Proteomics as the rest of the “omics” studies focuses on the global analysis of gene products, proteins, in the scope of identification, quantification and characterization. In contrast to mRNA expression studies, proteomics gives data about the functional state of the cell rather than the potential state (Zhang *et al*, 2010). The information obtained by the proteomic analysis enclose the identification of proteins in terms of sequence, changes of the levels of proteins in terms of abundance under different conditions or between the cell lines/types/mutants, modification, localization and the interaction of the proteins to provide a vision about the cellular state as a whole (Twyman, 2005).

Due to the mass limitation of the proteomic systems, proteins have to be digested into peptides. Additionally, independent of the scale of the study, protein analysis requires methods for separation from the mixtures to individual components. There are two main separation techniques in proteomics; liquid chromatography (LC) and gel electrophoresis.

Both techniques are completed by mass spectrometry for peptide and protein identification and relative quantification (McConkey, 2011).

Compared with the genome, proteome is a more dynamic system and comprises large subject to subject variations. Furthermore proteins undergo wide range of alterations such as phosphorylation, glycosylation, sulfation, nitration, glycation, acylation, methylation, oxidation and proteolytic cleavage which affects the function of the protein critically whereas creating a challenge in identification. Another challenge is the abundance of the constitutive proteins. For example, in blood 12 most abundant proteins compose 95% of the total protein mass. Thus the peptides obtained from these proteins will compete for the peptides generated from the less abundant proteins which may have significant importance. Therefore, for the effective analysis, the separation of the proteome, fractionation or excluding high abundant proteins are important steps as well as the selection of the proteomic separation, ionization and detection system (Zhang *et al*, 2010).

In Fig. 1.11 the major strategies for MS-based proteomics are represented. The bottom-up approach follows the order of separation of proteins before enzymatic digestion or peptides after enzymatic digestion followed by the peptide mass fingerprinting based identification simultaneously. On the other hand in top-down strategy, proteins are fractionated and separated into either pure simple proteins or less complex protein mixtures and then each fraction are analyzed by the MS system. In the bottom-up approach, generated peptides are of great complexity thus highly sensitive and efficient separation is required. It is preferred for large scale analysis despite the fact that the limited dynamic range of MS allows gathering information from highly abundant peptides rather than low abundance peptides. Top-down strategy is powerful in analysis of protein modification and less efficient for high-throughput studies (Han *et al*, 2008).

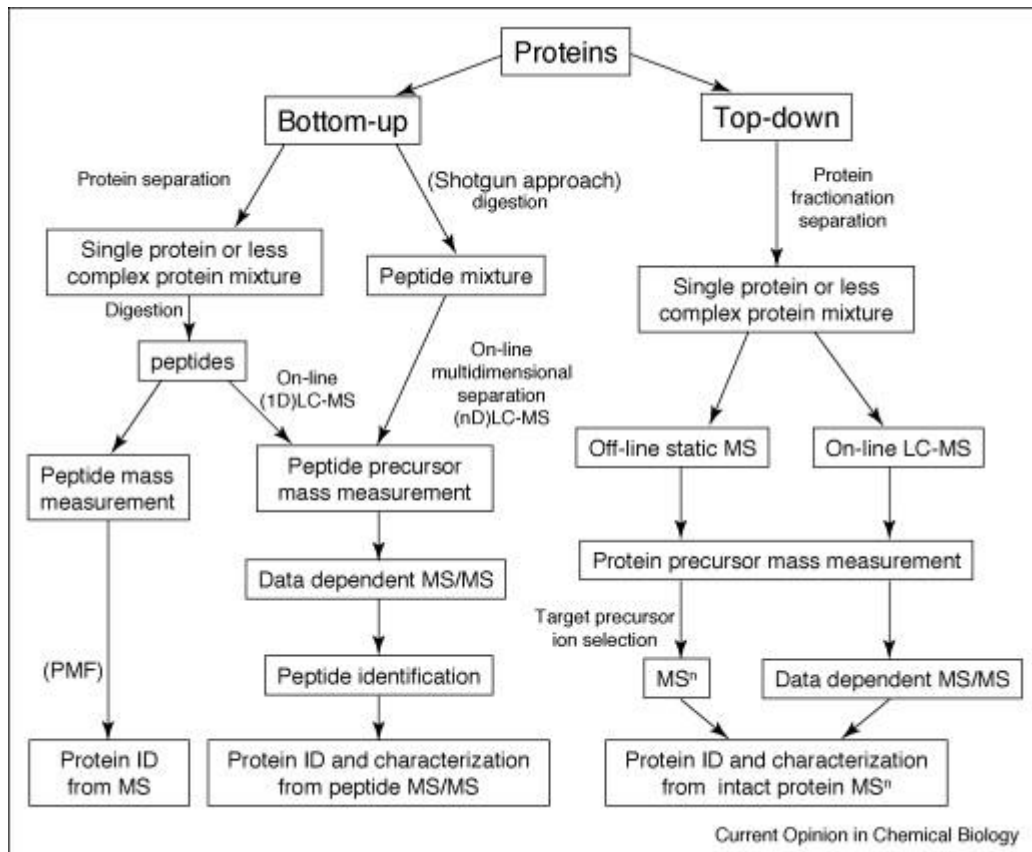


Figure 1.11 Strategies for MS-based proteomic analysis (Han *et al*, 2008)

Liquid chromatography coupled with mass spectrometry (LC/MS) is a widely used, robust and sensitive platform for the proteomic studies due to its sensitivity, selectivity, accuracy, speed and throughput (Chen and Pramanik, 2009).

1.6.1 LC-MS/MS

Basically, LC-MS/MS system is composed of a highly sensitive and selective liquid chromatography system for separation of peptides, an ion source to convert molecules to ions, a mass analyzer which sorts the ions by the electromagnetic field according to their masses and a detector.

The two commonly used ionization techniques are Matrix assisted Laser desorption/ionization (MALDI) and Electrospray ionization (ESI). MALDI is conventionally used for gel based separation techniques in which the protein band is excised, digested and

injected into MALDI system off-line. On the contrary, ESI system is preferred with the liquid chromatography based separation systems enabling continuous separation of the peptides and simultaneous ionization followed by mass detection. By means of ionization method, MALDI uses laser energy to ionize the acidified analyte and for the desorption of the ions with the matrix. In ESI system, high voltage is applied for electrospraying of the solution in which forms the ionized analyte-solvent droplets (Yates *et al*, 2009).

1.7 Proteomics studies of PNS bacteria

Recent studies on *Rhodobacter* proteome focuses mainly on the photosynthetic membranes. Woronowicz *et al*, analyzed the intracytoplasmic membrane of *Rhodobacter sphaeroides* during adaptation to low light intensity using LC-MS/MS system (2010). They used atomic force microscopy together with the proteomic analysis of the photosynthetic apparatus to understand the assembly of the complexes. In another recent study by Italiano *et al*, photosynthetic intracytoplasmic membranes of a carotenoidness *Rhodobacter sphaeroides* strain under high cobalt concentration were examined by non-denaturing blue native electrophoresis coupled to LC-MS/MS system (2011).

The efforts to study the proteome of *Rhodobacter sphaeroides* started earlier than *Rhodobacter capsulatus*. In 1999, the first genomic database of *Rhodobacter sphaeroides* is published including the sequence of small chromosome (CII) of the bacteria (Choudhary *et al*, 1999), however the physical map was constructed in 1989 (Suwanto *et al*). In 2001 the first analysis of nearly completed genome was published by Meckenzie *et al*. and the complete genome was published along with 2 other strains in 2007(Choudhary *et al*). For *Rhodobacter capsulatus* sequencing the whole genome efforts started earlier. In 1992 the physical map of the genome was published (Fonstein *et al*), whereas the genome project was completed after 9 years in 2001 (Haselkorn *et al*).

From 2004 to date, along with the microarray studies, there are several proteome analysis were done in different laboratories. Metabolic versatility of *Rhodobacter sphaeroides*, the comparison of different growth modes (Pappas *et al*,2004, Callister *et al*,2006), dynamics during the transition from photosynthetic to respiratory growth modes (Arai *et al*,2007) are the hot topics of “omics” studies. LC-MS/MS systems are the method of choice and yields high protein coverage as approximately 39% based on the current protein annotations from the available databases (Callister *et al*, 2006).

Finally in 2010, the first proteomic study published by Onder *et al.* This first glimpse revealed more than 450 proteins including the localization information by LC-MS/MS analyses coupled with 2-D gel electrophoresis method. Moreover, studies over the proteome provided evidence of hypothetical proteins annotated in genome studies.

1.8 Aim of this study

Proteomics studies provide comprehensive information about direct players of the cells. The data obtained enlarges the aspects of the cellular state, thus enables us to compare and highlight the differences of particular conditions. Hereby, in this study we aimed to compare the protein profiles of *Rhodobacter capsulatus* grown in different growth conditions. The ability of this organism to survive and adapt different conditions and growth modes stands out as a model to study photosynthesis, nitrogen fixation etc. Obtaining protein profiles in aerobic respiratory, photofermentative and anaerobic respiratory growth modes will give information about the cellular state and the key players in particular metabolism.

In photofermentative growth mode *R.capsulatus* produces hydrogen and understanding the metabolism of hydrogen production is also on the scope of this project. By comparing profiles of different growth conditions with photofermentative conditions, we aimed to highlight important identified or non-identified proteins involved in the hydrogen production.

As the consequence of these purposes LC-MS/MS experiments will give evidence for hypothetically annotated proteins. The optimization of the protocols as well as protein isolation and LC-MS/MS experiments will create a guide for the future studies.s

CHAPTER 2

MATERIALS AND METHODS

2.1 The Microorganism

Rhodobacter capsulatus SB1003 strain is used throughout the study. It is kindly gifted by Patrick Hallenbeck.

2.2 Culture media

Modified versions of the minimal Biebl and Pfening medium (1981) were used during the growth of *Rhodobacter capsulatus* and for the experimental conditions, which differed in the supplemented acetate and glutamate concentrations. During the experimental conditions, nitrogen source is limited to force the bacterial metabolism to hydrogen production. (Kars *et al.*, 2010). Minimal Biebl and Pfenning medium contain salts, trace elements, iron citrate and vitamins. The components are listed in appendix A.

2.2.1 Growth medium

Acetate (20mM) and Glutamate (10mm) as carbon and nitrogen sources respectively were supplemented to minimal Biebl and Pfenining media (1981). The composition of BP medium was given in Appendix A. Ingredients were dissolved in water and pH was adjusted to 6.3-6.4 using NaOH. Autoclaving was carried out at 121°C for 20 minutes. After cooling down the medium to room temperature, separately autoclaved iron citrate and trace elements were added together with vitamin solution sterilized using 0.2µm filters.

2.2.2 Hydrogen producing medium

For the experimental conditions hydrogen production medium containing 40mM acetate and 2mM glutamate was used. The preparation of the media is similar to growth medium. For

anoxygenic respiration with DMSO as the electron acceptor, DMSO is added to final concentration of 40mM.

2.2.3 Solid medium

Solid medium is used for the activation of the -80°C stocks of the bacteria. Basically 1.5% agar is added to MPYE medium before autoclaving. The preparation of MPYE medium was explained in Appendix A. Then cooled medium is supplemented with iron citrate, trace elements and vitamins, then poured into petri dishes to solidify.

2.2.4 Stock medium

For the preparation of long-term storage stocks at -80°C, stock medium is being used. It consists of 30% glycerol in growth medium. While preparing the stock, it has been diluted to 15% with the 50% inoculation of the bacteria.

2.3 Experimental set-up

2.3.1 Pre-cultivation of the bacteria

2.3.1.1 Single colony isolation

-80°C stocks of *Rhodobacter capsulatus* SB1003 was inoculated on the agar plates following the streak plate technique to obtain single colonies. Briefly the flame sterilized loop was dipped into the bacterial stock solution. First inoculation was done in one of the quadrants of the plate, then the loop is re-sterilized and the second inoculation was done dragging a streak from the first as shown in Fig. 2.1. Streaking was completed after the fourth quadrant and the plate was rapped with the aluminium foil to keep it in dark and incubated at 30°C.



Figure 2.1 Illustration of streak plate technique (public health image library PHIL#7925)

2.3.1.2 Growth of bacteria

Single colony selected from the agar plate was inoculated in growth medium containing 20mM acetate and 10mM glutamate at 30°C under dark conditions with constant agitation of 120 rpm. The bottles contain big head space to ensure the presence of oxygen for aerobic respiration.

2.3.2 Experimental conditions

Bacteria grown overnight in the growth medium at 30°C in dark with an agitation of 120 rpm was inoculated to hydrogen production medium in 10% ratio. For different metabolism different conditions were supplied, however for all conditions the total volume was 55mL and the temperature was kept at 30°C.

For aerobic growth mode 250 mL bottles sealed with rubber caps were used. Bottles were rapped with aluminum foil to be kept in the dark and placed in the incubator with 120rpm agitation.

For photofermentative growth condition 55mL small bottles sealed with rubber caps were used. After inoculation, argon was flashed for 30 seconds to remove the air in the headspace of the bottle thus to generate anoxygenic atmosphere. Two needles were inserted into the rubber cap one of which was connected to the argon tube. When argon was flushed from one

needle, air exited from the other one replacing argon with the air in the headspace. The illustration for the argon flush is shown in Fig. 2.2. The bottles were kept at 30°C with 2000 lux illumination using 75W tungsten lamps. The light intensity measurements were done with the luxmeter (Lutron LX-105 Light Meter).



Figure 2.2 Illustration of Argon Flush

For anaerobic growth with the presence of DMSO as the electron acceptor, 55mL small bottles sealed with rubber caps were used. DMSO was added to a final concentration of 40mM to the hydrogen producing medium. After the inoculation the bottles were flushed with argon to remove oxygen from the headspace atmosphere then rapped with aluminium foil to ensure the darkness and kept at 30°C with the constant agitation of 120 rpm.

2.3.3 Sampling procedures

For aerobic respiratory and photofermentative growth conditions, samples were taken 6 hours after the inoculation. For the anaerobic respiratory growth with the presence of DMSO condition, the sampling time was 48 hours due to slower bacterial growth. Sampling time was determined according to optical density (OD) of the culture at 660nm. Bacterial growth curves of each condition was determined before the experiments to give an opinion about the sampling time of the bacteria when OD reached approximately 0.5. In Fig. 2.3 illustration of the experimental procedures were shown.

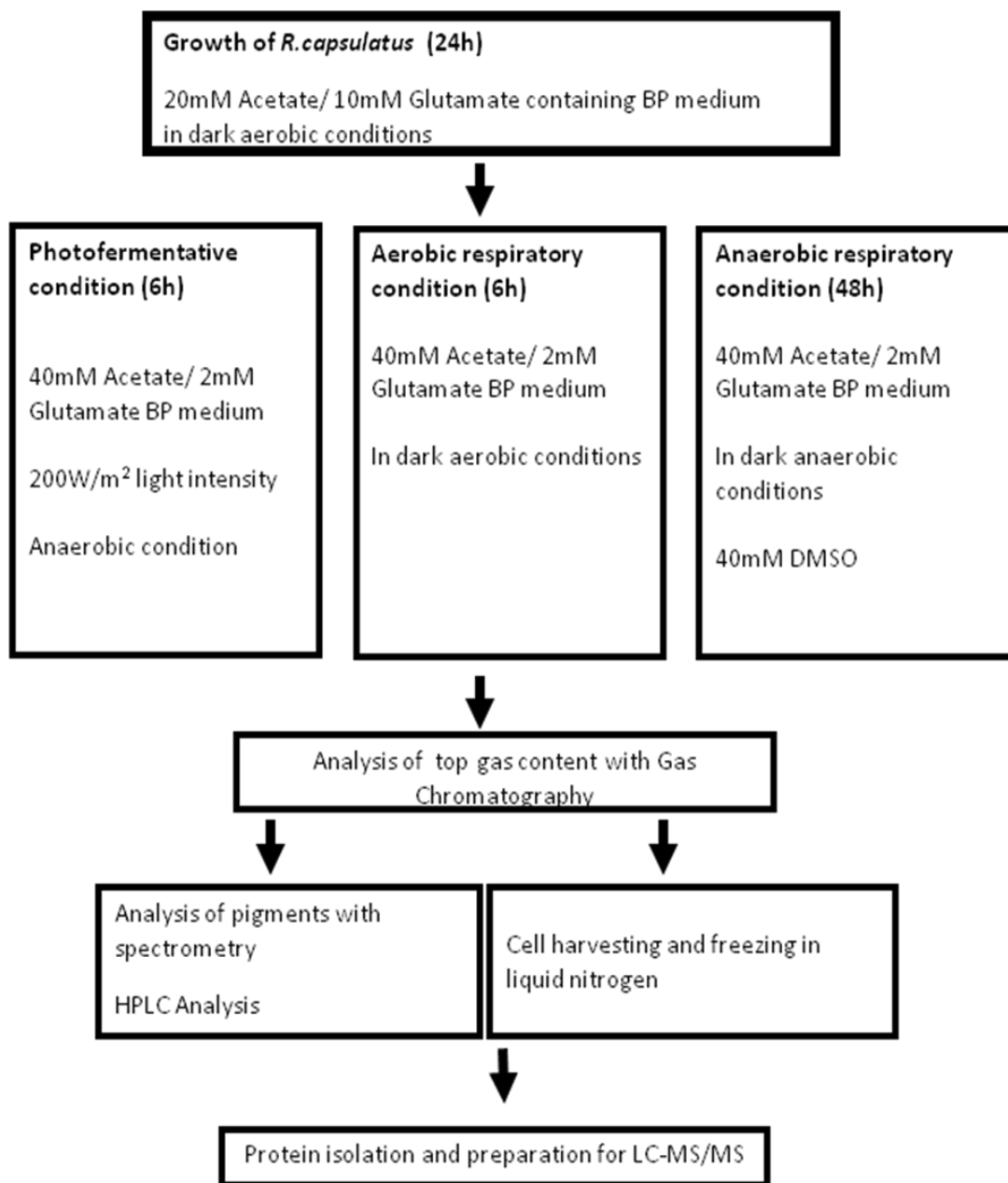


Figure 2.3 Experimental procedures for growth conditions and sampling

Before sampling, gas chromatography measurements were carried out to ensure the presence/ absence of oxygen/ hydrogen. 2 mL culture samples taken from the culture bottles were centrifuged at 13000 rcf for 10 min at 4°C. The supernatant was discarded and the pellet was washed 3 times using 50mM NH_4HCO_3 (Ammonium bicarbonate) with 5 minutes centrifugation steps at 5000 rcf. Finally, the supernatant was carefully aspirated and the tubes

were frozen in liquid nitrogen to be stored at -80°C. Additional samples were taken for HPLC, OD measurements and formation of absorption spectrum.

2.4 Analysis

2.4.1 Cell density measurement

Cell density measurements were carried out by reading the absorbance of the culture medium using a spectrometer (Shimadzu) at 660nm. Medium itself was used as blank solution for the measurement. Briefly 1 mL of culture sample was taken and used for the measurement. If the measured OD is not in the range of 0-0.5 dilutions were done using the fresh medium.

2.4.2 Gas composition analysis

For the gas analysis, 200uL gas samples were taken from the head space of the culture bottles using the gas tight Hamilton syringes (Hamilton, 500µL gas tight No. 1750) and then assayed using the Agilent (6890N) gas chromatography instrument. Instrument was equipped with Supelco Carboxen 1010 column and the detector used for gas analysis was thermal conductivity detector. Argon was used as the carrier gas with the flow rate of 20mL/ min. The temperature of the injector and detector was 160°C and 170°C. The program was started at 50°C for 6 min to obtain the hydrogen peak, and then a 40°C/min ramp was applied to heat the oven to 150°C. Ratio of the hydrogen (H₂), oxygen (O₂), nitrogen (N₂) and carbon dioxide (CO₂) were obtained using the instrument software.

2.4.3 Organic Acid analysis

Organic acid analysis were carried out using Shimadzu high-performance liquid chromatography (HPLC) LC 20A- Prominence Series. System was equipped with Alltech IOA-1000 (300 mm x7.8 mm) HPLC column. 1 mL culture samples were centrifuged at 14000 rpm (SIGMA-minifuge) for 10 minutes at room temperature. The supernatant was filtered using 0.45 µm nylon filters (Millipore) to remove any impurities that may interfere with the analysis. 0.085M H₂SO₄ was used as the mobile phase with 0.4mL/min flow rate. 20µL sample was injected with the auto sampler and organic acids were detected by an UV detector at 210 nm. The temperature of the oven was kept at 66°C during the 45 minutes analysis. The peaks were manually selected according to retention times and were assigned

for each organic acid. Concentration of the organic acids was calculated using the calibration curve plotted using the acetic acid, lactic acid, formic acid, propionic acid and butyric acid standards. Calibration curves for organic acids were shown in Appendix B.

2.4.4 Photosynthetic pigment analysis

For determination of the photosynthetic pigments, the acetone/ methanol extraction protocol was carried out. Briefly 2 mL culture samples were centrifuged at 14000 rpm for 10 min. 1 mL acetone: methanol mixture (7:2 v/v) was added to the pellet and solution was vortexed for 1 minute. Then the homogenate was centrifuged at 13400 rpm for 10 min and the absorbance spectrum was plotted by reading the absorbance of the supernatant at 350-950nm with Shimadzu spectrometer and the instrument software.

Bacteriochlorophyll a measurements were carried out by reading absorbance at 770nm and calculations were done according to the equation given by Clayton (1963). The extinction coefficient of bchl_a is 75mM⁻¹cm⁻¹ and the molecular weight is 911.5 g/mole.

2.4.5 Microscopy analysis

Phase-contrast images were taken using a hemacytometer, to visualize and count the bacteria. Zeiss LSM 510 was used as the instrument with 40x objective and no stain was applied.

For the visualization of the bacteria in the confocal microscope, bacteria were stained. Nonyl acridine orange which is a membrane stain is used in 1:100 dilution from 1 mM stock. Propidium iodide which is a DNA stain is used in 1:200 dilution from 25mg/mL stock. Propidium iodide is a membrane impermeable dye. Only non-living thus membrane integration disturbed cells were being stained. Non-living cells were stained with PI and living cells were stained with NAO. This method enabled us to visualize the non-living vs living cells. For the microscopy, OLYMPUS IX71 inverted research fluorescence microscope was used in 100x oil immersion objective.

NAO has excitation at 495nm and emission at 519 nm. For PI excitation is at 536nm and emission is at 617 nm.

2.4.6 Sodium dodecyl sulfate Polyacrylamide Gel Electrophoresis (SDS-PAGE)

SDS PAGE protocol was performed to visualize the quality of the isolated protein samples. The preparation of the solutions used in the protocol was explained in appendix C. 12% acrylamide gel was used with 6% stacking gel. Protein loading was calculated according to the volume to be able to have maximum protein amount in the gel, thus 25 μ L of proteins were loaded with 5 μ L of 6X loading dye. Fermentas Multicolor broad range protein ladder (SM1841) was used as the molecular weight marker.

For the coomassie staining, stacking gel was cropped and gel was washed with distilled water 2 times. Then 25mL of coomassie stain was added and incubated at room temperature overnight. Then, the stain was removed, gel was washed with distilled water thoroughly and kept in destaining solution for 30 min for 4 times in order to remove the unbound stain from the gel.

2.5 Proteome analysis

2.5.1 Protein isolation

Protein isolation was carried out with UPX Universal Protein Extraction kit and FASP Protein Digestion kit which follows Filter Aided Sample preparation Method (FASP) published by Wisniewski *et al.* (2009).

Bacterial samples of 2 mL correspond to approximately 30 mg wet bacterial weight. Cell pellet was dissolved completely with 2mL of UPX buffer which contains SDS and reducing agents. For homogenization sonication method was applied using Soniprep150-MSE instrument. Cells were kept on ice during 10 cycles of 10 seconds on 15 seconds off sonication to prevent heating. After homogenization solution becomes totally clear indicating a successful break down of cells. For the reduction of proteins as well as protease inactivation, solutions were boiled at 100°C waterbath for 5 min and kept on ice for 1 hour. It is important to clean up all the remaining cellular debris effectively to prevent UPLC system from blocking out. For this purpose centrifugation at high speeds as 45000 rpm was applied using Optima Max™ ultracentrifuge (Beckman Coulter) at 4°C for 2 hours. 5kDa cut-off spin columns (Vivaspin 500) was used to concentrate the supernatant simply by centrifuging at 14000 xg for 5-10 min until the 200 μ L liquid remained on the filter out of

500 μ L. The filtrate was removed and the process is repeated until the supernatant volume was reduced to 1/10 of it

2.5.2 Sample Preparation for LC-MS/MS

Isolated, reduced and concentrated protein solution was used for FASP kit (Protein discovery). FASP kit was designed to replace completely solubilized proteome in SDS with urea on a filter and elute pure peptides after trypsin digestion. The product usage guidelines were applied with no modification. Briefly 30 μ L of protein solution was washed with urea sample buffer, alkylated using iodoacetamide at dark and lastly washed with 50mM ammonium bicarbonate to be left for trypsinization. Trypsin (Proteomics Grade, SIGMA) was added according to 1:100 Trypsin:Protein ratio and incubated at 37°C for 18 hours. 50mM Ammonium bicarbonate and 0.5M Sodium chloride was used to elute the peptides. Concentrations were measured with nanodrop™ at 280nm using elution solution as blank.

For LC-MS/MS, taken the maximum capacity of the LC column into consideration, 500ng of peptide in 5 μ L injection volume was preferred. The peptide mixture was diluted to 100ng/ μ L and 10 fmol/ μ L of calibrant which was chosen as Rabbit- Glycogen Phosphorylase- b (P00489). Thus volumetric mistakes caused by pipetting were normalized during mass measurements.

2.5.3 LC-MS/MS method

The last step of experimental work flow was tandem mass spectrometry using shotgun proteomics approach. Waters SYNAPT- HDMS system being used was a quadrupole time of flight (qTOF) mass spectrometer having the advantage of ion mobility technology and electrospray ionization as ion source. Fig.2.4 shows the picture of the equipment.



Figure 2.4 Picture of the Waters Synapt HDMS

UPLC used upfront the MS system was based of reverse phase chromatography. Peptides were being separated according to hydrophobic interactions with 1.7 μ m BEH C18 nano LC column (75 μ m x250 μ m). Each injection was consisted of 500ng of peptide with 50fmol internal calibrant and lasted for 240 min with 300nL/min flow rate. Internal calibrant was selected as rabbit glycogen phosphorylase b (P00489). Peptides separated according to hydrophobicity properties were sprayed with ESI unit simultaneously to the qTOF analyzer. In fig. 2.5 Schematic illustration can be seen. In the quadrupole region peptides according to m/z ratio are separated. The ions with a particular m/z ratio were transferred to collision cell whereas the rest of the peptide ions were trapped. 5eV and then 25-40eV collision voltages were applied to create smaller ions. The ions were further separated with the advantage of tri-wave technology which guides the ions and separates according to ion mobility. Then the ions were transferred to time of flight analyzer and data was collected both for peptide as a whole and the amino acid sequence for 1.5 seconds. It is important to note that system calibrates itself in every 45 seconds with [Glu1]-fibrinopeptide B named as lock mass and can be seen in the fig. 2.5. This calibration is important to test the system itself and to create a normalization base during the long operating durations.

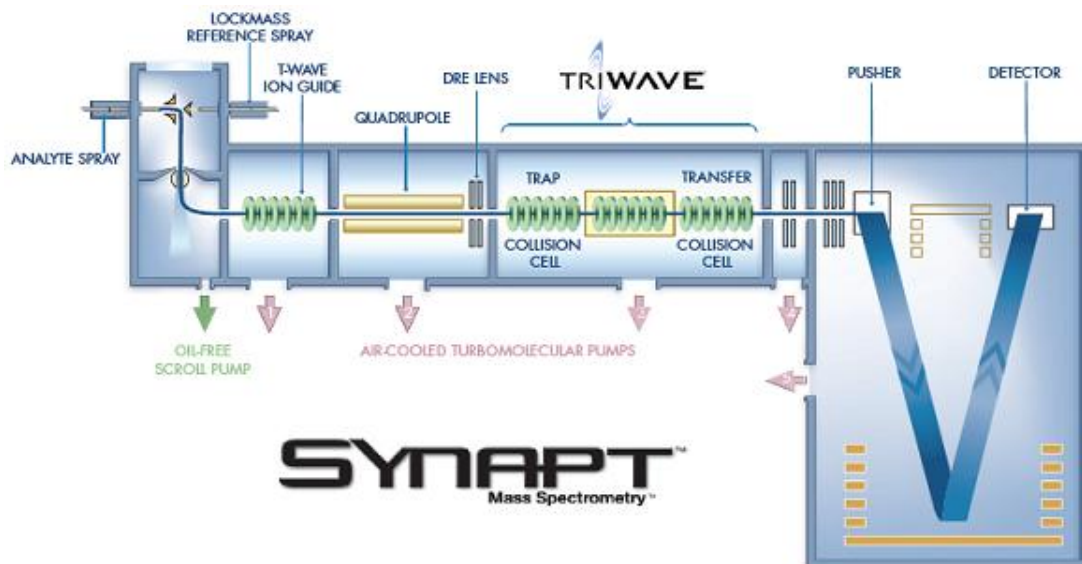


Figure 2.5 Schematic illustration of the LC-MS/MS system

Moreover the system was operated in MS^E mode which contributes to increased number of the peptides sampled during LC/MS-MS experiment and increased reproducibility. In MS^E mode, multiple precursor ions were analyzed simultaneously by the time align function of the system. As a result of MS^E method more peptides were being identified. LC-MS/MS experiments were performed at TÜBİTAK-Marmara Research Center- Genetic Engineering and Biotechnology Institute.

2.5.4 LC-MS/MS Data Analysis

LC-MS/MS experiment yielded very large amount of raw data due to vast number of mass spectra obtained from the total cell proteins. As a consequence, it was important to analyze the data to acquire qualitative protein identification and quantification. ProteinLynx Global SERVER™ (PLGS) which is the analytical platform for Waters proteomics systems was used for the data processing and data interpretation. PLGS™ was based on XML and appropriate to work on MS^E data. Identity^E module was used to identify peptides with high protein coverage and accurately. Expression^E module was used for data processing, expression analysis and visualization of data. Another software Progenesis was also used for the analysis of the data. This software uses ion intensities and ion abundance recorded in MS data, which obtained from PLGS in this case, to provide quantification. As a result, PLGS Expression module and Progenesis can give different results due to different algorithms and quantification strategies they have. Some proteins were excluded in a particular list, but

present in the other software's list. However, protein identification was done using the PLGS software of Waters and the software supplied the data for each analysis programs. For the quantitation purposes, both programs were used in order to cover as much information as possible and the software used was stated in the given tables. Another program used for visualization of the data was Scaffold. It enables the visualization of quantification results obtained from PLGS in a free-viewer version. Additionally, gene ontology (GO) file of *Rhodobacter capsulatus* obtained from European Bioinformatics Institute (EBI) database (ftp://ftp.ebi.ac.uk/pub/databases/GO/goa/proteomes/36379.R_capsulatus.goa) provided useful gene ontology, function, cellular localization information for each identified protein.

For each biological replicate, 3 injections were done. For a protein identification presence of the protein in minimum 2 out of 3 injections was selected to maintain a high confidence of the results.

CHAPTER 3

RESULTS AND DISCUSSIONS

In this study, metabolism of *R.capsulatus* was analyzed in aerobic respiration, anaerobic respiration in the presence of DMSO as the final electron acceptor and photofermentation in the scope of physiology and proteomics. In the physiological point of view growth profiles, hydrogen productions and pigmentation were evaluated for each growth condition. In proteomics studies, the protein isolation method was optimized and protein expression profiles were determined with LC-MS/MS method.

3.1 Physiological Analysis of *R.capsulatus* under different growth conditions

Three selected growth modes anaerobic light, photofermentative growth, aerobic dark, respiratory growth and anaerobic dark with the presence of DMSO were investigated. These analyses provided a first sight about the growth, pigment content of the cells and the gas produced. Additionally, the conditions were being tested in terms of oxygen and light availability.

3.1.1 Growth of *R.capsulatus* under different conditions

As can be expected, *R.capsulatus* did not show the same pattern when grown in aerobic dark, anaerobic light and anaerobic dark conditions. Fig. 3.1 shows the OD vs time graph for each growth condition and highlights anaerobic light condition. With a high growth rate and maximum cell number, anaerobic light condition in which the bacteria survive with the photofermentative abilities was the most suitable and can be referred as the preferred growth mode (Koku *et al*, 2002).

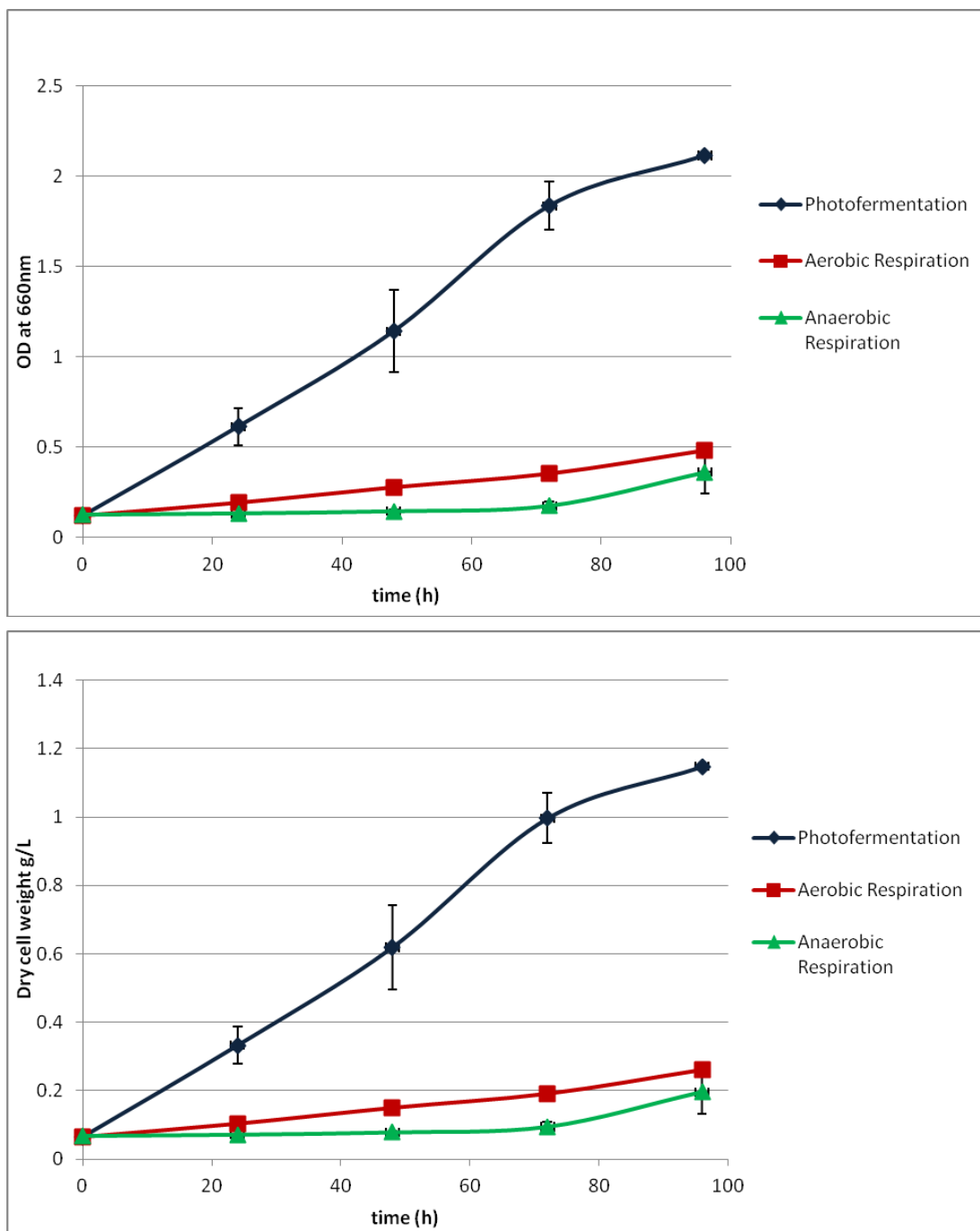


Figure 3.1 Growth profiles of *R.capsulatus* for different growth conditions

Moreover, the consumption of the main nutrient and carbon source acetate was in correlation with the growth as shown in Fig. 3.2. As shown in the graph 20mM acetate was the starting acetate concentration for all conditions and in anaerobic light condition

with photofermentative mode of growth, total consumption of the carbon source was obtained after 72 hours of incubation.

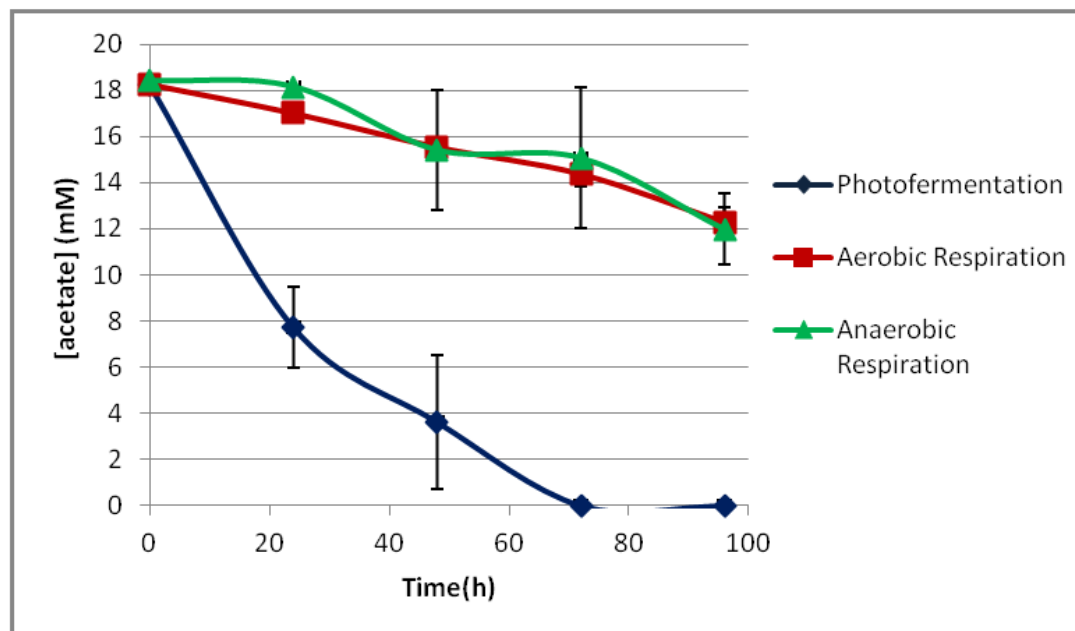


Figure 3.2 Acetate consumption graph of *R. capsulatus* for different growth conditions

For the proteomics experiments, cells were harvested when optical density (OD) reached 0.4-0.5 which corresponds to 0.5×10^9 - 0.7×10^9 cells/mL of culture to prevent micro-environmental differences such as light penetration or oxygen limitation when the cell culture is high. Cell count experiments were carried using a phase-contrast mode and the images can be found in the appendix D.

3.1.2 Optimization of DMSO concentration for the anaerobic respiratory growth condition

DMSO was used as the alternative electron acceptor for anaerobic dark growth mode. However for the optimal DMSO concentration to create a non-toxic but DMSO sufficient environment, growth and substrate consumption analysis was carried out. In the previous studies, DMSO was used in 30mM-70mM range with different nutrients such as lysogeny

Broth (LB), succinate containing BP medium (Mouncey *et al*, 1997, Pappas *et al*, 2004, Zeng *et al*, 2007, Öztürk *et al*, 2012). As shown fig. 3.3 and 3.4 growth of the bacteria and acetate consumption was examined for 0mM as control and 30mM, 40mM, 50mM DMSO concentrations.

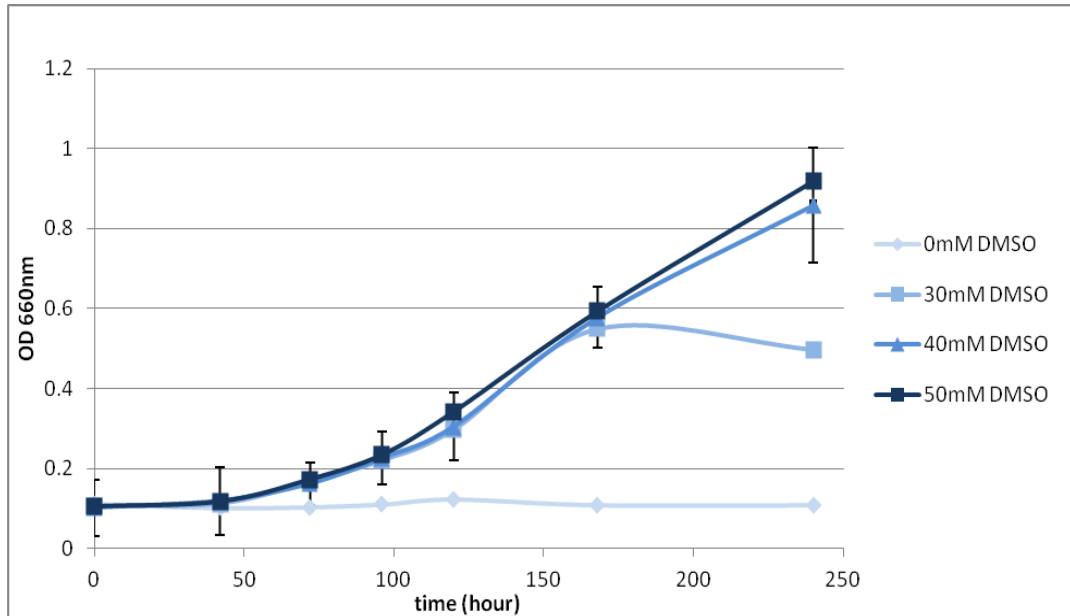


Figure 3.3 The growth profile of *Rhodobacter capsulatus* for different DMSO concentrations (0mM, 30mM, 40mM and 50mM)

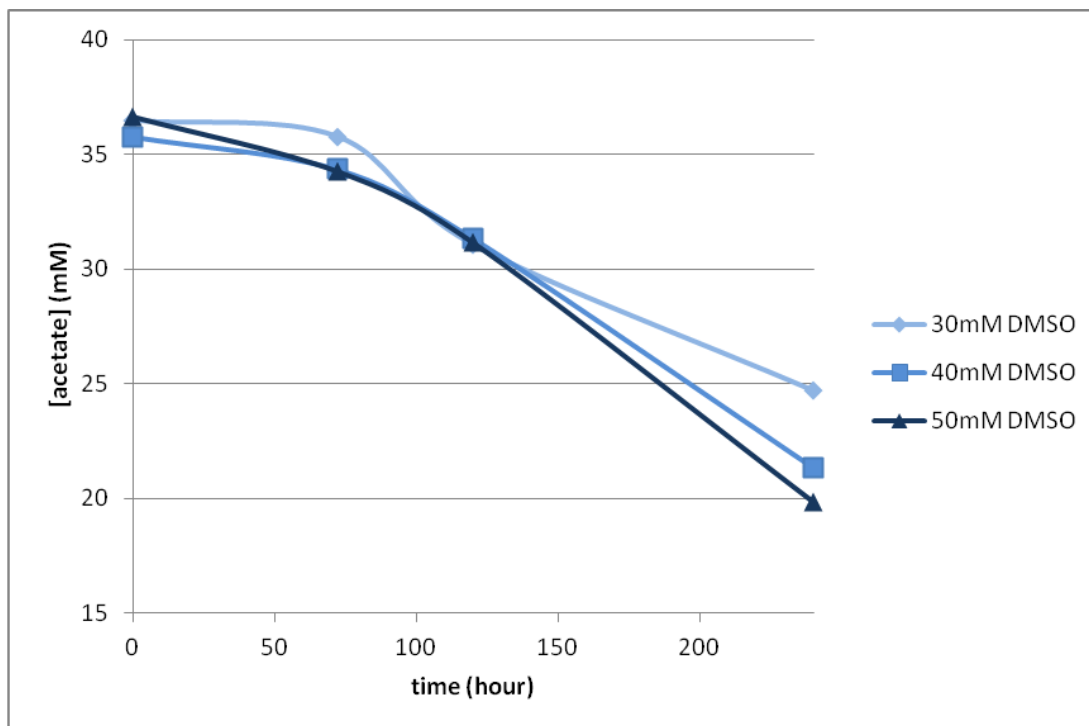


Figure 3.4 Acetate consumption graphs of *Rhodobacter capsulatus* for different DMSO concentrations (0mM, 30mM, 40mM and 50mM)

In control group (0 mM DMSO), no growth was observed as a consequence of no available energy source. This indicated that growth depended on DMSO in anaerobic conditions without light. In 30 mM DMSO containing group showed slower growth and acetate consumption rates compared to 40mM and 50mM DMSO containing growth. Thus 40mM DMSO concentration was selected for further studies, since growth was comparable with 50mM DMSO containing group and the toxic side effects of DMSO would be less in lower concentrations.

3.1.3 Analysis of Pigmentation in *Rhodobacter capsulatus* grown under different conditions

Rhodobacter capsulatus contains pigments regardless of the growth mode, however content and quantity of the pigments change (Madigan *et al*, 1982, Law *et al*, 2004). In the interest of observing pigmentation differences physiologically for different growth modes and light availability, pigments were isolated and further analyzed. Absorption

spectra for each growth condition were drawn and pigments were characterized according to the light emission properties. In Fig. 3.5 absorption spectrum of intact cells and in Fig. 3.4 acetone/methanol extracted cells grown under aerobic respiratory, photofermentative and anaerobic respiratory (in the presence of DMSO) growth modes are shown.

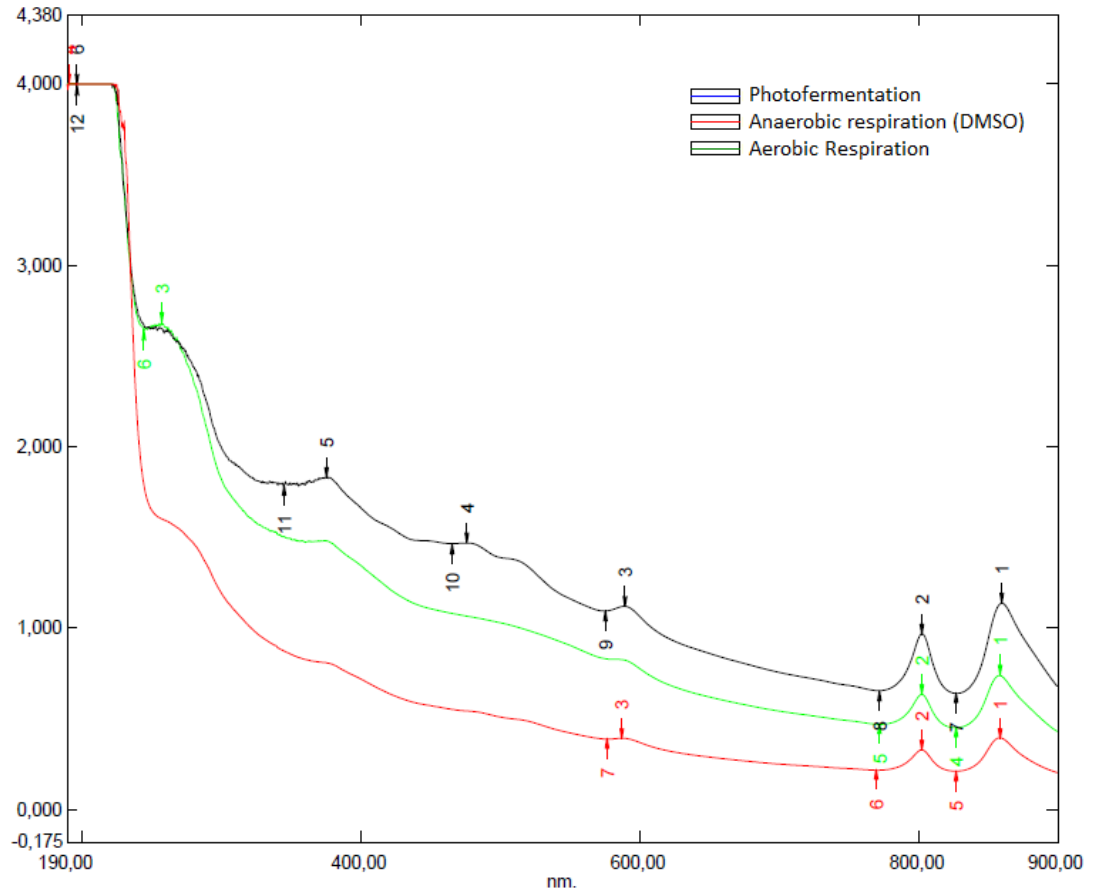


Figure 3.5 Absorption spectra of intact cells of *Rhodobacter capsulatus* grown on different growth conditions

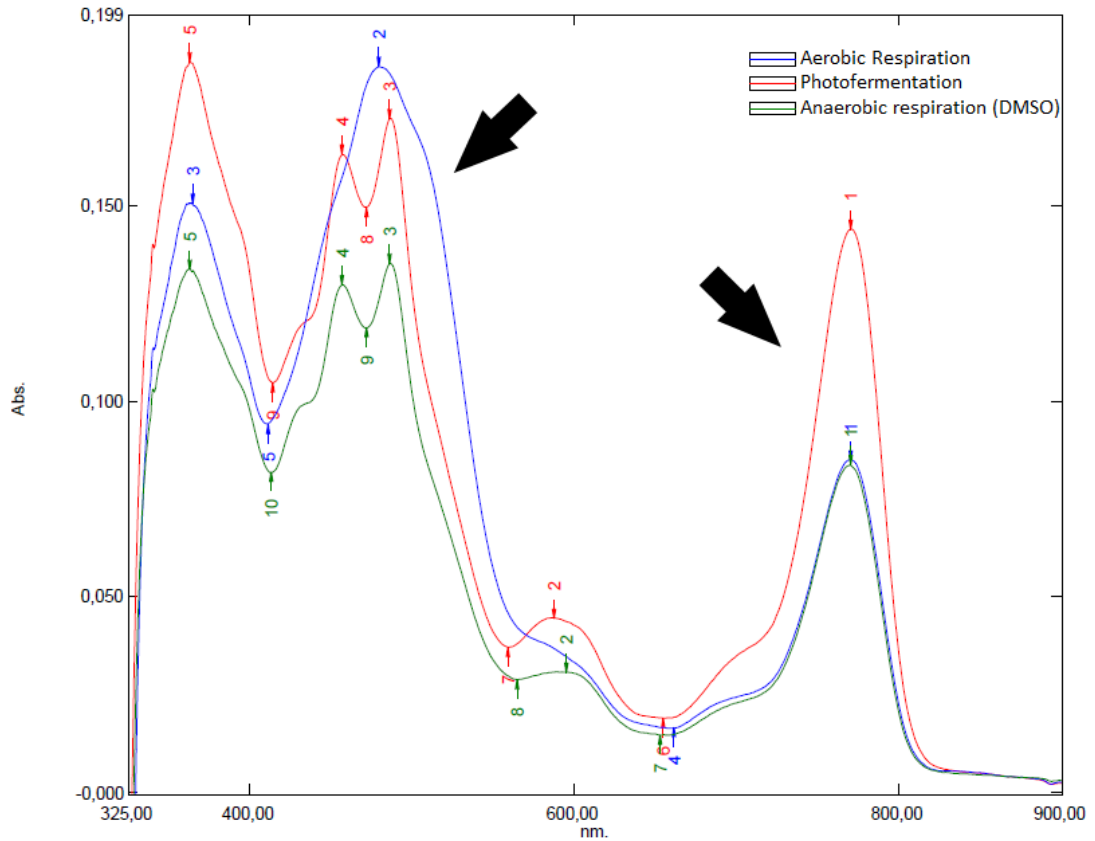


Figure 3.6 Absorption spectra of acetone/methanol extracted *Rhodobacter capsulatus* cells grown on different growth conditions

Carotenoids are responsible for the characteristic ‘three-fingered’ absorption peaks between 450nm-550nm (Law *et al*, 2004). As seen from the graph aerobic dark condition enabling respiratory growth mode lacks the carotenoid pigments. Moreover the color of the intact cells differs from the anaerobic light and anaerobic dark growth modes. In respiratory mode of growth in the dark, we observed pinkish red color whereas color shifts to orange-like red in the photofermentative mode of growth under anaerobic conditions in the presence of light and in the anaerobic respiratory growth mode in dark in the presence of DMSO.

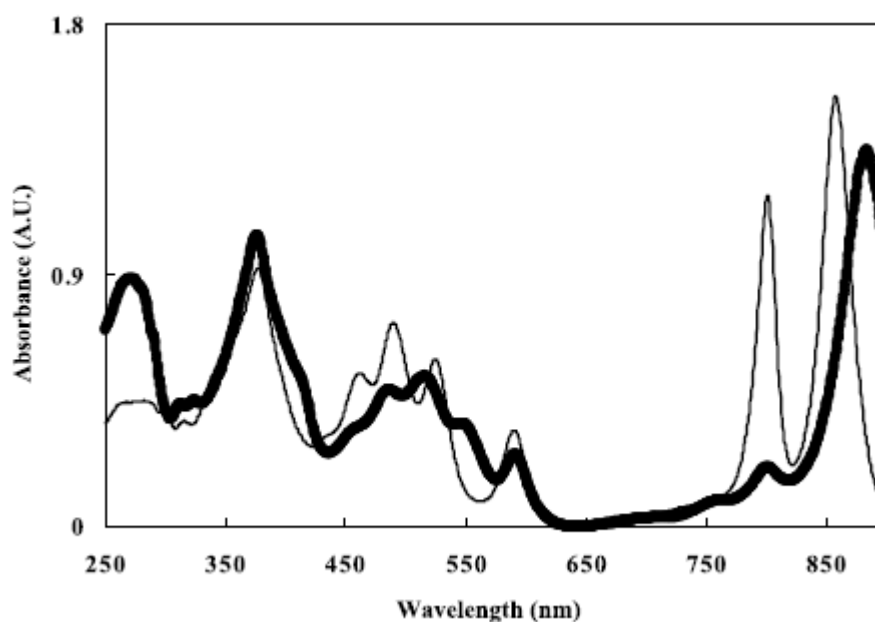


Figure 3.7 Absorption spectra of *Rhodospseudomonas acidophila* (Law et al, 2004)

The two intense near infrared absorption bands correspond to light harvesting (LH) complexes. LH1 has single large near infrared absorption band at 875 nm. On the other hand LH2 has two bands at 800 nm and 850 nm. Another minor peak at 800nm is due to Bchl molecules bound to reaction center (Law et al., 2004). In Fig. 3.6 a sample spectra is given in which the thicker line shows the spectrum of RC-LH1 complex and fine line shows the spectra of LH2 complex of *Rhodospseudomonas acidophila*.

In the absorption spectrum, we observe two peaks in the near infrared region in each growth condition. These peaks correspond to light harvesting complexes. Since the complexes are not separated after the isolation, the dominant peaks of light harvesting complexes are visible.

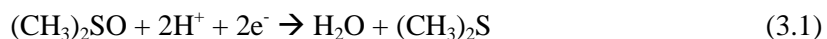
3.1.4 Analysis of top gas of *Rhodobacter capsulatus* grown under different conditions

As shown in Fig. 2.2, after argon flush space on the top of the bacteria bottles is filled with argon. After growth of the bacteria in the determined growth conditions, gas samples were taken from the top space and analyzed in order to examine the oxygen availability and the presence of CO₂ for respiratory growth mode under oxygenic dark conditions. For the case of anaerobic dark condition with the presence of DMSO, oxygen

availability was measured to assure the oxygen lacking conditions. In the photofermentative growth mode under anaerobic conditions and in the presence of light, bacteria produces hydrogen. However bacterial density is not optimal for the robust hydrogen production. Analyzing the top-gas resulted in observation of the hydrogen production.

Optimization experiments were carried out to successfully separate the nitrogen (N₂), hydrogen (H₂), oxygen (O₂) and carbondioxide (CO₂) peaks obtained in the gas chromatogram. Temperatures of the inlet and the column, as well as flow rate and temperature ramp were carefully adjusted to obtain optimum separation in shortest time.

Unknown peak for anaerobic respiratory growth is merging of CO₂ and an unknown gas. Dimethylsulfide (DMS) is a candidate for this peak as it evolves in the reaction of DMSO reduction. It has a disagreeable odor which was experienced during the experiments, however it must be verified by GC calibrated with DMS. The reduction reaction is as follows;



In Fig. 3.8 major peaks of the gas chromatograms for each condition were shown.

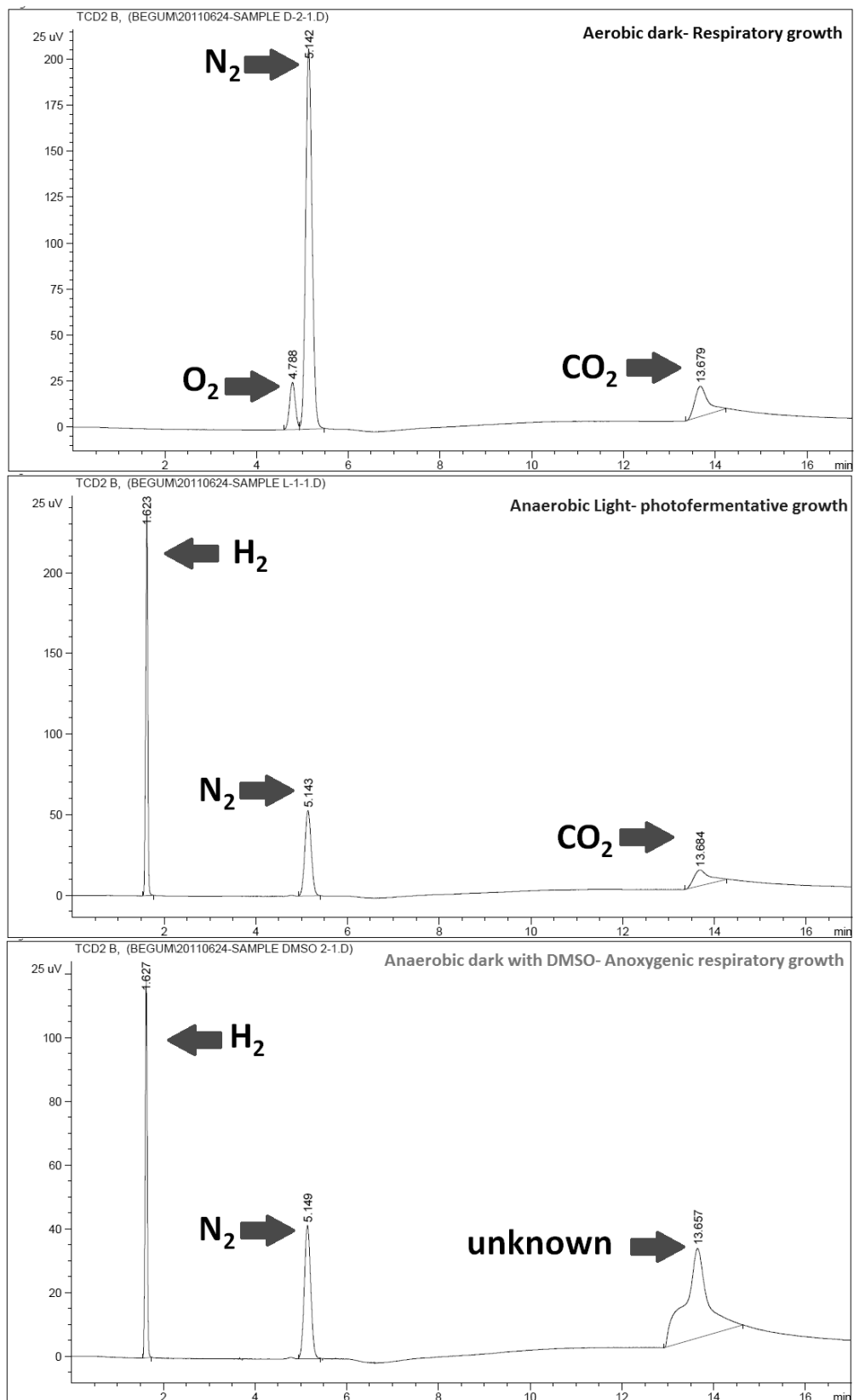


Figure 3.8 Gas chromatograms for different growth conditions

3.1.5 Physiological Analysis of the samples used for LC-MS/MS experiments

All the physiological analyses were done for the samples used for LC-MS/MS experiments to verify the requirements of each growth condition, such as oxygen availability, hydrogen production and acetate consumption.

Anaerobic respiratory and photofermentative growth modes were shown to have higher consumption of acetate, 40.70 ± 0.68 % and 39.39 ± 2.99 %, respectively. Moreover in aerobic respiratory growth mode was 10.97 ± 2.54 %. In appendix B table B.1 details of the measured concentrations were shown.

Gas chromatography analyses carried out without calibration the instruments for the quantitation of the compounds. Percentage of the particular gas over the total measured gas was used as the quantitation. For the case of aerobic respiration, 20.3 ± 2.22 % oxygen, 66.05 ± 7.62 % nitrogen and 13.64 ± 9.68 % CO₂ were measured after 6 hours of incubation and growth. It is known that 20% of the air is oxygen whereas CO₂ constitutes only 0.033%. Therefore, after 6 hours of respiratory growth oxygen levels are comparable for the bacteria whereas CO₂ production occurred as expected. For the photofermentative growth condition, hydrogen production is expected to occur, however vigorous hydrogen production occurs when the OD is reached to 1 (unpublished observation). The measurements were done after 6 hours when OD was approximately 0.5, thus no visible H₂ production was observed, nevertheless GC measurements showed that 82.62 ± 15.36 % of the total gas is hydrogen indicating an active hydrogen production. The remaining gas composition was measured as 11.54 ± 10.33 % nitrogen, 5.38 ± 4.58 % CO₂ and negligible amount (0.48 ± 0.58 %) oxygen. In the case of anaerobic respiratory growth, low amount of hydrogen production (0.03%) was observed, whereas the rest of the components were 2.21 ± 2.94 % oxygen, 32.88 ± 35.27 % nitrogen and 64.88 ± 38.7 % CO₂.

Absorption spectrum drawn for each sample showed that carotenoid pigments with three fingered characteristic peaks (shown in Fig. 3.7) were absent in aerobic respiratory growth condition. However the peak corresponding to bacteriochlorophyll at 770nm was present in all of the conditions with fluctuating quantities. In Fig. 3.9, concentration of Bchl_a for different conditions was shown.

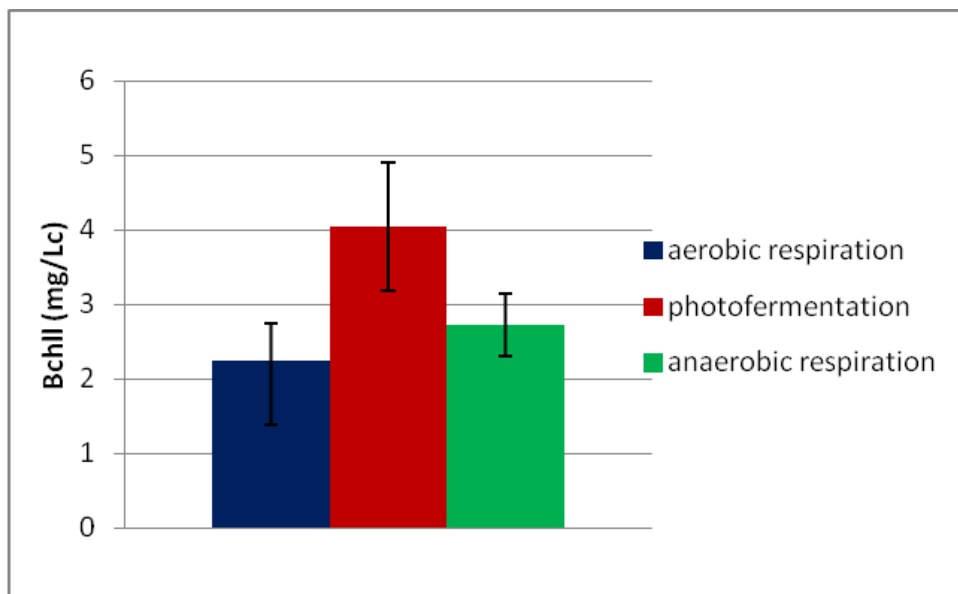


Figure 3.9 Bacteriochlorophyll concentration graph for different growth conditions

As shown in the graph, photofermentative growth mode exhibits the highest bchl a concentration. In spite of that, in aerobic respiratory and anaerobic respiratory growth modes expresses bchl a as well in lower levels.

3.1.6 Visualization of *Rhodobacter capsulatus* using fluorescence microscope

Rhodobacter capsulatus was visualized using nonyl acridine orange (NAO) staining the membrane and propidium iodide (PI) staining the non-intact thus non-living cells. 100X oil immersion objectives were used. The image of the bacteria was shown in Fig. 3.10.

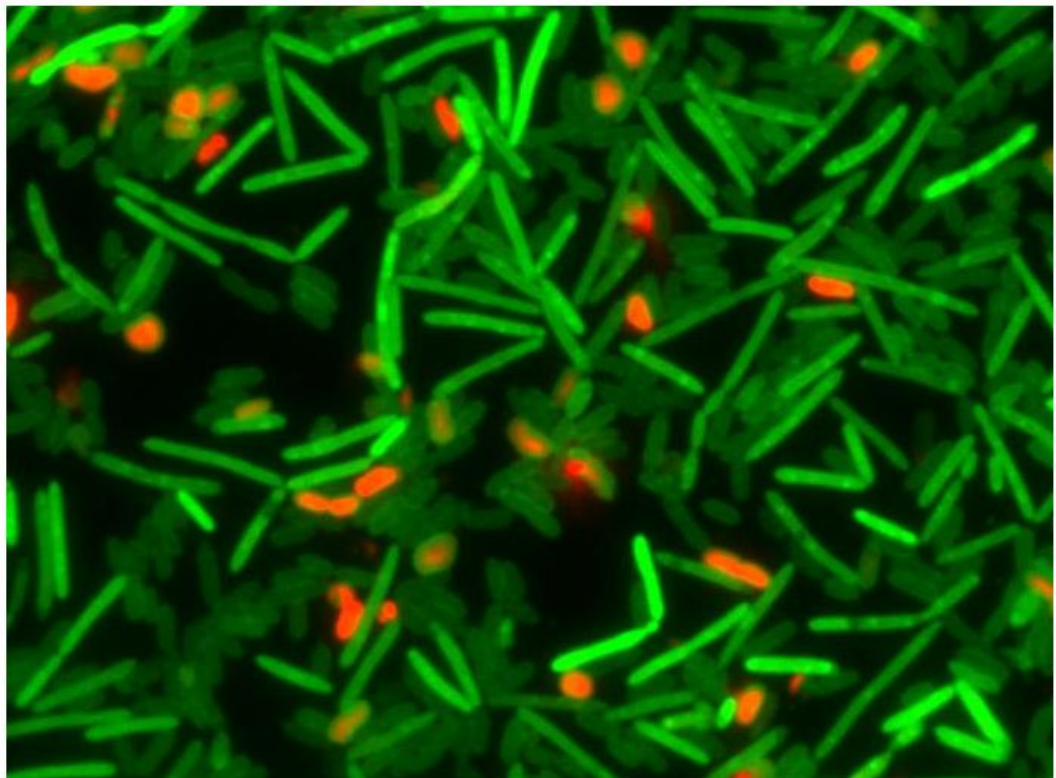
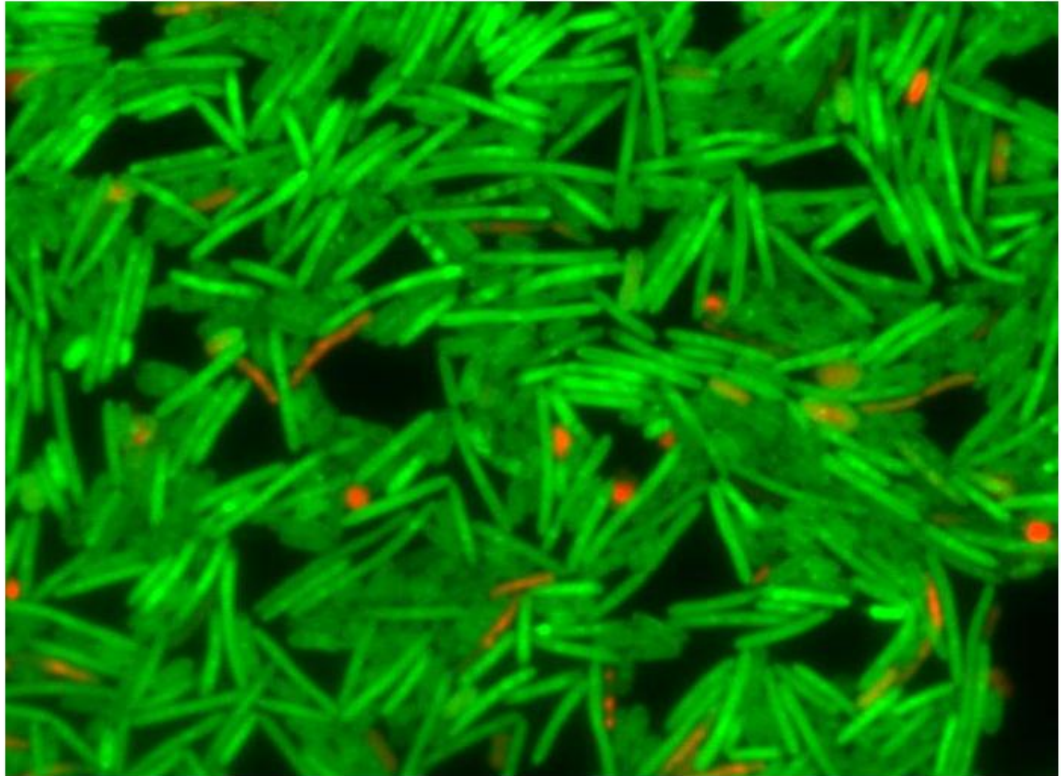


Figure 3.10 Fluorescence microscopy images of *Rhodobacter capsulatus*

3.2 LC-MS/MS Analysis

3.2.1 Optimization of Protein isolation and Protein quantification

Sample preparation method is a crucial step of the proteomics experiments. The quality and quantity of the proteins affects the number of proteins identified. The ratio of lowest and highest quantity of a protein which is named as dynamic range differs excessively among the cellular proteins. For an analytical system to detect a protein the dynamic range should be in the detection range of the instrument. The complexity of the sample, even in the detection range is a challenge because the scan speed of MS systems are limited and there is not sufficient time to resolve all peptide ions. The low abundance proteins are another concern as the MS systems are not very sensitive to detect without manipulations on the concentration of the protein. It is also important to note that protein degradation by the action of proteases and other protein modifying enzymes should be kept under control to have a better understanding of the cellular state of the enzymes. For the case of global protein extraction protocols, it is important to remove the nonprotein contaminants such as nucleic acids, lipids etc. and the incompatible detergents should be washed away not to disturb the following procedures such as chromatography or electrophoresis. Precipitation, aggregation or nonspecific surfaces causing adsorption may alter the original protein distribution and decrease the sensitivity. Therefore the protein extraction is an important step of proteomics studies.

For the extraction of the proteins, two different extraction solutions as chaotropic agents were used to denature and solubilize the proteins. Chaotropes solubilize and denatures the proteins by interacting with inter-molecular and intra molecular non-covalent interactions such as hydrogen bonds, dipole-dipole interactions etc. For global protein extraction, solubilization of membrane proteins along with cytosolic proteins requires strong chaotropes. Urea/Thiourea extraction solution is used previously for *Rhodobacter sphaeroides* (Callister *et al*, 2006). In another method by Wisniewski *et al*, 4% sodium dodecylsulfate (SDS) is recommended as the solubilization buffer for complete proteome. Thus we compared both buffers for the extraction of *Rhodobacter capsulatus* proteome using sonication technique. Below in Fig. 3.11, the SDS-PAGE picture for isolation of two samples with different extraction buffers were shown. The first 4 lanes in the gel are extracted by Universal protein extraction buffer which contains 4% SDS, but in the first two, 25mg of cells were harvested, in the second two 50mg of cells were used. The last 2

lanes contain 25mg cells extracted using 8M Urea/ 2M Thiourea buffer. As seen from the gel picture, highest concentration is obtained with UPX extraction of 50 mg cell.

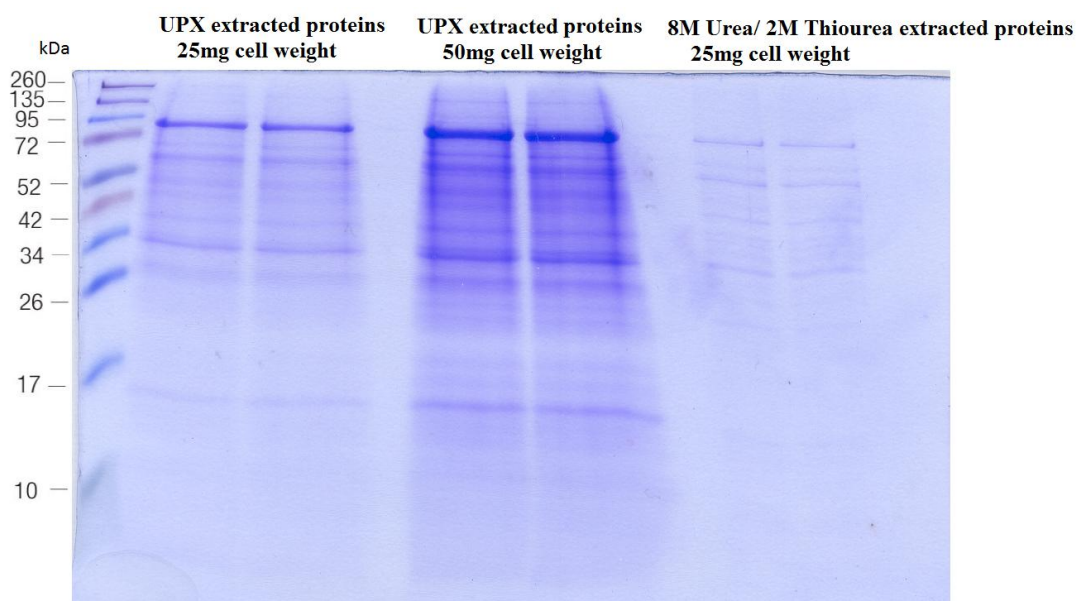


Figure 3.11 SDS-PAGE gel(12%) picture of proteins extracted with different extraction buffers stained with Coomassie

After the extraction protocol, high speed centrifugation was performed to pellet down small non-protein molecules such as pigments etc which blocks the LC system used for the separation of the peptides.

For cell concentration determination, absorbance readings were read using the nanodrop since the concentration of SDS and urea/thiourea was not compatible with the protein determination assays such as Bradford or BCA (thermo scientific kit user guides). After high speed centrifugation, most of the non-protein contaminants were removed, thus we obtained clear spectrum from the readings (Appendix E). Filtration using 5kDa cut-off columns enabled us further concentrating the protein. Another concentrating step was applied for the tryptic peptides by lyophilization to suffice the protein amount required in LC-MS/MS experiments. In table 3.1 Concentrations of the proteins after extraction protocols and peptides after lyophilization are shown.

Table 3.1 Concentration of UPX extracted proteins and peptides after trypsinization followed by lyophilization

Sample names	UPX extraction concentration (ng/uL)	peptide concentration after lyophilization (ng/uL)
Aerobic dark-1	2245	4960
Anaerobic light-1	2915	7810
Anaaerobic dark with DMSO-1	2490	7420
Aerobic dark-2	1860	4250
Anaerobic light-2	2300	3200
Anaaerobic dark with DMSO-2	1745	3080
Aerobic dark-3	3320	6670
Anaerobic light-3	2645	5410
Anaaerobic dark with DMSO-3	2025	6690

For determination of the extraction quality, we performed SDS-PAGE for all samples. As shown in Fig. 3.12, samples showed smear-like protein bands because of different weighted proteins in the whole proteome. There is a distinct band in 95-72 kDa molecular weight range of anaerobic dark with DMSO samples which addresses an essential protein used in anaerobic respiratory metabolism such as TMAO reductase. Moreover, bands found in all growth conditions are also visible in different molecular weight ranges.

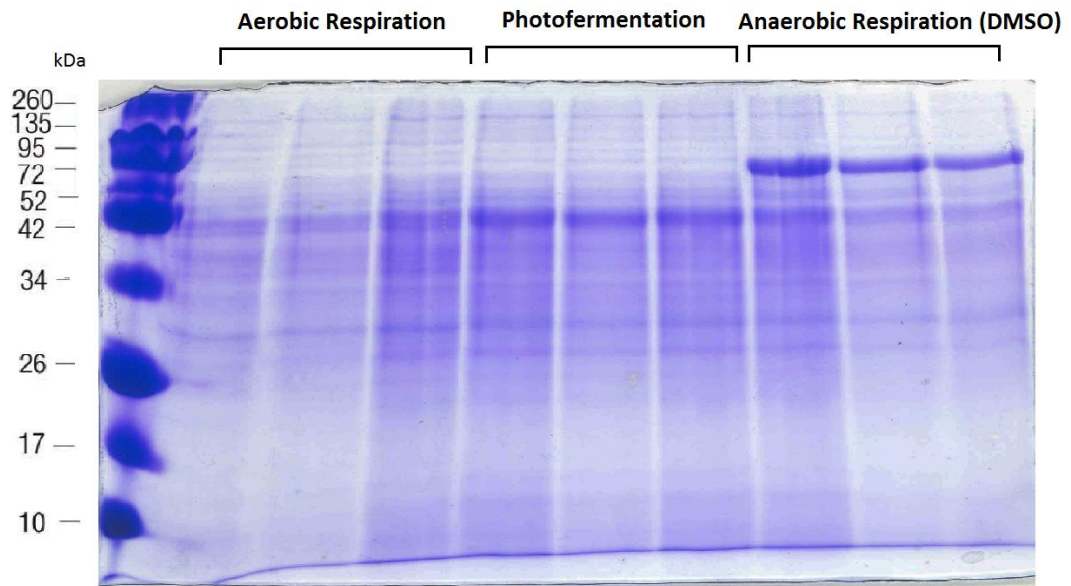


Figure 3.12 SDS-PAGE gel (12%) image of UPX extracted samples stained with Coomassie Blue

3.2.2 Quality assessment of the LC-MS/MS data

Principle component analysis (PCA) is a mathematical method to identify the patterns in a multivariate data. The aim of this technique is to reduce the size of the data set with extracting important information and simplifying the data set. PCA represents the data in a set of new orthogonal variables called principal components, so that the patterns in the data are identified, similarities and differences are highlighted as points in maps (Abdi and Williams, 2010).

PCA is actually a common technique for analyzing the data in MS studies. It describes the main sources of variation as the principal components will point in average directions of overall covariation (Harrington *et al*, 2005). Data matrix extracts the dominant patterns in a data set representing inter-correlated variables and displays them as points in the maps. Progenesis software was used for PCA analysis. Briefly, the program plots the variables thus the normalized values for each proteins or peptides against each other. A new axis representing the maximum variation through the data was determined by minimizing the sum of the squared distances from the points to the component. This new axis is named as principle component. Second principal component is orthogonal to the

first principle component and represents the second highest variation through the data. Finally, the data was centered into the new axes of the graph (Abdi and Williams, 2010).

In Fig. 3.13 and 3.14 PCA graphs of identified proteins and detected peptides were shown for each data set representing different growth conditions: aerobic dark, anaerobic light and anaerobic dark in the presence of DMSO. Each spot in the graph represents the principal component of a data set. In this study, we worked in triplicates for each 3 growth condition, and we performed 3 injections for each sample to reduce the errors occurred during the long operation time of LC-MS/MS instrument statistically, thus there are 27 spots in total. We expect to have 3 positionally close spots representing the 3 injections of a sample and the distance is the measure of variance of the samples. Therefore the distance between the spots measures the difference of the data sets. However the high-throughput nature of the system comes with the variance in the sample which in overall does not create inaccurate results. In the overall scheme, we clearly observed that each growth condition formed distinct groups indicating that the proteomes of three different growth conditions are different from each other as expected.

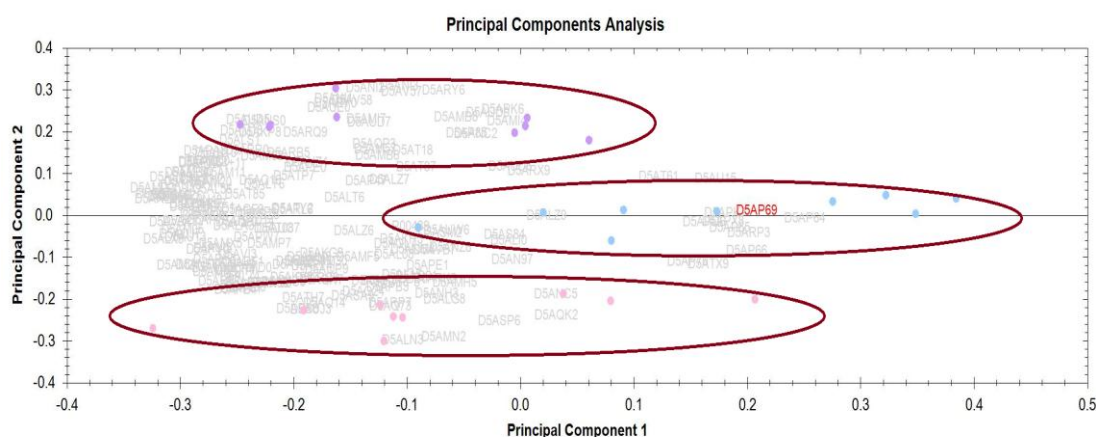


Figure 3.13 Principle Component Analysis of identified proteins in all growth conditions

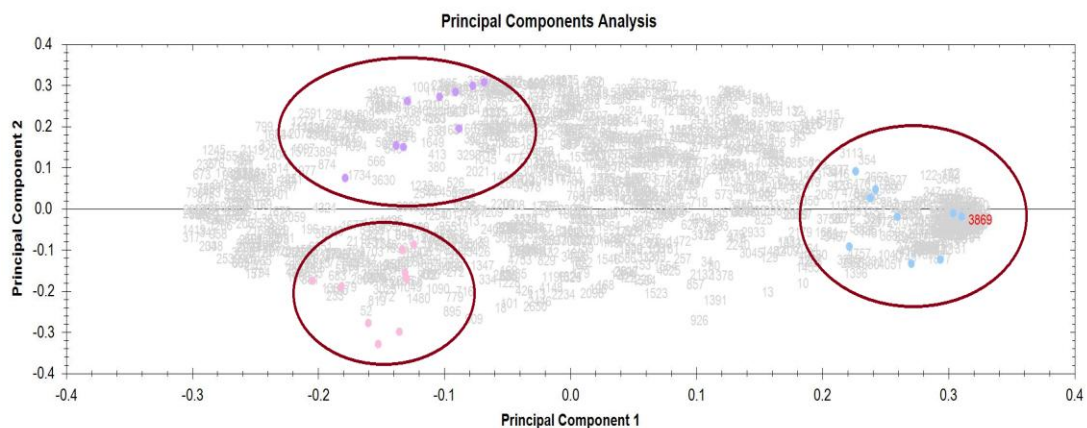


Figure 3.14 Principle Component Analysis of identified peptides in all growth conditions

3.2.3 Identification of Proteins of *Rhodobacter capsulatus* by LC-MS/MS

LC-MS/MS experiments resulted in identification of 460 proteins. The total list of proteins obtained by PLGS software was shown in Appendix I with the protein scores. Fig. 3.15 shows a representation of the peptide mass/charge (m/z) ratio versus retention time. Retention time is the measure of the hydrophobicity, a peptide with the longest retention time has the most hydrophobic nature whereas x axis represents the m/z ratio of the peptide. Each spot on the graph represents a peptide in the chromatogram obtained by the LC-MS/MS experiments. In appendix-H the representation of the features are shown for selected proteins.

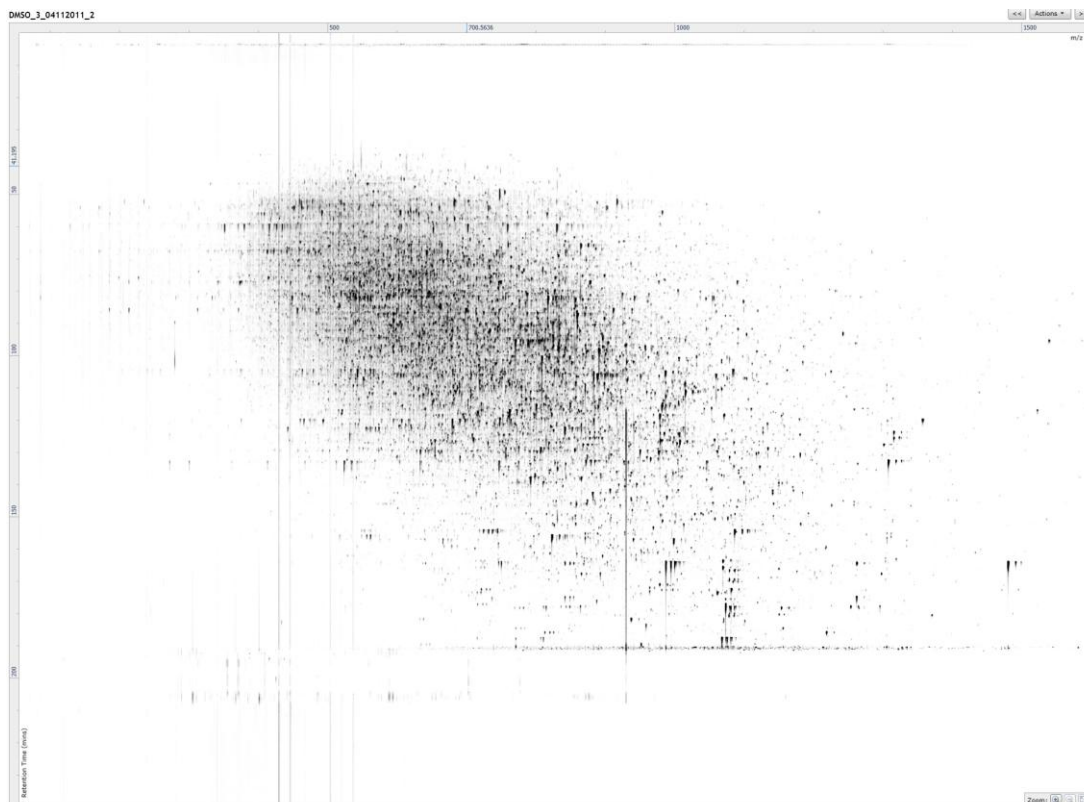


Figure 3.15 Plot of charge/mass ratio versus retention time of analyzed peptides by LC-MS/MS

Identified peptides were grouped according to available gene ontology (GO) information. Fig. 3.16 shows the pie-chart representation of gene ontology according to biological processes. In gene ontology guidelines, biological processes are defined as the collection of molecular events. There are 159 protein identified having role in metabolic processes, 137 proteins having role in cellular processes. Metabolic processes and cellular processes differ in the involvement in more than one cell-type. According to the GO terms, metabolic processes are organismal but can occur in different types of cells in the organism whereas cellular processes are restricted to a single cell. Thus the proteins identified are mostly involved in biosynthetic and catabolic processes in the bacteria. 24.5% of the proteins do not have gene ontology information about their involvement in biological processes.

By means of GO according to molecular functions as represented in Fig. 3.17, we identified 181 proteins with molecular function, 127 protein with binding functions and 106 proteins with catalytic activity. However there are still 24.5% of the proteins remained with unknown functions.

GO according to Biological Processes

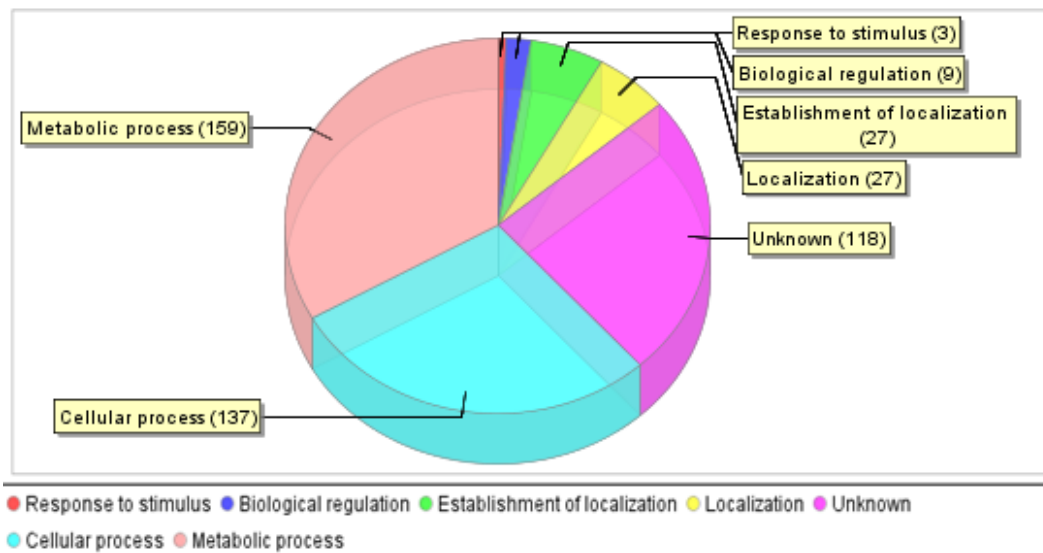


Figure 3.16 The pie-chart representation of gene ontology according to biological processes

GO according to Molecular Function

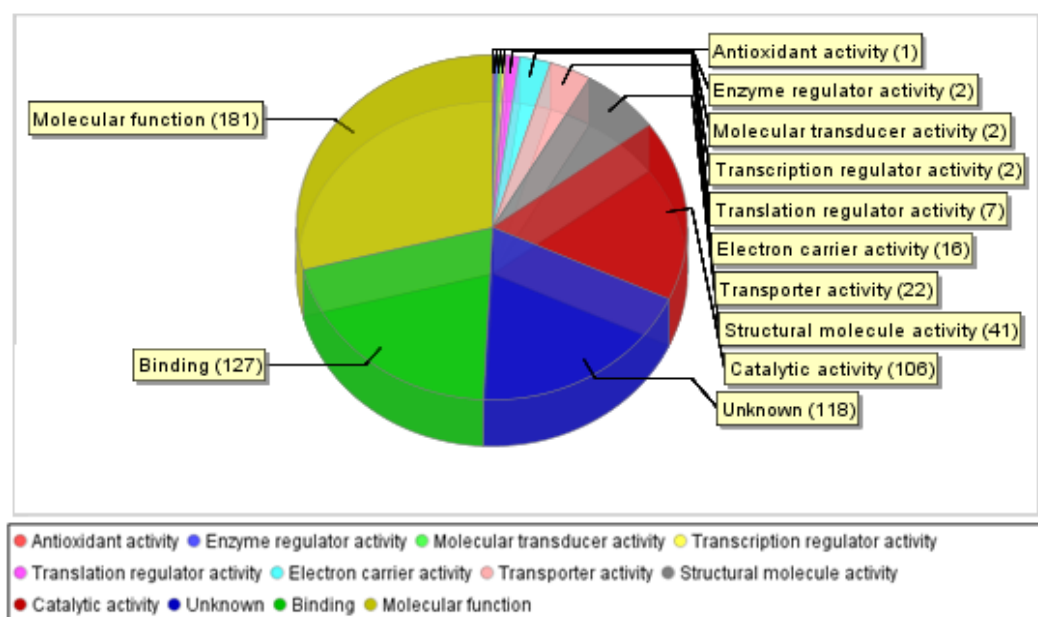


Figure 3.17 The pie-chart representation of gene ontology according to molecular function

3.3 Protein Profiles of *Rhodobacter capsulatus* Grown on Different Growth Conditions

In the following sections, the proteins are profiled according to the growth modes of *Rhodobacter capsulatus*. The changes in the levels of the proteins indicate the involvement of the protein in particular condition giving better understanding of the cellular state of the cell in the protein level. However it is important to note that, the high-throughput nature of the LC-MS/MS system does not measure the amount of protein exactly.

Identity^E module of the PLGS software identifies peptides using dedicated algorithms and acquires peptide ion accounting informatics. In Fig. 3.18 LC-MS ion chromatogram of anaerobic respiratory condition was shown in different energy levels as an example. Each run lasted for 240 minutes as can be seen from the chromatogram. Retention time for each peptide ion was determined to be used for quantitative analysis in MS^E mode. The software aligns the chromatograms for better identification. For a protein to be identified,

peptides should be present in minimum of 2 injections out of 3 as a prerequisite. Uniprot protein database for *Rhodobacter capsulatus* was used to identify the proteins. The more peptides used for the identification, the higher confidence attained in identifying the proteins.

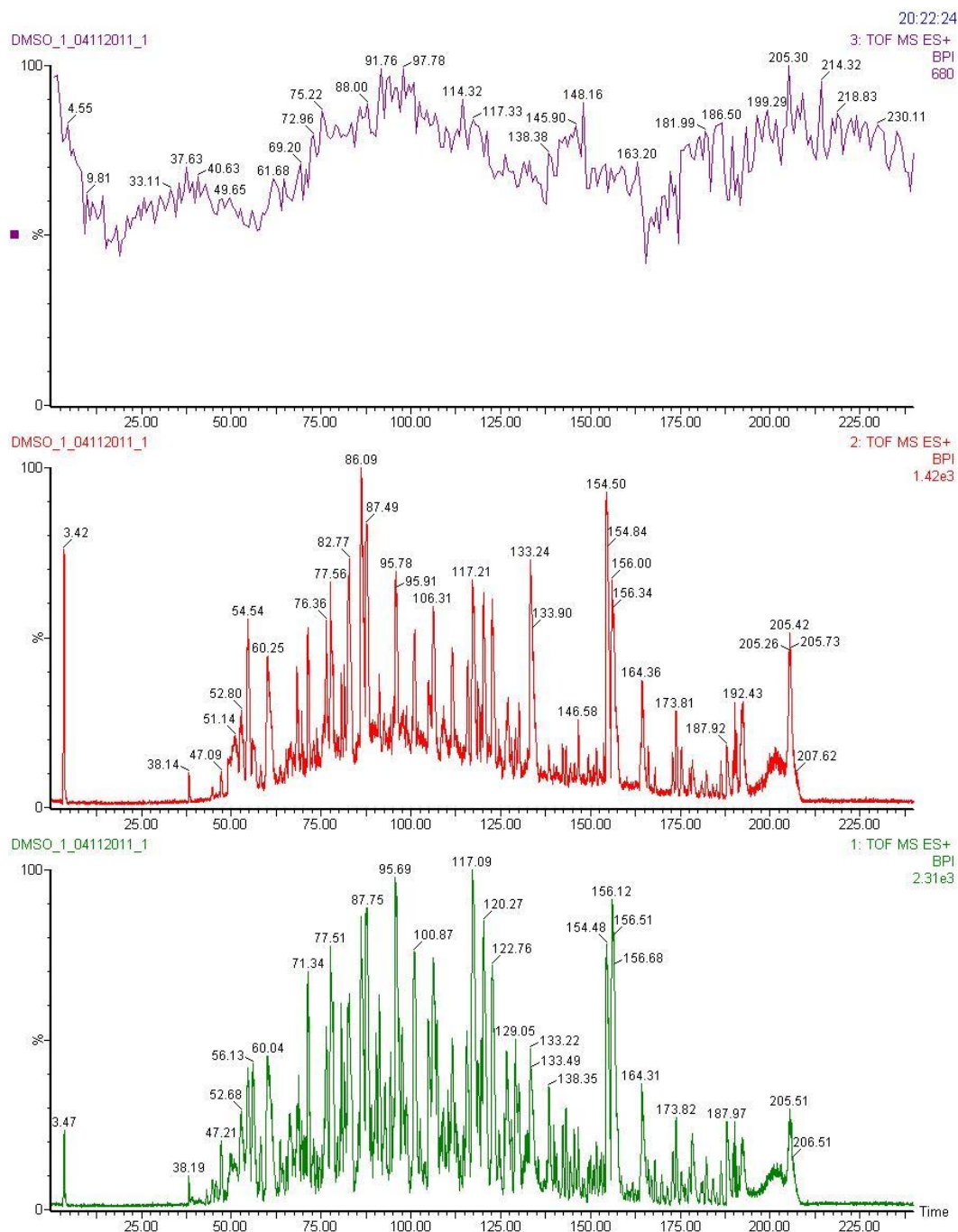


Figure 3.18 Base peak ion chromatogram obtained from LC-MS/MS experiment

As an overall scheme, the representation of identified proteins for each growth conditions are shown in venn diagrams in Fig. 3.19. Proteins are identified using peptides and peptides are identified using the spectra obtained by the LC-MS/MS. For aerobic dark growth condition referring to respiratory growth mode, no unique proteins were identified despite the fact that there are 885 spectra and 623 peptides were determined. The peptides identified did not result in protein identification due to the filtering applied for high confidence levels. For example if a peptide is not detected in at least 2 injections, it is not used for the protein identification. There are 254 proteins identified for both of the conditions, pointing up the requirement and importance of these proteins for the metabolism.

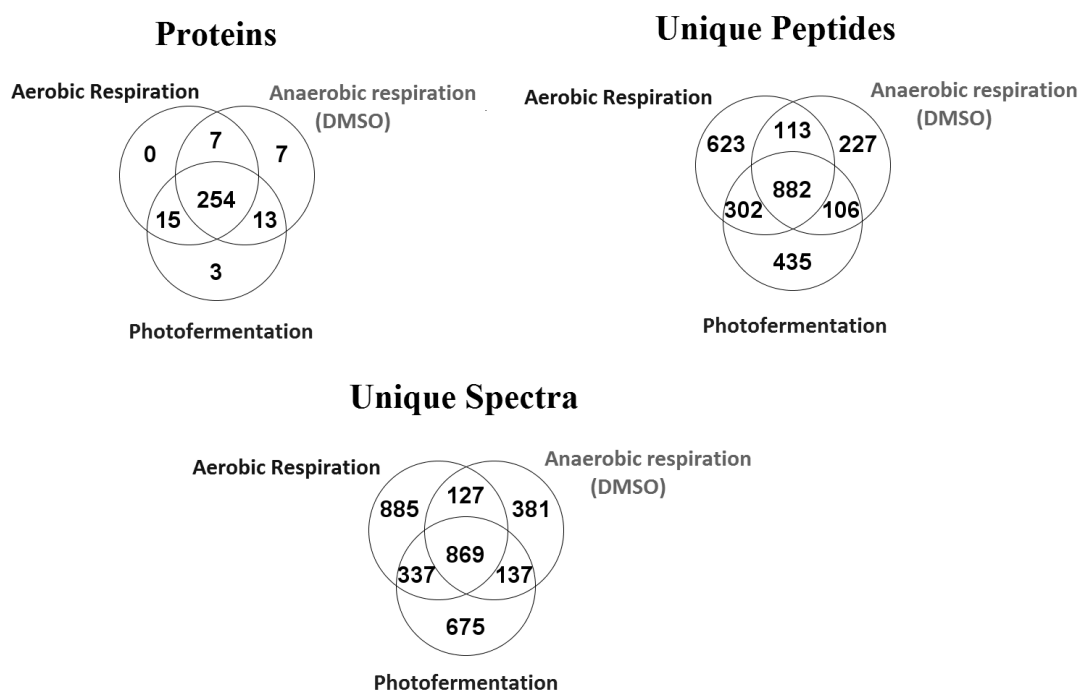


Figure 3.19 Schematic representation of unique spectra, peptides and proteins identified for different growth conditions

Unique proteins identified in anaerobic growth condition in dark in the presence of DMSO and in anaerobic growth condition in the presence of illumination are represented in table 3.2. As can be seen Trimethylamine N oxide (TMAO) reductase

which is the enzyme and the cytochrome are identified for anaerobic respiration in the presence of DMSO which is the final electron acceptor. The enzyme and the cytochrome are involved in the reduction of TMAO or DMSO (McEwan *et al*, 1991). The enzyme has a molybdenum cofactor of the pterin type, thus the proteins involved in the biosynthesis of cofactors and transport of the molybdate are identified. For photofermentative growth mode in anaerobic light condition, ferredoxins are identified uniquely which have roles in the hydrogen production metabolism.

Table 3.2 Unique peptides identified in a particular growth mode

	Accession number	Protein name
Unique to Anaerobic respiration in the presence of DMSO	D5AP69	Trimethylamine N oxide reductase
	D5APK7	Trimethylamine N oxide reductase c type cytoch
	D5AP70	Chaperone protein TorD
	D5AP65	Molybdenum cofactor biosynthesis protein B 2
	D5AP64	Molybdenum cofactor biosynthesis protein C 2
	D5AP66	Molybdenum cofactor biosynthesis protein D 1
	D5ANH3	Molybdenum ABC transporter periplasmic molybd
Unique to Photofermentative growth condition	D5ARX7	Ferredoxin III
	D5ARY7	Ferredoxin IV
	D5ARX8	Putative uncharacterized protein

3.3.1 Comparison of the protein levels in anaerobic respiratory growth in the presence of DMSO vs aerobic respiratory growth

In table 3.3 proteins are listed according to the fold change difference in particular conditions. The ration refers to the ratio of proteins in anaerobic respiratory condition in the presence of DMSO to proteins in aerobic respiratory condition.

Table 3.3 Changes in the protein levels in anaerobic respiratory growth in the presence of DMSO vs aerobic respiratory growth

Description	Ratio	software
D5AP69 Trimethylamine N oxide reductase	6.31	Progenesis
D5AP64 Molybdenum cofactor biosynthesis protein C 2	5.66	Progenesis
D5ARY6 Ferredoxin I	5.26	Progenesis
D5APD6 ATP synthase F0 B subunit	4.76	Progenesis
D5APK7 Trimethylamine N oxide reductase c type cytoch	3.61	Progenesis
D5AP87 Photosynthetic reaction center M subunit	2.27	PLGS
D5APX8 ATP synthase epsilon chain	2.16	Progenesis
D5AU15 Peptidyl prolyl cis trans isomerase	2.15	Progenesis
D5AP65 Molybdenum cofactor biosynthesis protein B 2	2.04	Progenesis
D5ANH3 Molybdenum ABC transporter, periplasmic molybdenum-binding protein ModA-1	2	PLGS
D5ANI1 Nitrogenase molybdenum-iron protein beta chain	2	PLGS
D5ANI2 Nitrogenase protein alpha chain	2	PLGS
D5ANI3 Nitrogenase iron protein 1	2	PLGS
D5ARY0 Nitrogen fixation protein NifX	2	PLGS
D5AV58 Multicopper oxidase family protein	2	PLGS
D5AMB6 Membrane protein putative	1.9	PLGS
D5AR82 Putative uncharacterized protein	0.52	Progenesis
D5ARY3 Peroxiredoxin	0.52	Progenesis
D5AM07 50S ribosomal protein L5	0.5	PLGS
D5AU26 Nucleoside diphosphate kinase	0.5	PLGS
D5AL83 dTDP-4-dehydrorhamnose reductase	0.49	PLGS
D5AMD0 Inorganic pyrophosphatase	0.49	PLGS
D5APY7 30S ribosomal protein S4	0.48	PLGS
D5ALZ0 30S ribosomal protein S7	0.47	PLGS
D5AMD1 10 kDa chaperonin	0.47	PLGS
D5ATK5 Putative uncharacterized protein	0.47	PLGS
D5AMD2 60 kDa chaperonin	0.46	PLGS
D5APC6 Succinate dehydrogenase flavoprotein subunit	0.46	PLGS

Table 3.3 continued

D5ATH7 NADH-quinone oxidoreductase, E subunit	0.46	PLGS
D5ALF8 DNA-binding protein HU-1	0.45	PLGS
D5ALY3 50S ribosomal protein L1	0.45	PLGS
D5AP40 Bifunctional sulfate adenylyltransferase/adenylyl-sulfate kinase	0.45	PLGS
D5ANF1 Aspartate-semialdehyde dehydrogenase	0.43	PLGS
D5AKP1 Sigma 54 modulation protein/ribosomal protein S30EA	0.41	PLGS
D5AQ04 Cell division protein ftsZ	0.4	PLGS
D5ATT1 Uridylate kinase	0.40	Progenesis
D5ANT4 Geranylgeranyl diphosphate reductase	0.37	PLGS
D5AR65 4-aminobutyrate aminotransferase-1	0.37	PLGS
D5APB3 Succinyl CoA ligase ADP forming subunit beta	0.36	PLGS
D5APB8 Dihydrolypoyllysine residue succinyltransferas	0.33	PLGS
D5AMX5 Putative uncharacterized protein	0.30	Progenesis
D5APB4 Succinyl CoA ligase ADP forming subunit alph	0.28	PLGS

In anaerobic respiratory growth mode in the presence of DMSO, up to 6 times higher levels of Trimethylamine N oxide reductase was observed together with Molybdenum cofactor biosynthesis protein C2 and B2 in comparable ratios. TMAO contains pterin molybdenum cofactor in its structure which is related with the increase in the molybdenum cofactor biosynthesis protein which is involved in Mo-molybdopterin cofactor biosynthetic process according to gene ontology information. Moreover almost 4 folds of increase in Trimethylamine N oxide reductase c type cytochrome was observed. 2 fold increase of Molybdenum ABC transporter, periplasmic molybdenum-binding protein ModA-1 may be due to higher demand of molybdenum in the cell.

Increase in proteins involved in nitrogen fixation during anaerobic respiratory growth condition indicates the activation of nitrogen fixation metabolism and explains the brief hydrogen production.

Putative membrane protein with the accession number D5AMB6 shown to have 2 fold change, thus may have importance in anaerobic respiratory metabolism.

In aerobic respiratory growth condition, we observed increased levels of TCA cycle proteins such as Succinyl CoA ligase ADP forming subunits (alpha and beta), dihydrolipoyllysine residue succinyltransferase, and succinate dehydrogenase flavoprotein subunit compared to anaerobic respiration.

Geranylgeranyl reductase, having 2.7 fold increase during anaerobic respiration has roles in bacteriochlorophyll synthesis.

D5AMX5 Putative uncharacterized protein and D5ATK5 Putative uncharacterized protein shown to have increased levels in aerobic respiratory growth condition and identification of these proteins may provide better understanding of the metabolism.

3.3.2 Comparison of the protein levels in anaerobic photofermentative growth in the presence of illumination vs aerobic respiratory growth

Table 3.4 represents the proteins with minimum of 2 fold change in the comparison of the protein levels in aerobic respiratory growth vs anaerobic photofermentative growth in the presence of illumination. The ratio refers to the ratio in the protein levels of anaerobic photofermentative growth condition in the presence of illumination to the protein levels of aerobic respiratory growth condition.

Table 3.4 Changes in the protein levels in anaerobic photofermentative growth in the presence of illumination vs aerobic respiratory growth

Description	Ratio	software
D5ARY6 Ferredoxin I	23.12	progenesis
D5ANI3 Nitrogenase iron protein 1	3.42	progenesis
D5AUD7 Glyceraldehyde-3-phosphate dehydrogenase-1 (Phosphorylating)	3.32	PLGS

Table 3.4 continued

D5ANI1 Nitrogenase molybdenum-iron protein beta chain	3	PLGS
D5ANI2 Nitrogenase protein alpha chain	3	PLGS
D5ANI3 Nitrogenase iron protein 1	3	PLGS
D5ARY0 Nitrogen fixation protein NifX	3	PLGS
D5AV58 Multicopper oxidase family protein	3	PLGS
D5AP87 Photosynthetic reaction center M subunit	2.8	PLGS
D5AUE0 Fructose 1 6 bisphosphatase class 1	2.73	progenesis
D5ARR0 Porphobilinogen deaminase	2.18	PLGS
D5AV57 Putative uncharacterized protein	2.09	progenesis
D5AUD4 Ribulose-phosphate 3-epimerase	2.05	PLGS
D5AMB6 Membrane protein putative	1.93	PLGS
D5AMN2 Iron III ABC transporter periplasmic iron II	0.57	progenesis
D5ALN3 Citrate synthase	0.52	PLGS
D5ATH7 NADH-quinone oxidoreductase, E subunit	0.51	PLGS
D5AUJ3 Isocitrate dehydrogenase [NADP]	0.5	PLGS
D5AP66 Molybdenum cofactor biosynthesis protein D 1	0.47	progenesis
D5APB8 Dihydrolipoyllysine residue succinyltransferas	0.47	PLGS
D5APB4 Succinyl CoA ligase ADP forming subunit alph	0.35	PLGS

In photofermentative growth mode 23 fold increase of ferredoxin was observed. Ferredoxin is an important player in the hydrogen production as it transfers electrons to nitrogenase. Moreover up to 3 folds of increase was observed in the proteins involved in nitrogen fixation such as Nitrogenase molybdenum-iron protein, Nitrogenase iron protein, Nitrogen fixation protein etc. Higher levels of photosynthetic reaction center protein compared to aerobic respiration was as expected.

Putative uncharacterized protein with the accession number D5AV57 and putative Membrane protein with the accession number D5AMB6 were shown to have almost 2 fold increase in photofermentative growth condition and may have important roles in processes like hydrogen production and light reactions.

In respiratory growth mode, proteins functioning in TCA cycle shown to have increased levels when compared to photofermentative growth highlighting the demand for TCA cycle to provide energy. Succinyl CoA ligase ADP forming subunit alpha, Dihydrolipoyllysine residue succinyltransferase, Isocitrate dehydrogenase NADP, Citrate synthase and Succinyl CoA ligase ADP forming subunit beta are examples having roles in TCA cycle with increased proteins levels.

3.3.3 Comparison of the protein levels in anaerobic photofermentative growth in the presence of illumination vs anaerobic respiratory growth in the presence of DMSO

In anaerobic respiration energy demand is satisfied from the respiratory chains using the DMSO as the final electron acceptor and in anaerobic photofermentative growth, the resource is light energy, thus the nitrogenase system as the bacteria are forced to produce H₂ in this growth mode.

Table 3.5 summarizes the changes of the protein levels. The ratio represents the ratio of the protein levels in anaerobic photofermentative growth condition in the presence of illumination to the protein levels in anaerobic respiratory growth condition in the presence of DMSO.

Table 3.5 Changes in the protein levels in anaerobic respiratory growth in the presence of DMSO vs anaerobic photofermentative growth in the presence of illumination

Description	Ratio	Software
D5ANI2 Nitrogenase protein alpha chain	8.58	PLGS
D5ANI1 Nitrogenase molybdenum-iron protein beta chain	7.92	PLGS
D5ANI3 Nitrogenase iron protein 1	5.26	PLGS
D5ARY6 Ferredoxin I	4.39	Progenesis
D5ANT4 Geranylgeranyl diphosphate reductase	3.97	PLGS
D5ARY0 Nitrogen fixation protein NifX	3.25	PLGS
D5AR65 4-aminobutyrate aminotransferase-1	3.1	PLGS
D5AR82 Putative uncharacterized protein	3	PLGS
D5AUD7 Glyceraldehyde-3-phosphate dehydrogenase-1 (Phosphorylating)	2.89	PLGS
D5AV58 Multicopper oxidase family protein	2.77	PLGS
D5AQ04 Cell division protein ftsZ	2.64	PLGS
D5AP40 Bifunctional sulfate adenylyltransferase/adenylyl-sulfate kinase	2.61	PLGS
D5AUD4 Ribulose-phosphate 3-epimerase	2.53	PLGS
D5AMX5 Putative uncharacterized protein	2.48	Progenesis
D5ALZ7 50S ribosomal protein L2	2.34	PLGS
D5AST0 Phosphoglycerate dehydrogenase	2.34	PLGS
D5ARR0 Porphobilinogen deaminase	2.29	PLGS
D5AL83 dTDP-4-dehydrorhamnose reductase	2.25	PLGS
D5AUE0 Fructose 1 6 bisphosphatase class 1	2.23	Progenesis
D5ALY3 50S ribosomal protein L1	2.2	PLGS

Table 3.5 continued

D5ALS1 Protease Do	2.14	PLGS
D5AM00 30S ribosomal protein S3	2.14	PLGS
D5APY7 30S ribosomal protein S4	2.12	PLGS
D5ASS9 Phosphoserine aminotransferase	2.12	PLGS
D5ALF8 DNA-binding protein HU-1	2.05	PLGS
D5ANH3 Molybdenum ABC transporter, periplasmic molybdenum-binding protein ModA-1	2	PLGS
D5AKP8 UTP--glucose-1-phosphate uridylyltransferase	1.97	PLGS
D5ANF1 Aspartate-semialdehyde dehydrogenase	1.95	PLGS
D5AQI5 50S ribosomal protein L25	1.95	PLGS
D5AMD1 10 kDa chaperonin	1.93	PLGS
D5AMJ1 Cysteine synthase	1.93	PLGS
D5AM19 30S ribosomal protein S13	1.9	PLGS
D5AM57 50S ribosomal protein L19	1.9	PLGS
D5ARP3 UspA domain protein	0.52	Progenesis
D5AP65 Molybdenum cofactor biosynthesis protein B 2	0.46	Progenesis
D5APX8 ATP synthase epsilon chain	0.43	Progenesis
D5AP66 Molybdenum cofactor biosynthesis protein D 1	0.29	Progenesis
D5APK7 Trimethylamine N oxide reductase c type cytoch	0.27	Progenesis
D5APD6 ATP synthase F0 B subunit	0.19	Progenesis
D5AP69 Trimethylamine N oxide reductase	0.16	Progenesis
D5AP64 Molybdenum cofactor biosynthesis protein C 2	0.14	Progenesis

Proteins involved in nitrogen fixation have 3 to 8 fold increase compared to anaerobic respiratory growth mode.

Moreover proteins involved in bacteriochlorophyll synthesis such as Geranylgeranyl reductase and Porphobilinogen deaminase have increased levels when compared to anaerobic respiratory growth mode. Molybdenum ABC transporter was shown to increase by 2 fold due to higher demand of for the metallic ions in photofermentative growth condition.

Putative proteins with the accession numbers D5AR82 and D5AMX5 has up to 3 fold increase in photofermentative growth condition, therefore may have important roles.

In anaerobic respiratory growth condition, TMAO reductase, TMAO reductase cytochromes and molybdenum cofactor synthesis proteins revealed higher levels compared to photofermentative growth condition.

CHAPTER 4

CONCLUSIONS

In the present study, the protein profiles of *Rhodobacter capsulatus* SB1003 grown under respiratory, photofermentative and anaerobic respiratory conditions were investigated. LC-MS/MS method which is a high throughput technique and gives comprehensive data was used to obtain the whole proteome of the bacteria. Additionally, physiological analysis such as GC analysis to examine the produced gas, absorption spectrum to determine the pigmentation differences and HPLC analysis to measure the organic acid consumption was carried out in order to show the physiological differences.

Based on the obtained data and results, the following conclusions are obtained:

- Growth rate was slower on anaerobic respiratory growth mode than respiratory and photofermentative growth modes. Preferred growth mode was photofermentation using 40mM Acetate and 2mM Glutamate as the carbon and nitrogen sources, respectively.
- Acetate utilization was higher on anaerobic respiratory and photofermentative growth modes than aerobic respiratory growth mode.
- “Three-fingered” characteristic carotenoid absorption peak was observed in photofermentative and anaerobic respiratory growth conditions in the presence of DMSO, whereas it was absent in aerobic respiratory growth condition.
- On anaerobic respiratory growth condition in the presence of DMSO, hydrogen production obtained in very low amounts, but the proteins involved in nitrogen fixation was found in this condition. This observation might be further

investigated to be used in out-door bioreactors for hydrogen production during night.

- Protein isolation protocol was optimized for *Rhodobacter capsulatus* revealing high peptide and protein identification for LC-MS/MS methodology.
- SDS-PAGE resulted in very distinctive protein band in 72-95 kDa range for anaerobic respiratory growth condition in the presence of DMSO. Further characterization can be done by gel extraction of the protein followed by the LC-MS/MS experiment.
- By LC-MS/MS method total of 460 proteins were identified.
- Trimethylamine N oxide reductase, Trimethylamine N oxide reductase c type cytochrome and Molybdenum cofactor biosynthesis proteins are shown to have important function in anaerobic respiratory metabolism.
- Nitrogen fixation proteins are in very high levels in photofermentative growth condition and maximum of 23 fold of increase was observed in ferredoxin when compared to aerobic respiratory growth condition.
- Ferredoxin III, Ferredoxin IV and a putative uncharacterized protein with the accession number D5ARX8 found to be uniquely expressed in anaerobic fermentative condition.
- Trimethylamine N oxide reductase, Trimethylamine N oxide reductase c type cytochrome , Chaperone protein TorD , Molybdenum cofactor biosynthesis protein B 2 , Molybdenum cofactor biosynthesis protein C 2 , Molybdenum cofactor biosynthesis protein D 1 and Molybdenum ABC transporter periplasmic are uniquely identified in anaerobic respiratory growth mode in the presence of DMSO.

REFERENCES

- Abdi H., Williams L. J., (2010). Principal component analysis. Wiley Interdisciplinary Reviews: Computational Statistics, 2, 433–459.
- Argun H., Kargi F., (2011). Bio-hydrogen production by different operational modes of dark and photo-fermentation: An overview. International Journal of Hydrogen Energy, 36(13), 7443-7459.
- Balat M., (2008). Possible Methods for Hydrogen Production. Energy Sources, Part A: Recovery, Utilization, and Environmental Effects, 31(1), 39-5.
- Bicakova O. and Straka P., (2010). The resources and methods of hydrogen production. Acta Geodyn. Geomater. 7(2), 175-188.
- Bieble, H., Pfennig, N., (1981). Isolation of members of the family Rhodospirillaceae. In: Starr, M.P., Stolp, H., Trüper, H.G., Balows, A., Schlegel, H.G. (Eds.). The prokaryotes, 1, 267–73.
- Callister S.J., Nicora C. D., Zeng X., Roh J. H., Dominguez M. A., Tavano C. L., Monroe M. E., Kaplan S., donohue T. J., Smith R. D., Lipton M. S., (2006). Comparison of aerobic and photosynthetic *Rhodobacter sphaeroides* 2.4.1 proteomes. Journal of Microbiological Methods, 67, 424-436.
- Chen G., Pramanik B.N., (2009). Application of LC/MS to proteomics studies: current status and future prospects. Drug Discovery Today, 14(9–10), 465-471.
- Chong M.L, Sabaratnam V., Shirai Y., Mohd A. H., (2009). Biohydrogen production from biomass and industrial wastes by dark fermentation. International Journal of Hydrogen Energy, 34(8), 3277-3287.

Choudhary M, Zanhua X, Fu YX, Kaplan S., (2007). Genome analyses of three strains of *Rhodobacter sphaeroides*: evidence of rapid evolution of chromosome II. *Journal of bacteriology*, 189(5), 1914-1921.

Choudhary M., Mackenzie C., Mouncey N. J., Kaplan S., (1999). RsGDB, the *Rhodobacter sphaeroides* Genome Database. *Nucleic Acids Research*, 27(1), 61-62.

Clayton R. K., (1971). Photochemical reaction centers from *Rhodospseudomonas sphaeroides*. *Methods Enzymol.* 23, 696-704.

Das D, Khanna N, Veziroğlu T. N., (2008). Recent developments in biological hydrogen production processes. *Chem Ind Chem Eng Q* 14, 57–67.

Elsen S., Ponnampalam S.N., Bauer C.E., (1998). CrtJ bound to distant binding sites interacts cooperatively to aerobically repress photopigment biosynthesis and light harvesting II gene expression in *Rhodobacter capsulatus*. *J Biol Chem* 273, 30762–30769.

Eroglu E, Melis A, (2011). Photobiological hydrogen production: Recent advances and state of the art. *Bioresource Technology*, 102(18), 8403-8413.

Geelhoed J.S., Hamelers H. V.M., Stams A.J.M., (2010). Electricity-mediated biological hydrogen production. *Current Opinion in Microbiology*, 13(3), 307-315.

Gregor J., Klug G., (1999). Regulation of bacterial photosynthesis genes by oxygen and light. *FEMS Microbiology Letters* 179, 1-9.

Guoxin H. , Hao H., (2009)., Hydrogen rich fuel gas production by gasification of wet biomass using a CO₂ sorbent. *Biomass and Bioenergy*, 33, 899–906.

Hallenbeck P. C., Benemann J. R., (2002). Biological hydrogen production; fundamentals and limiting processes. *International Journal of Hydrogen Energy*, 27(11–12), 1185-1193.

Han X., Aslanian A., Yates J.R., (2008). Mass spectrometry for proteomics. *Current Opinion in Chemical Biology*, 12(5), 483-490.

Harrington P. B, Vieira N. E., Espinoza J., Nien J.N., Romero R., Yergey A.L., (2005). Analysis of variance–principal component analysis: A soft tool for proteomic discovery. *Analytica Chimica Acta*, 544(1–2),118-127.

Holladay J.D., Hu J., King D.L., Wang Y.,(2009). An overview of hydrogen production technologies. *Catalysis Today*, 139(4), 244-260.

Imhoff J.F., (2006). The phototrophic alpha-proteobacteria. In Dworkin M., Falkow S., Rosenberg E., Schleifer K. H., Stackebrandt E. (Eds). *The Prokaryotes: a handbook on the Biology of Bacteria*, Springer.

International energy Agency-

http://www.iea.org/textbase/nppdf/free/2011/key_world_energy_stats.pdf, 3rd February, 2012.

Ishida M., Takenaka S., Yamanaka I., Otsuka K., (2006). Production of CO_x-free hydrogen from biomass and NaOH mixture: effect of catalysts. *Energy and Fuels*, 20, 748–753

Italiano F., D'Amici G.M., Rinalducci S., De Leo F., Zolla L., Gallerani R., Trotta M., Ceci L.R., (2011). The photosynthetic membrane proteome of *Rhodobacter sphaeroides* R-26.1 exposed to cobalt. *Research in Microbiology*, 162, 520-527.

Jain I.P., (2009). Hydrogen the fuel for 21st century, *International Journal of Hydrogen Energy*. 34(17), 7368-7378.

Junge, W., and Jackson, J. B., (1982). In *Photosynthesis: Energy Conversion by Plants and Bacteria*. Govindjee(eds) 1, 589-646, Academic Press,New York.

Kars G, Gündüz U., Yücel M, Rakhely G, Kovacs K. L., Eroğlu İ., (2009). Evaluation of hydrogen production by *Rhodobacter sphaeroides* O.U.001 and its hupSL deficient mutant using acetate and malate as carbon sources. *International Journal of Hydrogen Energy*, 34(5), 2184-2190.

Kars G., Gündüz U., (2010). Towards a super H₂ producer: Improvements in photofermentative biohydrogen production by genetic manipulations. *International Journal of Hydrogen Energy*, 35(13), 6646-6656.

Koku H, Eroğlu İ., Gündüz U., Yücel M., Türker L., (2002). Aspects of the metabolism of hydrogen production by *Rhodobacter sphaeroides*. *International Journal of Hydrogen Energy*, 27(11–12), 1315-132.

Kothari R, Buddhi D., Sawhney R.L., (2008). Comparison of environmental and economic aspects of various hydrogen production methods. *Renewable and Sustainable Energy Reviews*, 12(2), 553-563.

Law C J., Roszak A. W., Southall J., Gardiner A. T., Isaacs N. W., Cogdell R. J.,(2004). The structure and function of bacterial light harvesting complexes (Review), *Molecular Membrane biology* 21, 183-191.

Lee H. S, Vermaas W. F.J., Rittmann B. E., (2010). Biological hydrogen production: prospects and challenges, *Trends in Biotechnology*, 28(5), 262-271.

Levin D. B., Chahine R., 2010. Challenges for renewable hydrogen production from biomass. *International Journal of Hydrogen Energy*, 35(10), 4962-4969.

Levin D.B., Pitt L. , Love M., (2004). Biohydrogen production: prospects and limitations to practical application. *International Journal of Hydrogen Energy*, 29 ,173.

Mackenzie C., Choudhary M., Larimer F. W., Predki F. W., Stilwagen S., Armitage J. P., Barber R. D., Donohue T. J., Hosler J. P., Newman J. E., (2001). The home stretch, a first analysis of the nearly completed genome of *Rhodobacter sphaeroides* 2.4.1. *Photosynthesis Research*, 70(1), 19-41.

Madigan M, Cox JC, Gest H., (1982). Photopigments in *Rhodopseudomonas capsulata* cells grown anaerobically in darkness. *J Bacteriol.* 150(3),1422–1429.

Madigan M. T., Gest H., (1979). Growth of the photosynthetic bacterium *Rhodospseudomonas capsulata* chemoautotrophically in darkness with H₂ as the energy source. *Journal of Bacteriology*, 137(1), 524-530.

Madigan T. M., Jung D. O., (2009). An overview of purple bacteria: systematics, physiology and habitats. In Hunter N. C., Daldal F., Thurnauer M.C., Beatty J. T. (Eds), *The purple phototrophic bacteria*, Springer.

Maresca, J. A., Graham, J. E. & Bryant, D. A., (2008). The biochemical basis for structural diversity in the carotenoids of chlorophototrophic bacteria. *Photosynth Res* 97, 121–14.

Masepohl B., Hallenbeck P.C., (2010) Nitrogen and molybdenum control of nitrogen fixation in the phototrophic bacterium *Rhodobacter capsulatus*. In Hallenbeck P.C. (Eds) *Advances in Experimental Medicine and Biology* 675, Springer.

McConkey B.J., (2011). Theory and Applications of Proteomics, In Moo-Young M. (Eds), *Comprehensive Biotechnology* (Second Edition), Academic Press, Burlington, 461-469.

McEwan A. G., Ferguson S.J., Jackson J.B., (1991). Purification and properties of dimethyl sulphoxide reductase from *Rhodobacter capsulatus*. *Biochemical Journal*, 274, 305-307

McHugh K., (2005). *Hydrogen Production Methods*, MPR Associates Inc.

Melis A., Melnicki M. R., (2006). Integrated biological hydrogen production. *International Journal of Hydrogen Energy*, 31(11), 1563-1573.

Milliken J., (2008). Hydrogen generation from biomass-derived carbohydrates via aqueous phase reforming process. U.S. Department of Energy, Washington, DC, PD-6.

Mouncey N. J., Choudhary M., Kaplan S., (1997), Characterization of genes encoding dimethyl sulfoxide reductase of *Rhodobacter sphaeroides* 2.4.1T: an essential metabolic gene function encoded on chromosome II. *Journal of Bacteriology*, 179(24), 7617-7624.

Muradov N. , Smith F., (2008). Thermocatalytic conversion of landfill gas and biogas to alternative transportation fuels. *Energy and Fuels*, 22 , 2053–2060.

Onder O., Aygun-Sunar S., Selamoğlu N., Daldal F., (2010) A glimpse into the proteome of phototrophic bacterium *Rhodobacter capsulatus*. In Hallenbeck P.C. (Eds) *Advances in Experimental Medicine and Biology* 675, Springer.

Öztürk Y., Gökçe A., Peksel B., Gürkan M., Özgür E., Gündüz U., Eroğlu İ., Yücel M., (2012). Hydrogen production properties of *Rhodobacter capsulatus* with genetically modified redox balancing pathways. *International Journal of Hydrogen Energy*, 37(2), 2014-2020.

Öztürk Y., Yücel M., Daldal F., Mandacı S., Gündüz U., Türker L., Eroğlu İ., (2006). Hydrogen production by using *Rhodobacter capsulatus* mutants with genetically modified electron transfer chains. *International Journal of Hydrogen Energy*, 31(11), 1545-1552.

Pappas C. T., Sram J., Moskin O. V., Ivanov P. S., Mackenzie R. C., Choudhary M., Land M. L., Larimer F. W., Kaplan S., Gomelsky M., (2004). Construction and Validation of the *Rhodobacter sphaeroides* 2.4.1 DNA Microarray: Transcriptome Flexibility at Diverse Growth Modes. *Journal of Bacteriology*, 186(14), 4748-4758.

Reichman B, Mays W, Strebe J, Fetcenko M. (2007). Fuel reformation using alkaline enhancement. In: *Proceedings International Hydrogen Energy Congress and Exhibition*. Istanbul, Turkey.

Sabaty M, Gans P and Verméglio A., (1993). Inhibition of nitrate reduction by light and oxygen in *Rhodobacter sphaeroides* forma sp. denitrificans. *Arch Microbiol* 159, 153–159.

Scheuring S., Sturgis J. N., (2009) Atomic force microscopy of the bacterial photosynthetic apparatus: plan pictures of an elaborate machinery. *Photosynthesis research* 102, 197-211.

Schwarz C., Poss Z., Hoffman D., Appel J., (2010). Hydrogenases and hydrogen metabolism in photosynthetic prokaryotes. In Hallenbeck P.C. (Eds) *Advances in Experimental Medicine and Biology* 675, Springer.

Smart J.L., Willett J.W., Bauer C.E., (2004). Regulation of hem gene expression in *Rhodobacter capsulatus* by redox and photosystem regulators RegA, CrtJ, FnrL, and AerR. *J Mol Biol* 342, 1171–1186.

Sørensen B., (2005). *Hydrogen and Fuel Cells Emerging Technologies and Applications*. Elsevier Academic Press, New York.

Strnad H., Lapidus A., Paces J., Ulbrich P., Vlcek C., Paces V., Haselkorn R., (2010). Complete genome sequence of the photosynthetic purple nonsulfur bacterium *Rhodobacter capsulatus* SB 1003. *Journal of Bacteriology* 192, 3545–3546.

Suwanto A., Kaplan S., (1989). Physical and genetic mapping of the *Rhodobacter sphaeroides* 2.4.1 genome: presence of two unique circular chromosomes. *Journal of Bacteriology*, 171:11, 5850-5859.

Turner J., Sverdrup G., Mann M.K., Maness P.-C., Kroposki B., Ghirardi M., Evans R.J., Blake D., (2008). *International Journal of Hydrogen Energy*, 32, 379–407.

Twyman R.M., (2005). Proteomics, In Worsfold P., Townshend A., Poole C. (Eds), *Encyclopedia of Analytical Science (Second Edition)*, Elsevier, Oxford, 383-393.

US department of energy hydrogen analysis research center-
<http://hydrogen.pnl.gov/cocoon/morf/hydrogen/article/401>, 18th of February 2008.

Verméglio A., Joliot P., (1999). The photosynthetic apparatus of *Rhodobacter sphaeroides*. *Trends in microbiology* 7, 435-440.

Verméglio A., Joliot P., Joliot A., (2004). Organization of electron transfer components and supercomplexes. In Blankenship R., Madigan M., Bauer C.(eds) *Anoxygenic Photosynthetic Bacteria*, Kluwer Academic Publishers.

Wen G., Xu Y., Ma H., Xu Z., Tian Z., (2008). Production of hydrogen by aqueous-phase reforming of glycerol. *International Journal of Hydrogen Energy*, 33, 6657–6666.

Willett J., Smart J.L., Bauer C.E., (2007). RegA control of bacteriochlorophyll and carotenoid synthesis in *Rhodobacter capsulatus*. *Journal of Bacteriology*, 189,7765–7773.

Wisniewski J.R., Zougman A., Nagaraj N., Mann M., (2009). Universal sample preparation method for proteome analysis. *Nature Methods*, 6(5), 359-362.

World Energy Outlook 2011 Factsheet-

<http://www.iea.org/weo/docs/weo2011/factsheets.pdf>, 9th November, 2011.

Woronowicz K., niederman R. A., (2010). Proteomic analysis of the developing intracytoplasmic membrane in *Rhodobacter sphaeroides* during adaptation to low light intensity. In Hallenbeck P.C. (Eds) *Advances in Experimental Medicine and Biology 675*, Springer.

Yates J. R., Ruse C. I., Nakorchevsky A., (2009). Proteomics by mass spectrometry: Approaches, advances and applications. *Annual review of Biomedical Engineering*, 11, 49-79.

Zannoni D., (2004). Aerobic and anaerobic electron transport chains in anoxygenic phototrophic bacteria. In Blankenship R., Madigan M., Bauer C.(eds) *Anoxygenic Photosynthetic Bacteria*, Kluwer Academic Publishers.

Zappa S., Li K., Bauer C. E., (2010). The tetrapyrrole biosynthetic pathway and its regulation in *Rhodobacter capsulatus*. In Hallenbeck P.C. (Eds) *Advances in Experimental Medicine and Biology*, 675, Springer.

Zeilstra-Ryalls J. H., (2008). Regulation of the Tetrapyrrole biosynthetic pathway. In Hunter N. C., Daldal F., Thurnauer MC., Beatty J. T. (Eds), *The purple phototrophic bacteria*, Springer, Dordrecht.

Zeng X., Roh J. H., Callister S. J., Tavano C. L., Donohue T. J., Lipton M. S., Kaplan S., (2007). Proteomic Characterization of the *Rhodobacter sphaeroides* 2.4.1 Photosynthetic Membrane: Identification of New Proteins. 189(20), 7464-7474.

Zhang X., Fang A., Riley C.P., Wang M., Regnier F.E., Buck C., (2010). Multi-dimensional liquid chromatography in proteomics—A review. *Analytica Chimica Acta*, 664(2), 101-113.

Züttel A., Remhof A., Borgschulte A., Friedrichs O., 2010. Hydrogen: the future energy carrier. *Philosophical Transactions of the Royal A Society*, 368, 3329-3342.

APPENDIX A

COMPOSITION OF THE GROWTH AND EXPERIMENTAL MEDIA

Table A.1 The composition of MPYE medium for 1 L

Medium components	Amount
Bactopeptone	3 g
Yeast Extract	3 g
MgCl ₂	1.6 mL from 1M stock
CaCl ₂	1mL from 1M stock

The ingredients were dissolved in 1L of distilled H₂O, pH was adjusted to 7 and sterilization was carried out by autoclaving.

Table A.2 The components of the growth and experimental media

Medium Components	Amounts for 20mM Acetate/ 10mM Glutamate Growth Medium	Amounts for 40mM Acetate/ 2mM Glutamate Experimental Medium
KH ₂ PO ₄	3 g	3 g
MgSO ₄ .7H ₂ O	0.5 g	0.5 g
CaCl ₂ .2H ₂ O	0.05 g	0.05 g
Acetic Acid	1.15 mL	2.3 mL
Na-Glutamate	1.85 g	0.36 g
Vitamin Solution (10X)	0.1 mL	0.1 mL
Trace Element solution (10X)	0.1 mL	0.1 mL
Fe-citrate (50X)	0.5 mL	0.5 mL

All the constituents were dissolved in 1L of distilled H₂O except vitamin, trace element and Fe-citrate solution. pH was adjusted to 6.3-6.4 by 5M NaOH and sterilized by autoclaving.

Vitamin, trace elements and Fe-citrate were added separately in sterile conditions.

Vitamin and trace element solution were prepared according to table A.3 and A.4 and filter sterilized.

For Fe-citrate 5g ferric citrate was dissolved in 100mL distilled water and sterilized by autoclaving.

Table A.3 The composition of the 10X vitamin solution

Components	Amount
Thiamine	500 mg
Niacin (Nicotinate)	500 mg
Biotin	15 mg

All the components were dissolved in 100mL distilled H₂O and filter sterilized.

Table A.4 The composition of 10X trace element solution

Components	Amount
HCl (25% v/v)	1 mL
ZnCl ₂	70 mg
MnCl ₂ × 4H ₂ O	100 mg
H ₃ BO ₃ 60	60 mg
CoCl ₂ × 6 H ₂ O 200 mg	200 mg
CuCl ₂ × 2 H ₂ O	20 mg
NiCl ₂ × 6 H ₂ O	20 mg
NaMoO ₄ × 2 H ₂ O	40 mg

All of the constituents were added in 100 mL of distilled H₂O and filter sterilized.

APPENDIX B

SAMPLE HPLC CHROMATOGRAM AND CALIBRATION CURVES

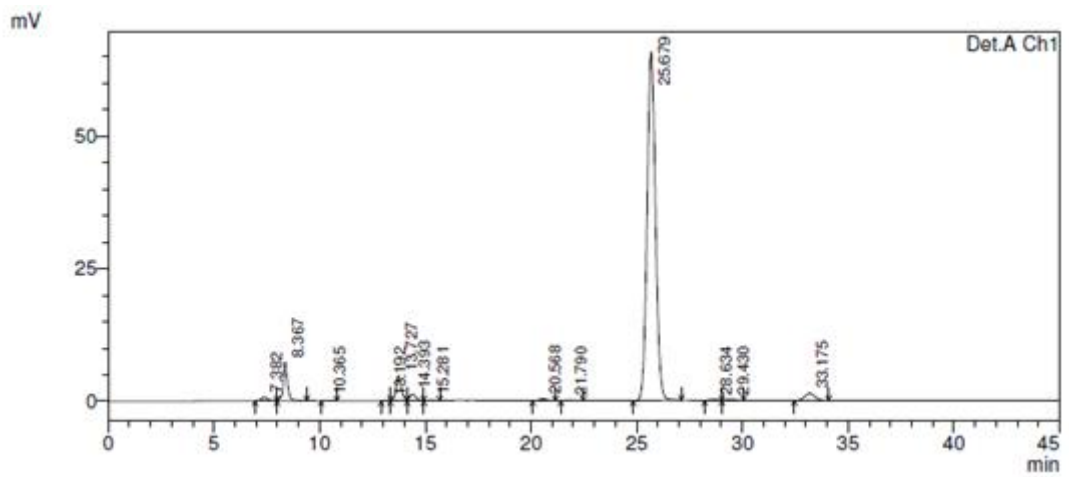


Figure B.1 Sample HPLC chromatogram for Aerobic respiratory growth condition

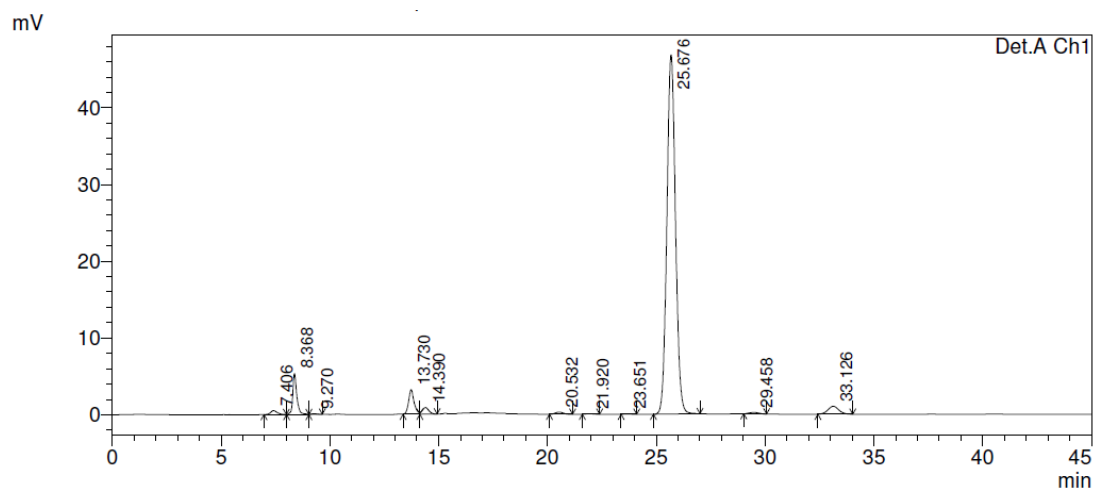


Figure B.2 Sample HPLC chromatogram for Anaerobic photofermentative growth condition

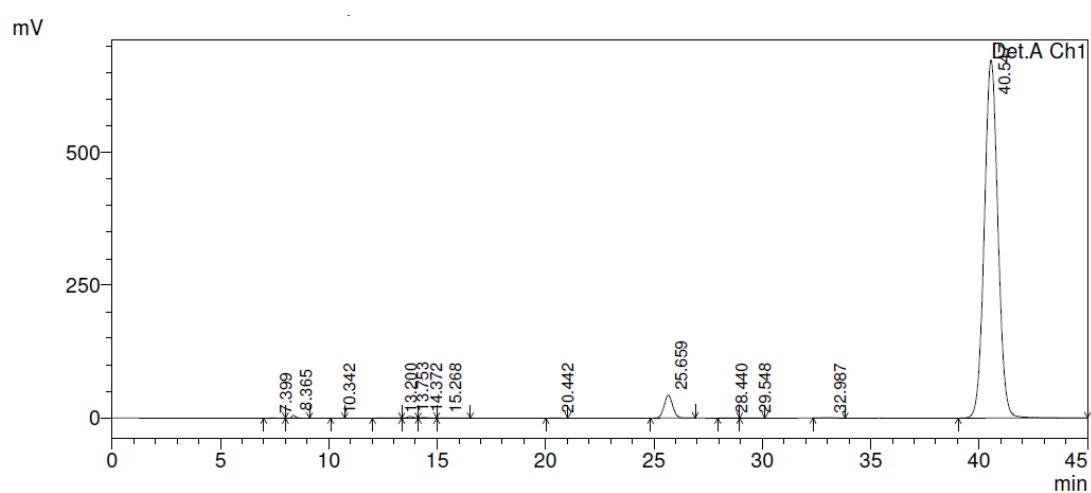


Figure B.3 Sample HPLC chromatogram for Anaerobic respiratory growth condition in the presence of DMSO

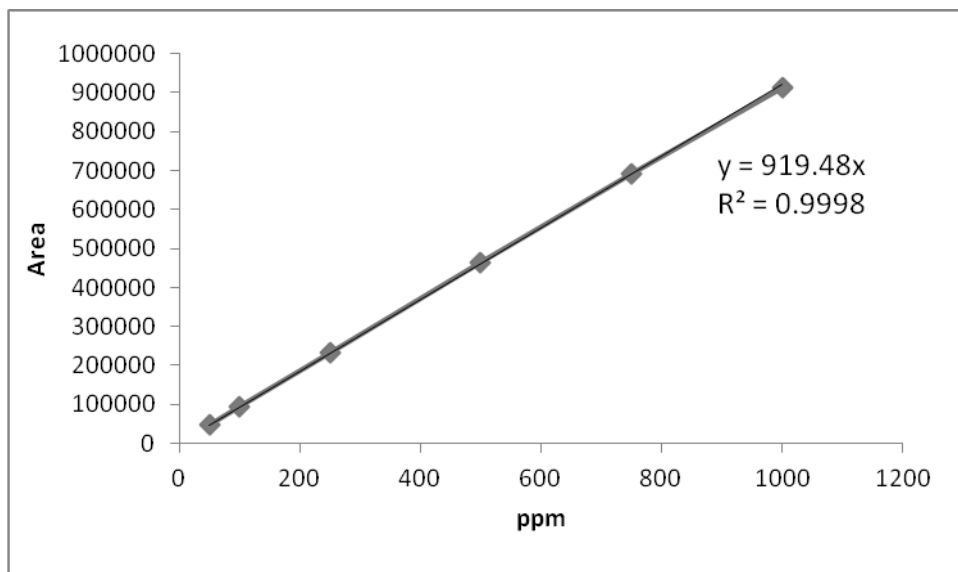


Figure B.4 Calibration Curve for Acetic Acid

Table B.1 HPLC analysis of LC-MS/MS samples

Acetate Concentrations	T_0	T_{final}	Consumption %
Aerobic respiratory 1	37.62	32.81	12.78
Aerobic respiratory 1	37.07	32.60	12.06
Aerobic respiratory 3	28.86	26.53	8.06
Photofermentative 1	37.22	23.35	37.27
Photofermentative 2	36.77	21.51	41.50
Photofermentative 3	36.24	33.72	6.96
Anaerobic respiratory 1	37.32	31.13	16.59
Anaerobic respiratory 2	36.80	22.00	40.22
Anaerobic respiratory 3	36.43	21.43	41.18

T_{final} corresponds the sampling time when the OD reached approximately 0.5 for each growth condition. Thus for aerobic respiratory and photofermentative growth it is approximately 6 hours, whereas in anaerobic respiratory condition 48 hours.

APPENDIX C

COMPONENTS OF THE SOLUTIONS USED IN SDS POLYACRYLAMIDE GEL ELECTROPHORESIS

1.5mM Tris pH 8.8, 0.4% SDS was prepared by adding 18g Tris Base and 0.4 g SDS in 100mL distilled H₂O, pH was adjusted to 8.8 with HCl.

0.5M Tris-HCL pH 6.8, 0.4% SDS was prepared by adding 6.055g Tris and 0.4 g SDS in 100 mL distilled H₂O and pH was adjusted to 6.8 with HCl.

10% Ammonium persulfate prepared by adding 1g APS in 10mL H₂O

Table C.1 The composition of 10X SDS Running Buffer

Components	Amount
25mM Tris	30.3 g
20mM Glycine	188 g
SDS (1%)	10g

All the components were added to 1 L of distilled H₂O pH was adjusted to 8.3

Table C.2 The composition of 6X Loading Buffer

Components	Amount
0.5 M Tris HCl (pH 6.8)	1.2 mL
Glycerol	4.7 mL
SDS	1.2 g
Bromophenol Blue	6 mg
Distilled H ₂ O	2.1 mL
β-Mercapto ethanol	50 μL (freshly added for 950μL)

Table C.3 The composition of the SDS Polyacrylamide gel

Components	Amounts in 12% Gel	Amounts in 6% stacking Gel
Distilled H ₂ O	2.6 mL	2.6 mL
30% Bis-Acrylamide	3.2 mL	1 mL
Tris	2.2 mL 1.5 M TRIS pH 8.8	1.25 mL 0.5 M TRIS pH 6.8
10% SDS	80 µL	50 µL
10 % APS	80 µL	50µL
TEMED	8 µL	5 µL
Total volume	8mL	5mL

Table C.4 The composition of Coomassie Gel stain and destaining solution

Components	Staning solution	Destaining Solution
Coomassie Brilliant Blue R-250	2.5 g	-
Ethanol	500 mL	165 mL
Ultrapure H ₂ O	400 mL	785 mL
Acetic Acid	100 mL	50 mL

APPENDIX D

CELL COUNT EXPERIMENTS AND MICROSCOPY IMAGES

For the cell count experiments, grown bacterial cells were observed under light microscope in phase-contrast mode using a hemocytometer plate with Zeiss LSM 510.

Total of 5 counts were done in 5 different regions in the hemocytometer.

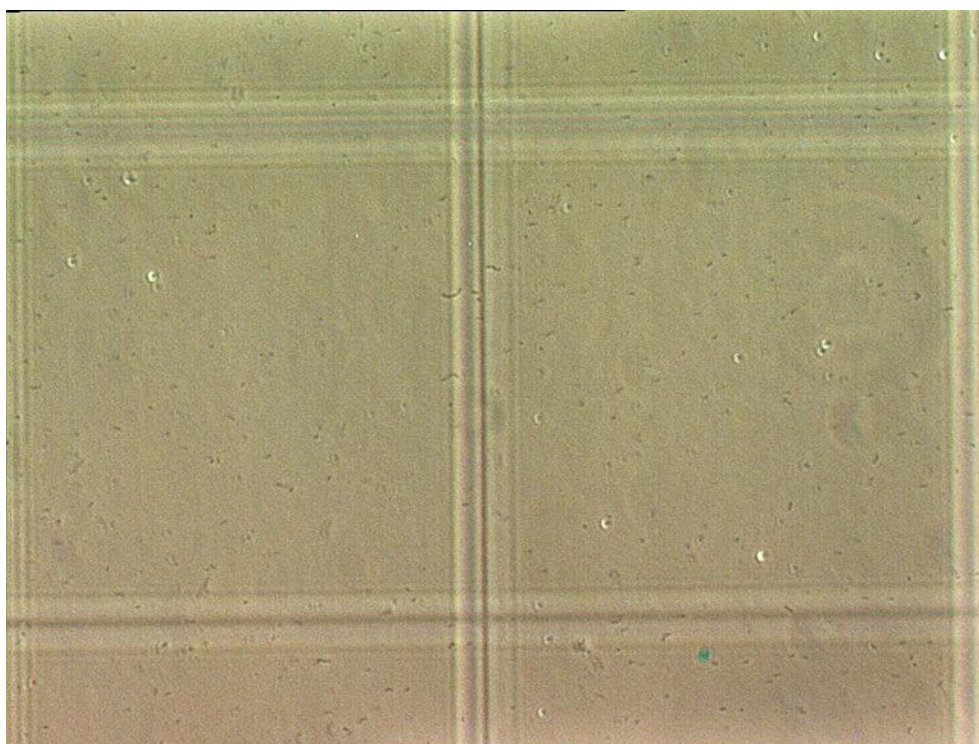


Figure D.1 Phase-contrast image of *R. capsulatus* used in cell counting experiments

According to the cell counts, optical density of 1 corresponds to 1.3×10^9 cells/ mL.

APPENDIX E

BACTERIA DRY CELL WEIGHT CURVES

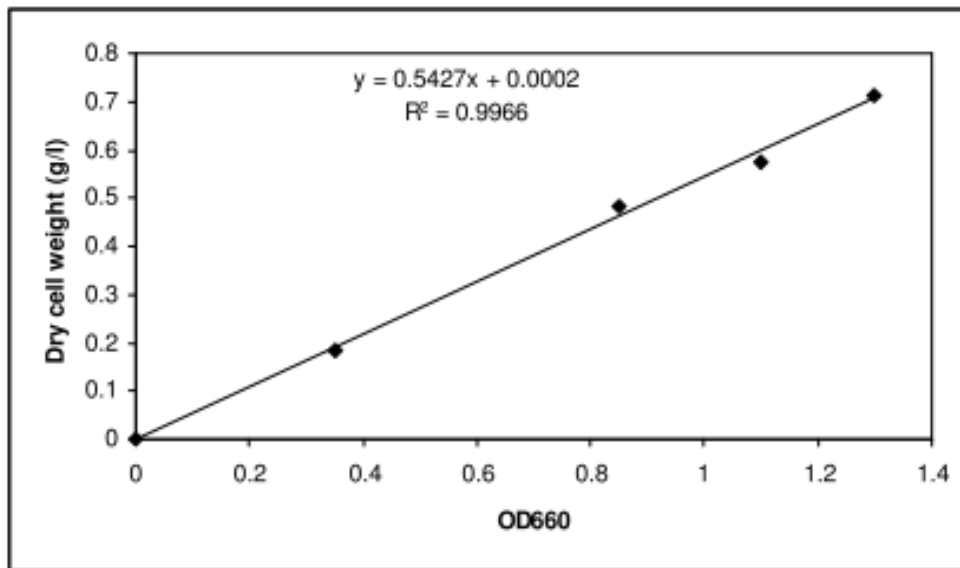


Figure E.1 Dry cell weight calibration curve of *Rhodobacter capsulatus*

APPENDIX F

SAMPLE NANO-DROP SPECTRUM FOR ISOLATED PROTEINS

The spectrum shown is composed of several readings represented in different colors.

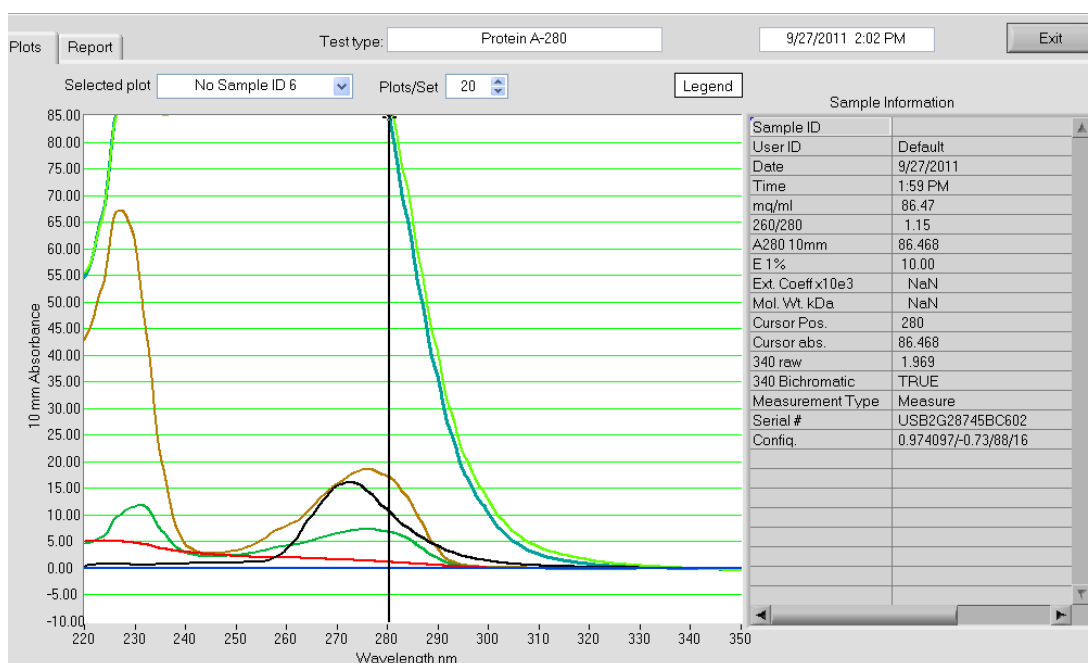


Figure F.1 A representative Nano-Drop spectrum for Protein readings at 280nm

APPENDIX G

PRINCIPLE COMPONENT ANALYSIS

Mathematically, Principle component analysis depends on the eigen-decomposition of positive semi-definite matrices and singular value decomposition of rectangular matrices. The components are obtained by the singular value decomposition of the data table X.

$$X = P\Delta Q^T \quad (G-1)$$

Whereas, P is the $I \times L$ matrix of left singular vectors, Q is the $J \times L$ matrix of right singular vectors and Δ is the diagonal matrix of singular values.

The inertia of a column is computed as ;

$$\gamma_j^2 = \sum_i x_{i,j}^2. \quad (G-2)$$

The center of gravity (g) of the rows is the vector of the means of each column in the data table X. The Euclidean distance of the i-th observation to g is equal to;

$$d_{i,g}^2 = \sum_j (x_{i,j} - g_j)^2. \quad (G-3)$$

When the data is centered, the equation G-3 becomes;

$$d_{i,g}^2 = \sum_j x_{i,j}^2. \quad (G-4)$$

Fig. G-1 summarizes the geometrical steps for finding the principles component analysis. First, the variables were plotted against each other, then the first principle component was obtained by pointing the main direction in the data, then the second component orthogonal to the first component was obtained.

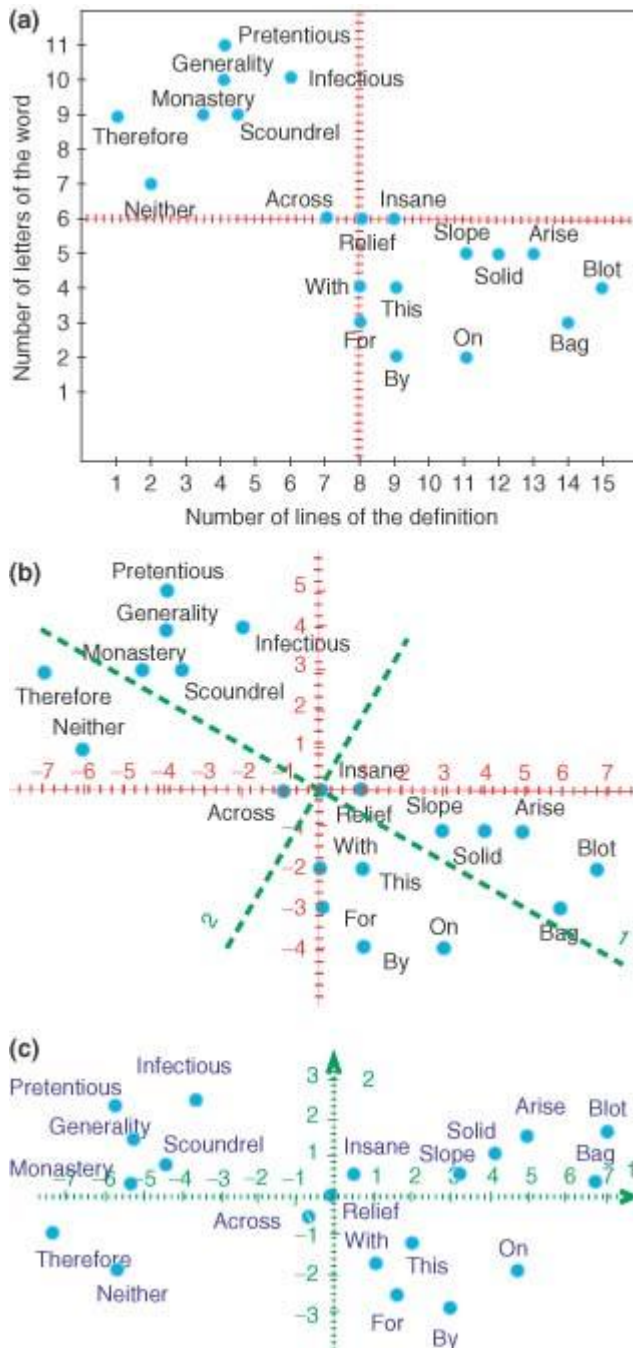



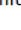
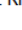
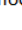

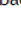
Figure G-1 Geometrical steps for finding components of principal component analysis (Abdi and Williams, 2010)

APPENDIX H

PROTEIN DETERMINATION AND QUANTIFICATION BY PROGENESIS SOFTWARE

In the following Fig. H-1, list of the peptides used in identification of Light harvesting protein B 870 alpha subunit is represented. In Fig. H-2, the identification of feature 1663 was represented along with the abundance values for each condition. A,B and C corresponds to growth conditions in which A corresponds to aerobic respiratory, B corresponds to anaerobic respiratory in the presence of DMSO and C corresponds to photofermentative growth modes of *Rhodobacter capsulatus*. Lastly, Fig. H-3 represents the abundance of the proteins in different growth conditions by box-plots.

D5AP85 RHOCB SubName Full Light harvesting protein B 870 alpha subunit Rhodobacter capsulatus
8 peptides

Sequence	Feature	Score	Hits	Mass	Charge	Tags	Conflicts	Modifications	In quantitation	Average Normalised Abundances		
										A	B	C
DPR	6171	0.00	2	386.1934	1		0		yes	29.04	46.75	53.96
HGYVAAAQ	4748	5.93	1	815.4274	2		1		no	95.52	104.07	105.82
IWL	1265	0.00	17	412.2501	1		0		yes	430.64	568.16	694.28
IWL	1475	0.00	16	511.3177	1		0		yes	892.40	766.44	973.79
IWL	434	8.54	17	1044.5806	1		0		yes	1270.59	2314.42	3138.93
IWL	32	8.54	17	1044.5726	2		0		yes	6366.03	8879.49	1.08e+004
L	93	0.00	15	745.4082	1		0		yes	8605.17	9476.50	1.03e+004
V	228	0.00	15	632.3262	1		0		yes	4624.10	4576.70	5791.76
W	1663	0.00	16	931.4912	1		0		yes	883.71	1163.54	1442.56
W	2834	0.00	15	931.4907	2		0		yes	244.29	304.98	470.37



Tags	
	Most Abundant
	Anova p-value \leq 0.05

Figure H-1 Representation of protein identification by Progenesis software

Charge 1
m/z 932.4985
Retention Time 129.8

Notes

- Anova p-value ≤ 0.05
- Most Abundant

Score	Protein	Description
0.00	D5AP85	D5AP85 RHO CB SubName Full Light harvesting protein B 870 alpha subunit Rhodobacter capsulatus

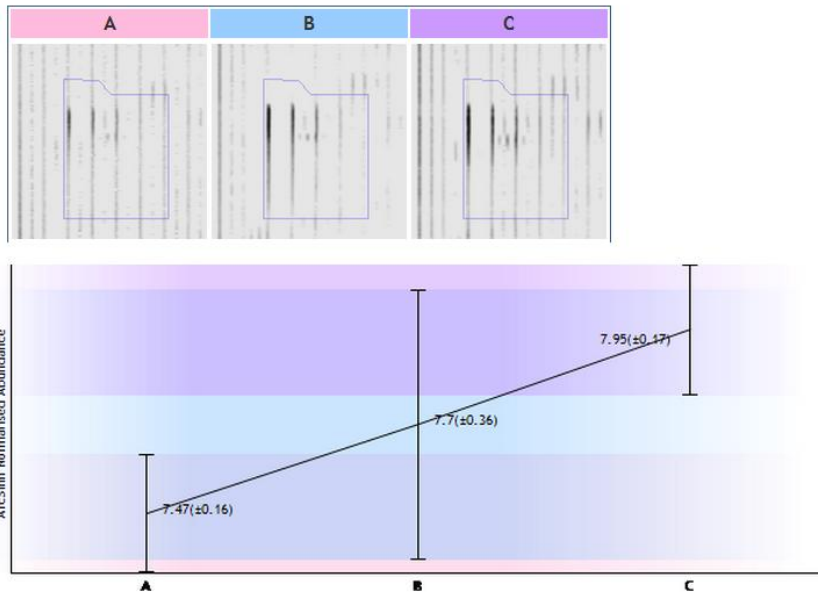


Figure H-2 Representation of peptide quantification by the feature on mass/charge ratio vs retention time graph

Description D5AP85 RHO CB SubName Full Light harvesting protein B 870 alpha subunit Rhodobacter capsulatus

Peptides 8 (7)

Score 23.01

Anova 0.01

Fold 1.44

● Anova p-value ≤ 0.05

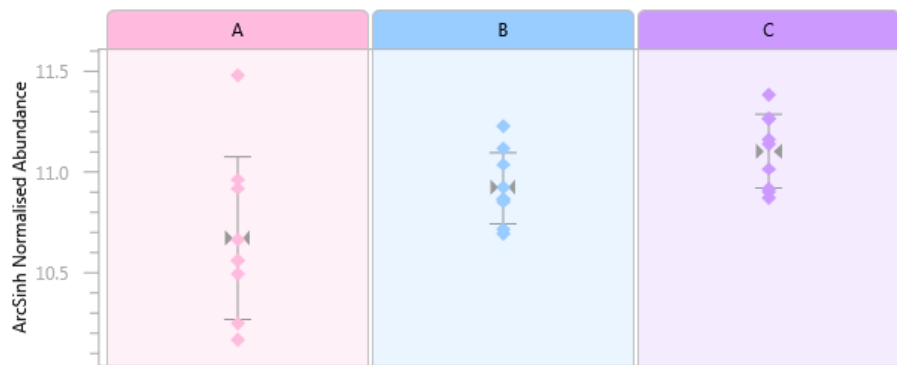


Figure H-3 Box plot representation of Light harvesting protein B 870 alpha subunit of *Rhodobacter capsulatus*

APPENDIX-I

LIST OF IDENTIFIED PROTEINS BY LC-MS/MS METHOD

The score calculated by the PLGS reports the probability that a protein in the mixture of proteins that constitutes the sample. Therefore, it is possible to obtain more than one hits with the highest probability of being correct.

The MS/MS data analysis, peptide sequence is constructed by the match of synthetic digestion of protein sequences in the databases with the precursor ion mass within the defined tolerance limits. For the given peptide sequence the probability of the fragment spectrum is calculated and the natural logarithm of this is peptide score.

Peptide scores are then used to compile the combinations of the proteins that are most likely to occur in the data set. The probability of the whole data set is then calculated with each given combinations and the probability for a protein is accumulated whenever it appears in a combination. According to Bayes' theorem probability of protein present in the mixture is calculated and it is assumed that the prior probability of each combination is related to the number of proteins in it. Only the highest scoring peptide match is being reported for each precursor ion and the related fragmentation data. Therefore the score represents;

$$\text{Probability of A in mixture GIVEN dataset} = \frac{(\text{SUM over Probabilities of Combinations Containing A})}{(\text{SUM over Probabilities of all Combinations})}$$

Comparison of the scores of the first two hits for a particular protein used to determine the correctness of the hit in practice. If there is a difference of five (factor of ~150) is

sufficient to indicate the top-scoring protein is correct. This curation was carried out automatically by the PLGS and the proteins listed are within the 95% of the significance threshold.

Table I.4 The list of identified proteins by LC-MS/MS and PLGS software

Description	Score
D5ALM7 RHO�B RecName Full Anthranilate phosphoribosyltransferase	113.74
D5AP47 RHO�B RecName Full Ribose phosphate pyrophosphokinase	156.5
D5ALM3 RHO�B SubName Full Peptidyl prolyl cis trans isomerase D	97.6
D5ARY6 RHO�B SubName Full Ferredoxin I	316.94
D5ARY3 RHO�B SubName Full Peroxiredoxin	1104.7
D5AP40 RHO�B SubName Full Bifunctional sulfate adenylyltransferase adeny	157.22
D5ARY1 RHO�B SubName Full Nitrogenase molybdenum iron cofactor biosynthe	119.86
D5ARY0 RHO�B SubName Full Nitrogen fixation protein NifX	402.9
D5ALL9 RHO�B SubName Full Enoyl acyl carrier protein reductase 1	322.66
D5ARX9 RHO�B SubName Full Putative uncharacterized protein	212.15
D5AS97 RHO�B SubName Full Ubiquinone biosynthesis hydroxylase UbiH UbiF	176.72
D5AS95 RHO�B SubName Full Urea ABC transporter ATP binding protein UrtD	168.04
D5AP32 RHO�B SubName Full Putative uncharacterized protein	449.48
D5ARX4 RHO�B SubName Full HesB YadR YfhF family protein	264.52
D5AS92 RHO�B SubName Full Urea ABC transporter urea binding protein Urt	244.88
D5AP25 RHO�B SubName Full Oligoendopeptidase F	127.91
D5AS84 RHO�B SubName Full Aromatic amino acid aminotransferase	603.23
D5ARW4 RHO�B SubName Full Putative uncharacterized protein	282.46
D5AS83 RHO�B SubName Full 3 mercaptopyruvate sulfurtransferase	133.52
D5ARW3 RHO�B SubName Full TOBE domain protein	7719.04

Table I.4 continued

D5AP15 RHO�B SubName Full Ferredoxin II	344.22
D5AP11 RHO�B SubName Full O acetylhomoserine aminocarboxypropyltransfera	612.26
D5ARV0 RHO�B RecName Full Ketol acid reductoisomerase	1807.82
D5ALI0 RHO�B RecName Full Bifunctional purine biosynthesis protein purH	88.37
D5ALH7 RHO�B SubName Full Peptidase M16 family	90.09
D5AUZ1 RHO�B SubName Full Nitrilotriacetate monooxygenase component B	341.28
D5ALG8 RHO�B SubName Full Porin family protein	2589.76
D5ALG7 RHO�B SubName Full Lipoprotein putative	489.88
D5ALG6 RHO�B RecName Full Leucyl tRNA synthetase	171.21
D5AUY8 RHO�B SubName Full DNA polymerase III beta subunit	517.84
D5ALF8 RHO�B SubName Full DNA binding protein HU 1	2580.94
D5ALF2 RHO�B RecName Full 2 3 4 5 tetrahydropyridine 2 6 dicarboxylate N	181.59
D5AS36 RHO�B SubName Full Thioredoxin 2	311.15
D5AV98 RHO�B SubName Full Aconitate hydratase	240.98
D5AV94 RHO�B SubName Full Transketolase 2	341.56
D5ARR0 RHO�B RecName Full Porphobilinogen deaminase	508.9
D5ARQ9 RHO�B RecName Full Uroporphyrinogen decarboxylase	119.04
D5AUW9 RHO�B SubName Full Putative uncharacterized protein	228.36
D5ALE0 RHO�B SubName Full Putative uncharacterized protein	410.73
D5AUW6 RHO�B RecName Full 30S ribosomal protein S6	116.32
D5AUW5 RHO�B RecName Full 30S ribosomal protein S18	223.46
D5AS22 RHO�B SubName Full Putative uncharacterized protein	125.04
D5AUW4 RHO�B RecName Full 50S ribosomal protein L9	3694.75
D5AUW3 RHO�B RecName Full Trigger factor	1322.52
D5AS20 RHO�B RecName Full DNA directed RNA polymerase subunit omega	796.19
D5ALD7 RHO�B SubName Full Oxidoreductase DSBA family	212.93

Table I.4 continued

D5ARP8 RHOCB SubName Full Cytochrome c oxidase Cbb3 type accessory pro	322.66
D5ALD3 RHOCB RecName Full Chaperone protein dnaK	483.01
D5ARP7 RHOCB SubName Full Cytochrome c oxidase Cbb3 type subunit III	194.84
D5ARP5 RHOCB SubName Full Cytochrome c oxidase Cbb3 type subunit II	1004.24
D5AS14 RHOCB SubName Full Signal peptidase I	210.63
D5ARP3 RHOCB SubName Full UspA domain protein	252.54
D5AS12 RHOCB RecName Full GTP binding protein era homolog	177.32
D5AV74 RHOCB RecName Full Acetyl coenzyme A synthetase 1	185.95
D5ARP1 RHOCB RecName Full 1 5 phosphoribosyl 5 5 phosphoribosylamino	157.73
D5ALC8 RHOCB SubName Full PpiC type peptidyl prolyl cis trans isomerase	146.21
D5ALC7 RHOCB SubName Full Arginine biosynthesis bifunctional protein Arg	128.46
D5ALC4 RHOCB RecName Full Translation initiation factor IF 2	118.16
D5AS08 RHOCB SubName Full Acyl CoA dehydrogenase medium chain specific	1497.15
D5ALC2 RHOCB SubName Full Transcription elongation factor NusA	132.97
D5ALB9 RHOCB RecName Full 3 demethylubiquinone 9 3 methyltransferase	366.23
D5ALB7 RHOCB RecName Full Argininosuccinate synthase	692.78
D5AV58 RHOCB SubName Full Multicopper oxidase family protein	199.35
D5ARN5 RHOCB SubName Full Pyrroline 5 carboxylate reductase	278.54
D5AV57 RHOCB SubName Full Putative uncharacterized protein	198.04
D5ARN1 RHOCB RecName Full Glycine dehydrogenase decarboxylating	106.24
D5ARM8 RHOCB SubName Full Glutamyl tRNA synthetase 1	168.69
D5ALA3 RHOCB SubName Full ErfK YbiS YcfS YnhG family protein Tat domain	171.39

Table I.4 continued

D5ALA2 RHOCB SubName Full SCP like extracellular protein	269.93
D5AV42 RHOCB SubName Full MaoC family protein	742.78
D5ARL6 RHOCB RecName Full Tryptophan synthase beta chain 1	200.45
D5ARL3 RHOCB RecName Full Integration host factor subunit beta	955.27
D5ARL2 RHOCB SubName Full 30S ribosomal protein S1	546.7
D5ARK7 RHOCB RecName Full S adenosylmethionine synthase	349.1
D5ARK3 RHOCB SubName Full PhoH family protein	207.86
D5ARK2 RHOCB SubName Full Lipoprotein putative	548.91
D5ARK1 RHOCB SubName Full OmpA MotB domain protein	239.57
D5AV20 RHOCB RecName Full Nicotinate nucleotide dimethylbenzimidazole p	219.73
D5ARG2 RHOCB SubName Full Crotonyl CoA reductase	129.63
D5ARG1 RHOCB SubName Full Putative uncharacterized protein	235.78
D5ARG0 RHOCB SubName Full Methylmalonyl CoA mutase large subunit	123.96
D5AUM1 RHOCB RecName Full Inosine 5 monophosphate dehydrogenase	338.23
D5ARF8 RHOCB SubName Full Transcriptional regulator AsnC Lrp family	1149.97
D5AUL8 RHOCB RecName Full Integration host factor subunit alpha	340.67
D5AUL5 RHOCB RecName Full 50S ribosomal protein L32	1334.38
D5ARF1 RHOCB SubName Full Basic membrane lipoprotein family	730.81
D5AL83 RHOCB SubName Full dTDP 4 dehydrorhamnose reductase	280.03
D5AL82 RHOCB RecName Full Glucose 1 phosphate thymidyltransferase	205.47
D5AUJ3 RHOCB RecName Full Isocitrate dehydrogenase NADP	1024.21
D5ARC9 RHOCB RecName Full Probable transaldolase	659.94
D5AL74 RHOCB SubName Full NAD dependent epimerase dehydratase family pro	211.04
D5AUI7 RHOCB SubName Full FeS assembly protein SufB	103.8
D5AUI5 RHOCB SubName Full FeS assembly ATPase SufC	228.21
D5AUI4 RHOCB SubName Full FeS assembly protein SufD	144.73

Table I.4 continued

D5AUH8 RHO�B RecName Full UDP 3 O 3 hydroxymyristoyl glucosamine N acy	223.29
D5ARB5 RHO�B RecName Full Protein tolB	225.15
D5ARB4 RHO�B SubName Full OmpA MotB domain protein	1211.11
D5AUH5 RHO�B SubName Full Invasion associated locus B family protein	189.61
D5ARB1 RHO�B SubName Full Cell division protease FtsH	200.66
D5AL56 RHO�B RecName Full Elongation factor Tu	8390.03
D5ANZ8 RHO�B SubName Full Polar amino acid ABC transporter periplasmic	827.46
D5AL53 RHO�B SubName Full Electron transfer flavoprotein beta subunit	1018.79
D5AL52 RHO�B SubName Full Electron transfer flavoprotein alpha subunit	210.55
D5ANZ4 RHO�B SubName Full Ubiquinol cytochrome c reductase cytochrome	649.58
D5AL51 RHO�B RecName Full Superoxide dismutase	1031.97
D5ANZ2 RHO�B RecName Full Ubiquinol cytochrome c reductase iron sulfur s	803.26
D5AUG5 RHO�B RecName Full 3 dehydroquinate synthase	198.44
D5ANY9 RHO�B SubName Full Branched chain amino acid transaminase 1	445.09
D5AKS6 RHO�B SubName Full Polyamine ABC transporter periplasmic polyami	619.06
D5AL43 RHO�B SubName Full PQQ enzyme repeat family protein	123.12
D5AKS2 RHO�B SubName Full Aminotransferase class III	87.84
D5AUF8 RHO�B SubName Full Branched chain amino acid ABC transporter per	337.67
D5AL40 RHO�B RecName Full 50S ribosomal protein L21	840.01
D5ANY2 RHO�B RecName Full UPF0133 protein RCAP rcc02758	373.31
D5AUF6 RHO�B SubName Full 3 deoxy 7 phosphoheptulonate synthase	177.01

Table I.4 continued

D5AL39 RHOCB RecName Full 50S ribosomal protein L27	1039.5
D5ANX7 RHOCB RecName Full Glutamyl tRNA Gln amidotransferase subunit A	288.65
D5ANX3 RHOCB RecName Full 50S ribosomal protein L33	167.46
D5AUE5 RHOCB RecName Full Glycogen synthase	141.13
D5AUE3 RHOCB SubName Full Phosphoglucomutase	274.53
D5AUE0 RHOCB RecName Full Fructose 1 6 biphosphatase class 1	297.68
D5AKQ6 RHOCB SubName Full Putative uncharacterized protein	151.41
Random Sequence 3028	146.12
D5AUD9 RHOCB RecName Full Phosphoribulokinase	403.78
D5AUD8 RHOCB SubName Full Transketolase 1	104.69
D5AUD7 RHOCB SubName Full Glyceraldehyde 3 phosphate dehydrogenase 1	316.48
D5AKQ0 RHOCB SubName Full 3 2 5 bisphosphate nucleotidase	553.67
D5AUD6 RHOCB SubName Full Fructose bisphosphate aldolase	132.43
D5AUD5 RHOCB RecName Full Ribulose bisphosphate carboxylase	145.29
D5AUD4 RHOCB SubName Full Ribulose phosphate 3 epimerase 1	357.43
D5AUD0 RHOCB SubName Full Putative uncharacterized protein	141.83
D5AKP8 RHOCB SubName Full UTP glucose 1 phosphate uridylyltransferase	375.68
D5AL18 RHOCB SubName Full Oligopeptide ABC transporter ATP binding prot	141.49
D5AL15 RHOCB SubName Full Oligopeptide ABC transporter periplasmic olig	3120.26
D5AL14 RHOCB RecName Full Proline iminopeptidase	110.88
D5AL13 RHOCB SubName Full Putative uncharacterized protein	151.4
D5AUC8 RHOCB RecName Full Elongation factor Ts	819.12
D5AKP1 RHOCB SubName Full Sigma 54 modulation protein ribosomal protein	759.18
D5AUC7 RHOCB RecName Full 30S ribosomal protein S2	2095.04
D5AL08 RHOCB SubName Full Polyamine ABC transporter periplasmic polyami	125.73

Table I.4 continued

D5AUB4 RHOCB RecName Full Delta aminolevulinic acid dehydratase	129.11
D5ANT8 RHOCB SubName Full Magnesium chelatase ATPase subunit I	262.96
Random Sequence 913	160.89
D5ANT4 RHOCB SubName Full Geranylgeranyl reductase	134.58
D5AQZ4 RHOCB SubName Full Membrane protein putative	901.48
D5ANT0 RHOCB SubName Full Magnesium protoporphyrin IX monomethyl ester a	130.66
D5ANS5 RHOCB RecName Full Light independent protochlorophyllide reductas	102.75
D5ANS3 RHOCB RecName Full Light independent protochlorophyllide reductas	92.31
D5ANS0 RHOCB SubName Full Photosynthetic reaction center H subunit	2203.48
D5AR98 RHOCB SubName Full Acetoacetyl CoA reductase	1398.4
D5AR97 RHOCB SubName Full Acetyl CoA acetyltransferase 2	891.93
Random Sequence 3334	553.76
D5AKK8 RHOCB RecName Full 3 isopropylmalate dehydrogenase	382.02
D5AKK4 RHOCB RecName Full 3 isopropylmalate dehydratase large subunit	91.11
D5AKK1 RHOCB RecName Full Ribosomal RNA large subunit methyltransferase	373.7
D5AKK0 RHOCB RecName Full 2 3 bisphosphoglycerate independent phosphogly	179.68
D5AR84 RHOCB RecName Full Acetyl coenzyme A carboxylase carboxyl transfe	134.46
D5AR83 RHOCB SubName Full Citrate lyase beta subunit 2	253.31
D5AR82 RHOCB SubName Full Putative uncharacterized protein	309.06
D5AR80 RHOCB SubName Full D amino acid transaminase	152.87
D5AKJ8 RHOCB SubName Full C terminal processing peptidase	163.36
D5AR73 RHOCB RecName Full 50S ribosomal protein L20	236.05

Table I.4 continued

Random Sequence 3311	229.07
D5AKI8 RHOCB SubName Full Transcription termination factor Rho	173.75
D5AR65 RHOCB SubName Full 4 aminobutyrate aminotransferase 1	4606.1
D5AR60 RHOCB SubName Full Cold shock like protein CspD	11264.61
Random Sequence 2577	251.96
D5AKH5 RHOCB SubName Full Putative uncharacterized protein	191.35
D5ANN5 RHOCB SubName Full Amino acid ABC transporter periplasmic amino	418.74
D5AKH2 RHOCB RecName Full Adenosylhomocysteinase	251.33
D5ANN2 RHOCB SubName Full Signal transduction histidine kinase	142.09
D5AKG9 RHOCB SubName Full Trans acting regulatory protein HvrA	244.79
D5AKG8 RHOCB SubName Full Photosynthetic apparatus regulatory protein Re	1133.79
D5ANM8 RHOCB SubName Full Secretion protein HlyD family	158.95
D5AR48 RHOCB RecName Full 50S ribosomal protein L28	294.41
D5AQS6 RHOCB SubName Full Putative uncharacterized protein	454.5
D5AR44 RHOCB SubName Full Heavy metal transport detoxification protein f	798.27
D5ATY6 RHOCB SubName Full 3 oxoacyl acyl carrier protein synthase II 1	245.82
D5ATY2 RHOCB SubName Full 3 oxoacyl acyl carrier protein reductase	102.77
D5ATY1 RHOCB SubName Full acyl carrier protein S malonyltransferase	193.77
D5ATY0 RHOCB RecName Full Glutamine synthetase	2748.73
D5AKF9 RHOCB SubName Full Thioredoxin 1	888.74
D5AKF4 RHOCB SubName Full Import inner membrane translocase subunit Tim	81.2
D5ATX9 RHOCB SubName Full Nitrogen regulatory protein P II 1	2195.59
D5AKF2 RHOCB RecName Full Protein export protein secB	233.37
D5AKE1 RHOCB SubName Full Xylose ABC transporter xylose binding protein	1000.43

Table I.4 continued

D5AU87 RHO�B SubName Full Preprotein translocase YajC subunit	492.56
D5AQP9 RHO�B SubName Full Type I secretion outer membrane protein TolC	294.69
D5AQP3 RHO�B SubName Full Putative uncharacterized protein	226.91
D5AU74 RHO�B SubName Full Glucokinase	250.22
D5ANI4 RHO�B SubName Full Ferredoxin V	332.66
D5ANI3 RHO�B RecName Full Nitrogenase iron protein 1	2753.36
D5AU67 RHO�B SubName Full Putative uncharacterized protein	197.49
D5ANI2 RHO�B RecName Full Nitrogenase protein alpha chain	1278.98
D5ANI1 RHO�B SubName Full Nitrogenase molybdenum iron protein beta chain	597.66
D5AR01 RHO�B SubName Full Iron siderophore cobalamin ABC transporter pe	323.09
D5AQN7 RHO�B SubName Full Succinyl CoA 3 ketoacid CoA transferase subun	271.6
D5AQN6 RHO�B SubName Full Succinyl CoA 3 ketoacid CoA transferase subun	422.51
D5ATT8 RHO�B SubName Full Outer membrane protein assembly factor YaeT	178.1
D5AU58 RHO�B RecName Full Alanyl tRNA synthetase	133.4
D5ANH3 RHO�B SubName Full Molybdenum ABC transporter periplasmic molybd	474.73
D5AU57 RHO�B RecName Full Protein recA	178.51
D5ATT6 RHO�B SubName Full Peptidase M50 family	153.05
D5ATT2 RHO�B RecName Full Ribosome recycling factor	206.08
D5ATT1 RHO�B SubName Full Uridylate kinase	181.15
D5ANG4 RHO�B RecName Full N acetyl gamma glutamyl phosphate reductase	128.43
D5ANG0 RHO�B RecName Full Phosphoribosylformylglycinamide synthase 2	348.95
D5ANF8 RHO�B SubName Full Glutaredoxin family protein	248.36
D5AQL7 RHO�B SubName Full Lipoprotein putative	633.89

Table I.4 continued

D5ANF1 RHOCB SubName Full Aspartate semialdehyde dehydrogenase	286.29
D5ANF0 RHOCB SubName Full Putative uncharacterized protein	156.58
D5AQL0 RHOCB SubName Full 3 4 dihydroxy 2 butanone 4 phosphate synthase	143.2
D5ATR1 RHOCB SubName Full Thiamine monophosphate synthase	380.75
Random Sequence 2849	320.98
D5ANE2 RHOCB SubName Full Cytochrome c b561 family protein	105.55
D5AU26 RHOCB RecName Full Nucleoside diphosphate kinase	729.95
D5AQL2 RHOCB SubName Full Putative uncharacterized protein	241.21
D5ATQ4 RHOCB RecName Full Triosephosphate isomerase	108.53
D5AU21 RHOCB RecName Full Enolase	1806.08
D5ATQ0 RHOCB SubName Full Sulfite reductase	161.94
D5AQJ7 RHOCB SubName Full Fructose 1 6 biphosphatase	120.64
D5ATP7 RHOCB SubName Full Ferredoxin NADP reductase	284.01
D5AU16 RHOCB RecName Full Peptidyl prolyl cis trans isomerase	220.17
D5AND1 RHOCB SubName Full Chaperone SurA	136.68
D5AU15 RHOCB RecName Full Peptidyl prolyl cis trans isomerase	168.94
D5AU14 RHOCB RecName Full Phosphoglycerate kinase	763.37
D5AU13 RHOCB SubName Full Fructose biphosphate aldolase	997.39
D5AU10 RHOCB SubName Full Pyruvate dehydrogenase complex E1 component	99.64
D5ANC8 RHOCB SubName Full Putative uncharacterized protein	868.52
D5ANC5 RHOCB SubName Full Glutathione S transferase family protein	201.49
D5ANC4 RHOCB SubName Full Polyphosphate kinase 2 domain protein	129.02
D5AQI5 RHOCB RecName Full 50S ribosomal protein L25	556.82
D5ANC2 RHOCB SubName Full Cytochrome c	2357.67
D5ANC1 RHOCB SubName Full Cytochrome b561 family protein	149.46
D5ANB1 RHOCB RecName Full Elongation factor P	735.98
D5ATN4 RHOCB SubName Full Lipoprotein putative	399.33

Table I.4 continued

D5ATN2 RHO�B SubName Full Orotate phosphoribosyltransferase	242.39
D5ANA8 RHO�B SubName Full 3 oxoacyl acyl carrier protein synthase I	148.33
D5ATM5 RHO�B RecName Full Amidophosphoribosyltransferase	113.68
D5ATM1 RHO�B SubName Full Methylmalonate semialdehyde dehydrogenase	225.45
D5AQF9 RHO�B SubName Full TRAP dicarboxylate transporter DctP 3 subunit	611.92
D5AQF1 RHO�B SubName Full Aldolase DeoC LacD family	238.46
D5ATL2 RHO�B RecName Full Dihydrolipoyl dehydrogenase	338.33
PYGM RABIT SubName Full Glycogen phosphorylase muscle form Rabbit	719.58
D5ATK7 RHO�B SubName Full Peroxiredoxin	115.66
D5ATK5 RHO�B SubName Full Putative uncharacterized protein	818.68
D5ATI3 RHO�B RecName Full NADH quinone oxidoreductase	88.33
D5ATH8 RHO�B SubName Full Putative uncharacterized protein	1584.71
D5ATH7 RHO�B SubName Full NADH quinone oxidoreductase E subunit	316.79
D5ATH6 RHO�B SubName Full NADH quinone oxidoreductase D subunit	135.97
D5AMY9 RHO�B SubName Full Electron transfer flavoprotein ubiquinone oxid	163.98
D5AMY7 RHO�B RecName Full 4 diphosphocytidyl 2 C methyl D erythritol kin	189.34
D5ATF1 RHO�B SubName Full Translation elongation factor G 2	433.81
D5AN97 RHO�B SubName Full Monosaccharide ABC transporter periplasmic mon	448.59
D5AMX5 RHO�B SubName Full Putative uncharacterized protein	4732.42
D5ATE9 RHO�B RecName Full GTP cyclohydrolase folE2	230.87
D5ATE7 RHO�B RecName Full 30S ribosomal protein S20	1141.63
D5AMX2 RHO�B RecName Full Valyl tRNA synthetase	201.58
D5ATE6 RHO�B SubName Full Enoyl CoA hydratase	148.93

Table I.4 continued

D5ATC8 RHOCB SubName Full Ribonuclease D 2	161.45
D5AMV2 RHOCB SubName Full Putative uncharacterized protein	168.61
D5ATC6 RHOCB RecName Full Phosphoribosylformylglycinamide cyclo ligase	254
D5AMU5 RHOCB SubName Full Tryptophanyl tRNA synthetase	112.45
D5AN60 RHOCB RecName Full Acetyl coenzyme A synthetase 2	182.77
D5AN57 RHOCB SubName Full 5 nucleotidase	142.01
D5AN49 RHOCB RecName Full ATP dependent Clp protease proteolytic subunit	123.76
D5AN48 RHOCB RecName Full ATP dependent Clp protease ATP binding subunit	1139.44
D5APY9 RHOCB RecName Full Histidinol phosphate aminotransferase	123.85
D5APY7 RHOCB RecName Full 30S ribosomal protein S4	616.33
D5AMS3 RHOCB RecName Full Uracil phosphoribosyltransferase	405.58
D5APY5 RHOCB SubName Full ATP dependent Clp protease ATP binding subunit	196.59
D5AN42 RHOCB SubName Full Acetyl CoA carboxylase biotin carboxylase	112.01
D5AN41 RHOCB SubName Full Acetyl CoA carboxylase biotin carboxyl carrier	300.58
D5APY2 RHOCB RecName Full ATP synthase subunit delta	558.36
D5APY1 RHOCB RecName Full ATP synthase subunit alpha	3126.67
D5APY0 RHOCB RecName Full ATP synthase gamma chain	210.29
D5AMR8 RHOCB SubName Full Propionate CoA ligase	92.37
D5APX9 RHOCB RecName Full ATP synthase subunit beta	5093.86
D5APX8 RHOCB RecName Full ATP synthase epsilon chain	694.01
D5AMR4 RHOCB RecName Full Serine hydroxymethyltransferase	125.17
D5AQ93 RHOCB RecName Full Phosphatidylserine decarboxylase proenzyme	179.5
D5AQ91 RHOCB RecName Full Bacterioferritin	151.14
D5AQ89 RHOCB SubName Full Propionyl CoA carboxylase alpha subunit	249.21

Table I.4 continued

D5AMQ6 RHOCB SubName Full ErfK YbiS YcfS YnhG family protein	227.94
D5APW8 RHOCB SubName Full Sialic acid synthase	88.85
D5APW7 RHOCB SubName Full Polyamine ABC transporter periplasmic polyami	1176.15
D5AN24 RHOCB SubName Full DNA binding protein HU 3	900.74
D5AQ86 RHOCB SubName Full Lipoprotein putative	21446.31
D5AMQ3 RHOCB RecName Full Pantothenate synthetase	89.47
D5AQ84 RHOCB SubName Full Propionyl CoA carboxylase beta subunit	111.29
D5APW3 RHOCB RecName Full Cysteine synthase	339.17
D5AMP7 RHOCB RecName Full Aspartokinase	124.63
D5AN14 RHOCB SubName Full Methylmalonyl CoA epimerase	682.25
D5AMP1 RHOCB SubName Full Oxidoreductase short chain dehydrogenase redu	206.07
D5AQ73 RHOCB SubName Full Glycine betaine L proline ABC transporter per	218.06
D5AN08 RHOCB RecName Full Aspartyl tRNA synthetase	228.82
D5AN07 RHOCB RecName Full Carbamoyl phosphate synthase large chain	107.39
D5AN06 RHOCB SubName Full Putative uncharacterized protein	120.84
D5AN00 RHOCB SubName Full Glyoxylate reductase 1	221.56
D5AMN9 RHOCB SubName Full Succinate semialdehyde dehydrogenase	316.85
D5AMN8 RHOCB SubName Full Arylformamidase	382.82
D5AMN2 RHOCB SubName Full Iron III ABC transporter periplasmic iron II	235.92
D5ASZ4 RHOCB SubName Full HemY domain protein	230.39
D5ASZ3 RHOCB SubName Full Putative uncharacterized protein	146.68
D5AMM3 RHOCB SubName Full Putative uncharacterized protein	403.33
D5ASY6 RHOCB SubName Full Phosphate ABC transporter periplasmic phospho	199.49

Table I.4 continued

D5AQ42 RHO�B RecName Full 30S ribosomal protein S9	112.83
D5AQ41 RHO�B RecName Full 50S ribosomal protein L13	1058.12
D5ASX7 RHO�B RecName Full Protein grpE	141.77
D5AT96 RHO�B RecName Full Sec independent protein translocase protein ta	371.98
D5ASX5 RHO�B RecName Full Ribonuclease PH	147.82
D5AQ32 RHO�B RecName Full Arginyl tRNA synthetase	101.17
D5ASX3 RHO�B SubName Full Endoribonuclease L PSP family	122.14
D5AMK4 RHO�B SubName Full Translation initiation factor IF 1	487.11
D5AT87 RHO�B RecName Full 4 hydroxy 3 methylbut 2 en 1 yl diphosphate sy	181.98
D5AQ24 RHO�B SubName Full Dipeptide ABC transporter periplasmic dipepti	405.37
D5AT85 RHO�B SubName Full 5 aminolevulinate synthase	108.2
D5ASW5 RHO�B SubName Full Flagellar M ring protein FliF	190.9
D5AT84 RHO�B SubName Full Peptidase M20 family	375.04
Random Sequence 2795	250.18
D5AQ19 RHO�B RecName Full Aspartyl glutamyl tRNA Asn Gln amidotransfera	232.24
D5AMJ2 RHO�B RecName Full Tryptophan synthase beta chain 2	292.4
D5AQ14 RHO�B SubName Full Cobaltochelataſe CobS subunit	211.26
D5AMJ1 RHO�B RecName Full Cysteine synthase	662.17
D5AQ11 RHO�B SubName Full Acetate kinase 1	112.05
D5AQ10 RHO�B SubName Full Phosphate acetyltransferase	336.06
D5AMI7 RHO�B SubName Full Light harvesting protein B 800 850 gamma chai	1121.83
D5AMI4 RHO�B SubName Full Light harvesting protein B 800 850 beta chain	243.67
D5AQ04 RHO�B RecName Full Cell division protein ftsZ	197.75
D5AT61 RHO�B SubName Full Putative uncharacterized protein	1211.71
D5AMH5 RHO�B SubName Full Pyrimidine ABC transporter periplasmic pyrimi	150.89

Table I.4 continued

D5APN7 RHOCB SubName Full Monosacharide ABC transporter periplasmic mon	191.73
D5APN6 RHOCB SubName Full Aldolase DeoC LacD family	225.92
D5AST7 RHOCB SubName Full Putative uncharacterized protein	585.62
D5AST0 RHOCB SubName Full Phosphoglycerate dehydrogenase	519.43
Random Sequence 1318	308.85
D5ASS9 RHOCB SubName Full Phosphoserine aminotransferase	485.53
D5AMG3 RHOCB SubName Full Toxic anion resistance protein TelA family	164.79
D5AT41 RHOCB SubName Full ABC transporter substrate binding protein	201.8
D5APL9 RHOCB RecName Full Acetyl coenzyme A synthetase 3	183.82
D5AMF5 RHOCB SubName Full Cytochrome c class I	1209.08
D5AME8 RHOCB SubName Full Oxygen independent coproporphyrinogen III oxid	113.27
D5AME4 RHOCB SubName Full OmpA family protein	386.07
D5APK6 RHOCB SubName Full Putative uncharacterized protein	109.12
D5ASP9 RHOCB SubName Full Endoribonuclease L PSP family protein	107.62
D5AT18 RHOCB SubName Full Iron containing alcohol dehydrogenase	310.1
D5AT17 RHOCB SubName Full Aldehyde dehydrogenase family protein	119.12
D5AMD2 RHOCB RecName Full 60 kDa chaperonin	2344.48
D5ASP6 RHOCB SubName Full Peroxiredoxin	373.04
D5AMD1 RHOCB RecName Full 10 kDa chaperonin	8927.3
D5AMD0 RHOCB SubName Full Inorganic pyrophosphatase	1672.69
D5AT08 RHOCB SubName Full ABC transporter periplasmic substrate binding	1638.97
D5AT02 RHOCB SubName Full 2 isopropylmalate synthase	123.15
D5AMB8 RHOCB SubName Full Prolyl tRNA synthetase	133.47
D5APH9 RHOCB SubName Full Basic membrane lipoprotein family	2433.11
D5AMB6 RHOCB SubName Full Membrane protein putative	406.5

Table I.4 continued

D5AMB4 RHO�B SubName Full Cold shock protein CspA 2	1018.73
D5APG5 RHO�B SubName Full Hydrogenase expression formation protein HupG	348.85
D5ASM2 RHO�B SubName Full Toluene tolerance family protein	235.06
D5ASM0 RHO�B SubName Full Nitrogen regulatory protein P II 2	4339.96
Random Sequence 463	230.02
D5APE5 RHO�B RecName Full Adenylosuccinate synthetase	157.79
D5APE1 RHO�B SubName Full Polyhydroxyalkanoate synthesis repressor PhaR	97.84
D5APE0 RHO�B SubName Full Putative uncharacterized protein	163.39
D5APD7 RHO�B SubName Full ATP synthase F0 B subunit	1226.98
D5APD6 RHO�B SubName Full ATP synthase F0 B subunit	860.06
D5APC9 RHO�B SubName Full Succinate dehydrogenase iron sulfur subunit	421.21
D5APC6 RHO�B SubName Full Succinate dehydrogenase flavoprotein subunit	137.88
D5APC3 RHO�B SubName Full MaoC domain protein	305.83
D5APC0 RHO�B SubName Full Citrate lyase beta subunit 1	114.88
D5APB9 RHO�B RecName Full Dihydrolipoyl dehydrogenase	149.53
D5APB8 RHO�B SubName Full Dihydrolipoyllysine residue succinyltransferas	695.71
D5APB7 RHO�B SubName Full Oxoglutarate dehydrogenase	400.56
D5APB4 RHO�B RecName Full Succinyl CoA ligase ADP forming subunit alph	383.1
D5APB3 RHO�B RecName Full Succinyl CoA ligase ADP forming subunit beta	2931.04
D5APB1 RHO�B RecName Full Malate dehydrogenase	2913.43
D5ALZ9 RHO�B RecName Full 50S ribosomal protein L22	432.42
D5ALZ8 RHO�B RecName Full 30S ribosomal protein S19	604.06
D5ALZ7 RHO�B RecName Full 50S ribosomal protein L2	161.53
D5ALZ6 RHO�B RecName Full 50S ribosomal protein L23	371.65

Table I.4 continued

D5APA8 RHOCB SubName Full Pyridine nucleotide transhydrogenase alpha su	187.82
D5ALZ5 RHOCB RecName Full 50S ribosomal protein L4	288.78
D5ALZ4 RHOCB RecName Full 50S ribosomal protein L3	785.73
D5ALZ3 RHOCB RecName Full 30S ribosomal protein S10	1158.5
D5APA4 RHOCB SubName Full Universal stress family protein	531.48
D5ALZ1 RHOCB RecName Full Elongation factor G	597.35
D5ALZ0 RHOCB RecName Full 30S ribosomal protein S7	1120.5
D5ASG4 RHOCB SubName Full CRISPR associated protein Cas2 family	178.77
D5ALY9 RHOCB RecName Full 30S ribosomal protein S12	156.47
D5ALY7 RHOCB RecName Full DNA directed RNA polymerase	241.92
D5ALY6 RHOCB RecName Full DNA directed RNA polymerase subunit beta	210.75
D5ALY5 RHOCB RecName Full 50S ribosomal protein L7 L12	4998.83
D5ALY4 RHOCB RecName Full 50S ribosomal protein L10	120.33
D5ALY3 RHOCB RecName Full 50S ribosomal protein L1	223
D5ALY2 RHOCB RecName Full 50S ribosomal protein L11	441.07
Random Sequence 1903	269.96
D5ALY1 RHOCB RecName Full Transcription antitermination protein nusG	152.18
D5ALX9 RHOCB RecName Full Polyribonucleotide nucleotidyltransferase	412.74
D5ALX6 RHOCB RecName Full 30S ribosomal protein S15	788.8
D5AVJ6 RHOCB SubName Full Nitrous oxide reductase	383.21
D5AM78 RHOCB SubName Full FAD dependent oxidoreductase	431.6
D5ALV0 RHOCB SubName Full DnaK suppressor protein 1	282.7
D5AVI3 RHOCB SubName Full TRAP transporter solute receptor TAXI family	621.45
D5ALU3 RHOCB SubName Full Oxidoreductase short chain dehydrogenase redu	382.35
D5AM62 RHOCB RecName Full 30S ribosomal protein S16	1429.61

Table I.4 continued

D5ASB0 RHOCB SubName Full Polyamine ABC transporter periplasmic polyami	1770.09
D5AM57 RHOCB RecName Full 50S ribosomal protein L19	503.96
D5AM56 RHOCB RecName Full 50S ribosomal protein L31	1663.62
D5ALT6 RHOCB SubName Full TRAP dicarboxylate transporter DctP 2 subunit	1065.77
D5ASA9 RHOCB SubName Full Polyamine ABC transporter ATP binding protein	189.36
D5ASA6 RHOCB SubName Full Cytochrome c2 1	1044.69
D5ASA2 RHOCB SubName Full Transcriptional regulator GntR family	159.42
D5AM45 RHOCB RecName Full 50S ribosomal protein L34	584.45
D5ALS1 RHOCB SubName Full Protease Do	190.65
D5AM40 RHOCB RecName Full Inner membrane protein oxaA	174.04
D5ALR9 RHOCB SubName Full HflC protein	188.23
D5ALR8 RHOCB SubName Full HflK protein	291.79
D5AP99 RHOCB SubName Full Oligopeptide ABC transporter periplasmic olig	784.16
D5AM36 RHOCB RecName Full Acetylglutamate kinase	244.39
D5AM30 RHOCB SubName Full Glutamate aspartate ABC transporter periplasm	1628.49
D5ALQ9 RHOCB SubName Full Alkane 1 monooxygenase	156.25
D5AP87 RHOCB SubName Full Photosynthetic reaction center M subunit	102.66
D5AP86 RHOCB SubName Full Photosynthetic reaction center L subunit	711.29
D5ALQ3 RHOCB SubName Full Mrp NBP35 family protein	400.32
D5AP85 RHOCB SubName Full Light harvesting protein B 870 alpha subunit	3443
D5AM22 RHOCB RecName Full 50S ribosomal protein L17	402.4
D5AM21 RHOCB RecName Full DNA directed RNA polymerase subunit alpha	1268.81
D5AM20 RHOCB RecName Full 30S ribosomal protein S11	653

Table I.4 continued

D5AP81 RHOCB SubName Full Chlorophyllide reductase BchY subunit	108.01
D5AP80 RHOCB SubName Full Chlorophyllide reductase BchX subunit	277.92
D5AM19 RHOCB RecName Full 30S ribosomal protein S13	1864.69
D5AM18 RHOCB RecName Full Adenylate kinase	421.4
D5AP79 RHOCB SubName Full 2 desacetyl 2 hydroxyethyl bacteriochlorophyll	215.37
D5AM16 RHOCB RecName Full 50S ribosomal protein L15	200.57
D5AP77 RHOCB SubName Full Farnesyltranstransferase	196.31
D5AM13 RHOCB RecName Full 50S ribosomal protein L30	757.58
D5AM12 RHOCB RecName Full 30S ribosomal protein S5	311.61
D5AM11 RHOCB RecName Full 50S ribosomal protein L18	902.35
D5AM10 RHOCB RecName Full 50S ribosomal protein L6	984.71
D5AP72 RHOCB SubName Full Phytoene dehydrogenase	519.88
D5AP71 RHOCB SubName Full Spheroidene monooxygenase	652.55
D5AM09 RHOCB RecName Full 30S ribosomal protein S8	413.67
D5AM07 RHOCB RecName Full 50S ribosomal protein L5	1792.53
D5AM05 RHOCB RecName Full 50S ribosomal protein L14	3969.96
D5AM04 RHOCB RecName Full 30S ribosomal protein S17	483.4
D5AP66 RHOCB SubName Full Molybdenum cofactor biosynthesis protein D 1	90.04
D5AM03 RHOCB RecName Full 50S ribosomal protein L29	1593.02
D5AVB8 RHOCB RecName Full Phosphoribosylaminoimidazole succinocarboxamid	315.82
D5AM01 RHOCB RecName Full 50S ribosomal protein L16	690.04
D5AVB7 RHOCB SubName Full Phosphoribosylformylglycinamide synthase Pu	771.99
D5AM00 RHOCB RecName Full 30S ribosomal protein S3	749.97
D5AVB6 RHOCB SubName Full Phosphoribosylformylglycinamide synthase Pu	420.62

Table I.4 continued

D5AP61 RHO�B RecName Full Phosphoenolpyruvate carboxykinase ATP	929.56
D5AVB4 RHO�B SubName Full C4 dicarboxylate transport transcriptional reg	81.32
D5AVB3 RHO�B SubName Full Ribonuclease E	192.6
D5ALN3 RHO�B RecName Full Citrate synthase	475.9
D5AVA8 RHO�B SubName Full Glyceraldehyde 3 phosphate dehydrogenase 3	1677.83
D5AVA5 RHO�B SubName Full Adenylosuccinate lyase	311.21
D5AP50 RHO�B SubName Full Fumarate hydratase	299.12